Physics-based modeling of fire behavior and smoke plume development, how much is enough?

RC19-1132 (Limited scope proposal)

USDA Forest Service
Pacific Northwest Research Station
Seattle, WA

August 30, 2021

William Mell[1], Anthony Bova[1], Tom Milac[2]

[1]USFS PNW Research Station, Seattle; [2]University of Washington, Seattle

REPORT DOCUMENTATION PAGE

Form Approved
OMB No. 0704-0188

1. REPORT DATE *(DD-MM-YYYY)*
30/08/2021

2. REPORT TYPE
SERDP Final Report

3. DATES COVERED *(From - To)*

4. TITLE AND SUBTITLE
Physics-based Modeling of Fire Behavior and Smoke Plume Development, How Much is Enough?

5a. CONTRACT NUMBER

5b. GRANT NUMBER

5c. PROGRAM ELEMENT NUMBER

5d. PROJECT NUMBER
RC19-1132

5e. TASK NUMBER

5f. WORK UNIT NUMBER

6. AUTHOR(S)
William Mell and Anthony Bova
USFS PNW Research Station, Seattle

Tom Milac
University of Washington, Seattle

7. PERFORMING ORGANIZATION NAME(S) AND ADDRESS(ES)
U.S. Forest Service PNW Research Station, Seattle
Pacific Wildland Fire Science Laboratory
400 North 34th Street, Suite 201
Seattle, WA 98103

8. PERFORMING ORGANIZATION REPORT NUMBER
RC19-1132

9. SPONSORING/MONITORING AGENCY NAME(S) AND ADDRESS(ES)
Strategic Environmental Research and Development Program (SERDP)
4800 Mark Center Drive, Suite 16F16
Alexandria, VA 22350-3605

10. SPONSOR/MONITOR'S ACRONYM(S)
SERDP

11. SPONSOR/MONITOR'S REPORT NUMBER(S)
RC19-1132

12. DISTRIBUTION/AVAILABILITY STATEMENT
DISTRIBUTION STATEMENT A. Approved for public release: distribution unlimited.

13. SUPPLEMENTARY NOTES

14. ABSTRACT
Over the last decade there has been a significant increase in the availability of affordable and capable computing power (e.g., Amazon Web Services cloud computing). As a result, there is a potential to use more advanced (e.g., greater physical fidelity) fire behavior and smoke plume development models as tools for prescribed burn planning. Basing these models on a computational fluid dynamic (CFD) solver is one path forward. CFD models have been used in weather prediction and engineering applications (e.g., airplane design and structure fire safety) for many years. While CFD models are used in larger-scale smoke transport modeling, their use in applications relevant to wildland fire behavior and near-field smoke plume development is nearly nonexistent outside of research activities.

15. SUBJECT TERMS
Fire behavior model, CFD, WFDS, FDS, Smoke, Plumes

16. SECURITY CLASSIFICATION OF: a. REPORT	b. ABSTRACT	c. THIS PAGE	17. LIMITATION OF ABSTRACT	18. NUMBER OF PAGES	19a. NAME OF RESPONSIBLE PERSON
UNCLASS	UNCLASS	UNCLASS	UNCLASS	87	William Mell
					19b. TELEPHONE NUMBER *(Include area code)* 206-430-2072

Physics-based modeling of fire behavior and smoke plume development, how much is enough?

RC19-1132 (Limited scope proposal)

William Mell[1], Anthony Bova[1], Tom Milac[2]

[1]USFS PNW Research Station, Seattle; [2]University of Washington, Seattle

Executive Summary

Introduction

Over the last decade there has been a significant increase in the availability of affordable and capable computing power (e.g., Amazon Web Services cloud computing). As a result, there is a potential to use more advanced (e.g., greater physical fidelity) fire behavior and smoke plume development models as tools for prescribed burn planning. Basing these models on a computational fluid dynamic (CFD) solver is one path forward. CFD models have been used in weather prediction and engineering applications (e.g., airplane design and structure fire safety) for many years. While CFD models are used in larger-scale smoke transport modeling, their use in applications relevant to wildland fire behavior and near-field smoke plume development is nearly nonexistent outside of research activities.

Some applications of interest in prescribed fire planning that could potentially be addressed in a useful way with higher physical fidelity CFD-based models, but lie outside the scope of simpler models, are listed below.

- For smoke applications:
    - the influence of various prescribed burn firing patterns on smoke plume rise
    - the influence of multiple regions of distinct burning (i.e., plume cores) on the behavior of the overall plume (versus a single region of burning)
    - the effects of atmospheric temperature profiles, wind and heat release rate on plume rise and on the plume fractions above and below the mixed layer

- For fire behavior application:
    - the influence of different prescribed burn firing patterns on local fire behavior (e.g., head versus back fires) throughout a burn plot
    - identifying locations of relatively high vegetation consumption as dependent on the characteristic of the vegetation (e.g., spatial distribution and physical characteristics), firing patterns, and atmospheric conditions.
- Addressing the trade-off between the need to ensure the smoke stays aloft (i.e., sufficiently high intensity fire) versus ensuring a desired environmental impact (i.e., removing vegetation only in selected locations).

A modeling tool that sufficiently captures the interaction of the fire generated wind and the surrounding atmosphere is more capable of addressing the example objectives listed above. The methods of CFD are capable of accounting for fire-atmosphere interactions.

Objectives

There are two main questions addressed in this limited scope study, from a model usability point view:

1. What is the lowest level of CFD-based model physical fidelity that results in predictions that are useful for the application in question (e.g., plume rise)?
2. How computationally expensive are the models considered here? For example, can they be run on a desktop computer or are cloud computing resources needed? Provide measures of computing time and cost in dollars.

Another objective is the development of a prototype tool for running simulations on Amazon Web Services (AWS). Many of the simulations in this project made use of AWS. A prototype was developed and a five-minute presentation, from this project's February 2021 progress presentation is available here.

It is important to note that it is outside the scope of this project to validate the predictions of the models considered here or provide an evaluation of their use for prescribed burn planning. Instead, we focus on comparing models of different physical fidelity through simulations of idealized scenarios. In some cases, it is clear that a higher fidelity model captures a fire or smoke behavior that is important while a lower fidelity model does not. A more complete identification of what level of physical fidelity is needed for a given model application requires a larger effort that includes end users and, ideally, appropriate observational data sets.

Technical Approach

Four models were used for fire behavior predictions and three models for smoke plume predictions. The models had different levels of physical fidelity as briefly described next.

Fire behavior models (in order of decreasing physical fidelity)

1. WFDS-PB (or PB) is a three-dimensional, time dependent, CFD-based approach that explicitly models the thermal degradation (drying and pyrolysis) of the vegetation. Gas phase combustion and all modes of heat transfer are explicitly modeled. Fire generated wind and the surrounding atmosphere influence each other (e.g., they are coupled through the model equations).
2. WFDS-LS (or LS) uses the same modeling approach as PB except for fire in surface vegetation. Instead of explicitly modeling the thermal degradation, a level set based approach is used to model the spread of the surface fire front. LS requires a formula for the potential head fire spread rate as a function of the local wind speed. The spread rate at any point on the surface-fire perimeter is determined based on the potential head fire spread rate and direction of spread relative to the direction of the local wind. This results in spread rates and flaming areas that differ across the fire perimeter (e.g., head versus flank fire). The motivation for the level set approach is the capability to model surface fire spread on computational grids with spatial resolutions that are too coarse to resolve the processes driving smaller, lower intensity, fires characteristic of prescribed burns.

3. WFDS-LS5 (or LS5) uses the same modeling approach as LS with the simplification that the potential head fire spread rate is constant (not a function of the local wind speed) but does depend on the direction of spread relative to the direction of the local wind.
4. WFDS-LS1 (or LS1) is not CFD based. There is no interaction of fire induced wind and the atmosphere. LS1 only requires a wind direction and speed (both are held constant) and can implemented with the Rothermel surface head-fire spread rate model to be equivalent to FARSITE.

Smoke plume models (in order of decreasing physical fidelity)

1. FDS is a three-dimensional, time dependent, CFD-based approach. It shares the same, but more current, CFD solver as WFDS-PB. Gas phase combustion is explicitly modeled. There is full coupling between the fire generated wind and the atmosphere.
2. ALOFT-FT is a two-dimensional, time dependent, CFD-based approach (with 3D projection) initially designed to model smoke plume rise from burning oil spills. Gas phase combustion is not explicitly modeled. The heat release rate from a spreading fire(s) is approximated by a stationary fire(s) with an equivalent heat release rate and the resulting buoyancy induced flow interacts with the atmosphere.
3. MW94 is not a CFD based model and was designed to simulate a two-dimensional vertical cross section of a plume from a line fire.

Predictions of various quantities from the models above are compared in a number of test scenarios. Two validation studies (crown ignition and grass fire spread - summarized below), using measurements from experiments, were conducted to provide some confidence in the capabilities of the higher fidelity CFD-based models. In this study, the highest fidelity models were used as a standard against which the lower fidelity models were evaluated. It is important to note that observational measurements are lacking for a comprehensive validation study of fire behavior and smoke plume development in a prescribed burn setting. For example, observations are needed to evaluate predictions of fire line interaction and the influence of different firing patterns on subsequent fire behavior and smoke plume rise. It is hoped that currently ongoing, SERDP funded, field experiment efforts will significantly expand the observational data base.

Results and Discussion

This section is split into two subsections. The first considers the results of comparing the fire behavior models and the second considers the smoke models.

Results from fire-behavior model comparisons

--- *PB, LS5, and LS fire behavior validation*

Two validation studies were conducted. The first compared the PB and LS5 model predictions of ignition thresholds for chamise shrub-crowns to observations in laboratory experiments. The PB and LS5 model predictions agreed with each other for all cases. The models over predicted the shrub-crown height threshold by 50%: the observed threshold height was 40 cm (16 inches) and predicted height was 60 cm (24 inches). However, the model predictions of the wind threshold agreed with the observations (1.8 m/s = 4 mph). This is for a shrub-crown base height of 20 cm (8 inches) which was the only height considered in experiments with an imposed wind.

The second validation study compared the PB and LS predictions of fire perimeter evolution to observations in an Australian grassland experiment. The PB predictions quantitatively matched the observed spread rate and depth of the head fire, but were unable resolve the flank fires. Rather than run the PB simulations with a finer grid, sufficient to resolve the flank fires, the PB simulations were used to develop a formula for the head fire spread rate as a function of the local wind speed for use in the LS model (see Appendix 1 of the technical report). With this formula, the LS approach predicted the spread rate and depth of the head fire and, by design, retained the flank fires.

--- *Comparison of fire behavior predictions for a prescribe fire scenario*
The distribution of vegetation and location of three ATV ignition lines for the idealized prescribed burn scenario is shown in Figure 1. The vegetation consists of a surface fuel (grass), understory (longleaf pine, turkey oak, persimmon), and overstory (longleaf pine, turkey oak) representative of southeastern US longleaf pine stands (see Appendix 2 of the technical report).[1] The center 100m x 100m portion of the domain containing the three ATV ignition tracks (red lines) is allowed to burn. ATVs are spaced 40 m (131 ft) apart and travel in the positive Y direction at 1.5 m/s (3.5 mph); these specifications can be easily changed. The ambient wind flows in the positive X direction at 2 m/s (4.5 mph) at 2 m (6.4 feet) above ground.

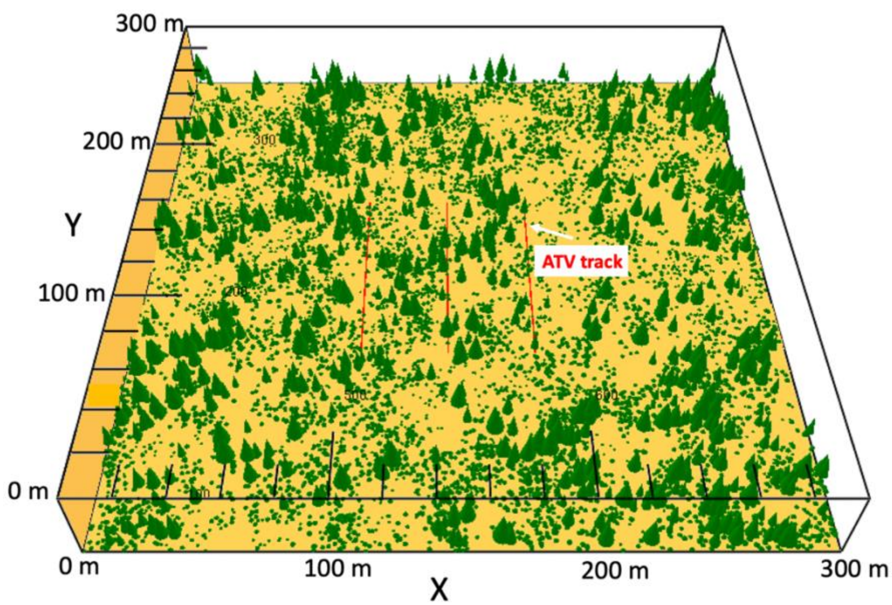

Figure 1: The 300 m x 300 m x 40 m computational domain used for comparing WFDS-PB and WFDS-LS predictions of a prescribed burn scenario. The visualization tool Smokeview (designed for FDS and WFDS) is used. The locations of three simulated ATV ignition lines are shown in red.

The influence of fire generated winds on the surface-fire behavior is clearly seen in Figure 2 which shows results of a PB simulation of the prescribed burn scenario. For example, at 120 s the fires initiated by the rightmost ATV line spread in a manner determined by the wind generated by the large head fire spreading from the leftmost ATV line: a head fire spreads to the left and a backing fire to the right of the rightmost ATV line. Models which cannot account for

[1] The authors thank Dr. Justin Ziegler and Prof. Chad Hoffman, of Colorado State University, for providing the characteristics of the raised vegetation used in the idealized prescribed burn scenario.

fire generated winds, such as FARSITE or FARSITE-WindNinja, are unable to predict this fire behavior.

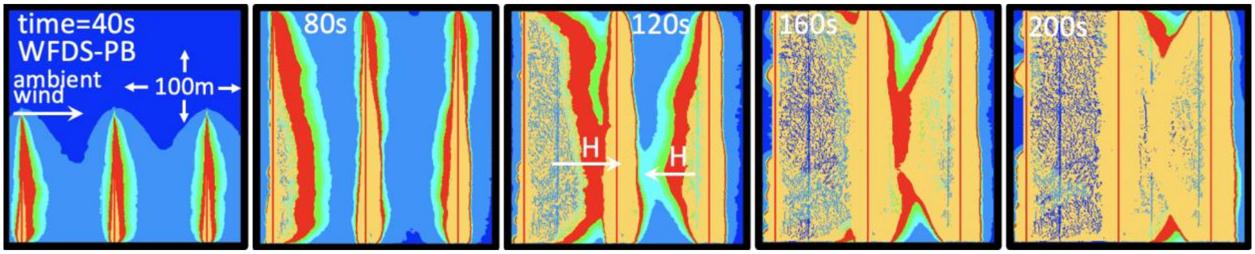

Figure 2: Color contours of the grass temperature at five times (every 40 s) from the PB simulation of the prescribed burn scenario shown in Figure 1 (only the center 100 m x 100 m is shown here). Red denotes the location of the flaming base of the fire; dark blue is ambient. The straight red lines are the simulated ATV tracks. The letter H denotes a head fire.

Figure 3 shows the time of arrival (TOA), in 20 s increments, of the leading edge of the fire fronts from LS1 (on left) and LS (on right), both run with a 1 m grid resolution. The LS1 model, which is consistent with FARSITE, shows fire spreading from all ATVs lines predominantly as a head fire, as determined by the ambient wind direction. Fire behavior from the LS model closely matches the PB model results in Figure 2. Fire behavior predicted by LS at a coarser grid resolution (2 m), and by LS5, is also consistent with the PB results (not shown).

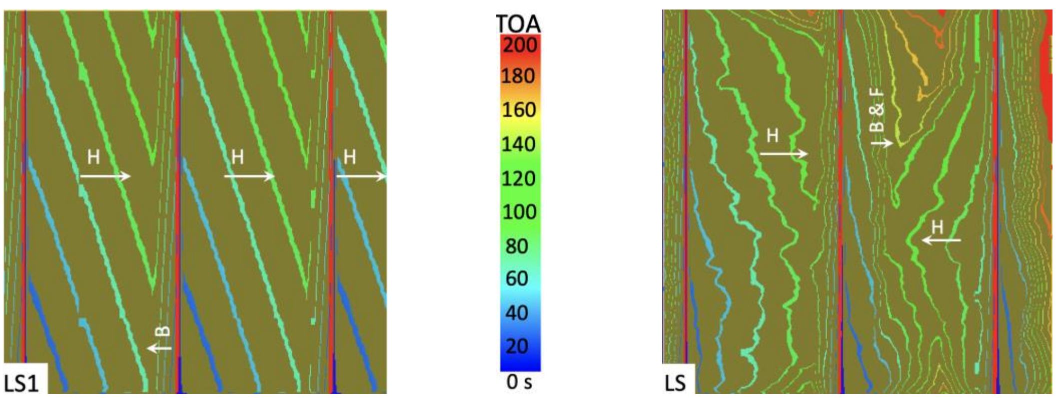

Figure 3: Surface-fire time of arrival contours in the center 100 m x 100 m area from of the prescribed burn scenario. The location of the leading edge of the fire front is plotted every 20 s (see legend). On the left are WFDS-LS1 predictions; on the right are WFDS-LS predictions, both with a 1 m grid resolution. Some locations of head, back, and flank fire spread are identified by H, B, F, respectively. Arrows show direction of fire spread.

The locations of understory consumption, from PB and LS, in Figure 4 agree well qualitatively. More consumption occurred in head fires, less in locations of flank and back fires. The PB model has significantly finer grids than LS and, therefore, requires significantly more computational resources and compute time (see Table 1).

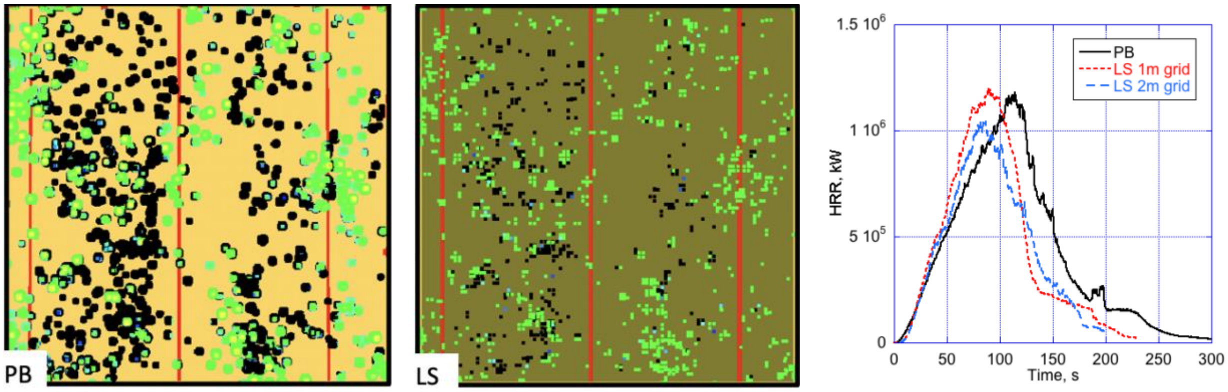

Figure 4: Comparison of the location of understory consumption from WFDS-PB and WFDS-LS (1 m grid resolution). Black denotes complete consumption; green denotes no consumption. The overstory is not shown. Rightmost plot is the time history of the global heat release rate (HRR).

Results from smoke-plume model comparisons

The agreement between PB and LS fire behavior predictions translates to the reasonable agreement in the overall heat release rate (HRR) seen in Figure 4. HRR drives plume rise and is dominate by the surface fuel consumption rate (not shown). For this reason, we use LS, instead of the more computationally expensive PB, at larger domains appropriate for smoke plume development such as shown in Figure 5. It was found that the ATV ignited fires reached a steady-state (see fires at the base of the plume in Figure 5, on left). In this case, static burners of the same size and heat release per unit area (HRRPUA) produced very similar smoke profiles (see Figure 5, on right) with coarser computational grids and significantly less computational expense (see Table 1).

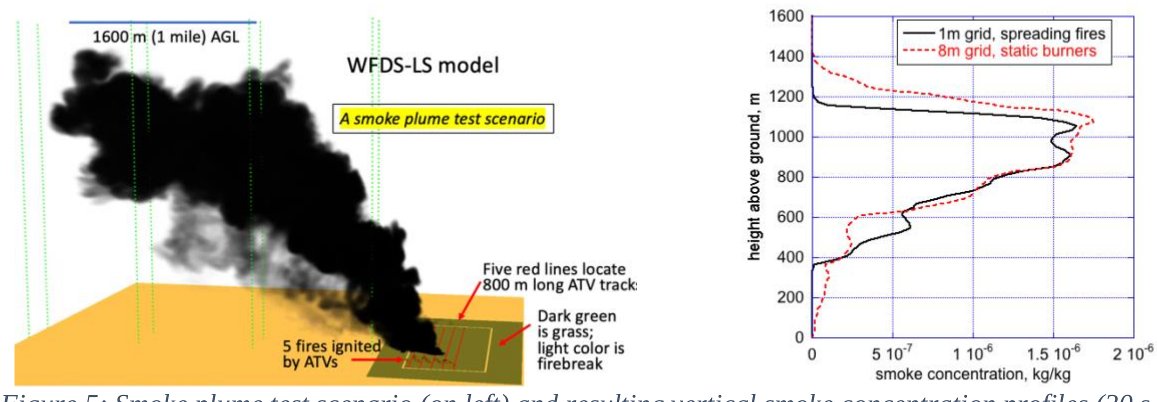

Figure 5: Smoke plume test scenario (on left) and resulting vertical smoke concentration profiles (30 s average, 2 km downwind of burn plot center) from WFDS-LS with spreading fires (1 m grid) and WFDS with a simplified representation of the fire (8 m grid).

Further smoke plume simulations were conducted to compare results from three smoke plume models (MW94, ALOFT-FT and FDS) and to compare FDS and ALOFT-FT to empirical data. Sensitivity studies and model modifications are described in the appendices of the report.

All three models were compared using simulations of line fires. An example of the results is shown in Figure 6 (left column). All models give adequate estimates of plume centerline height, but plumes in FDS and ALOFT-FT differ in spatial profiles and plume concentrations (MW94 does not provide concentrations). In general, initial plume rise is more vertical in FDS than in ALOFT-FT. This is likely due to the use of only a single transport windspeed in ALOFT-FT, as opposed to a boundary layer profile, which results in more plume bending near ground level.

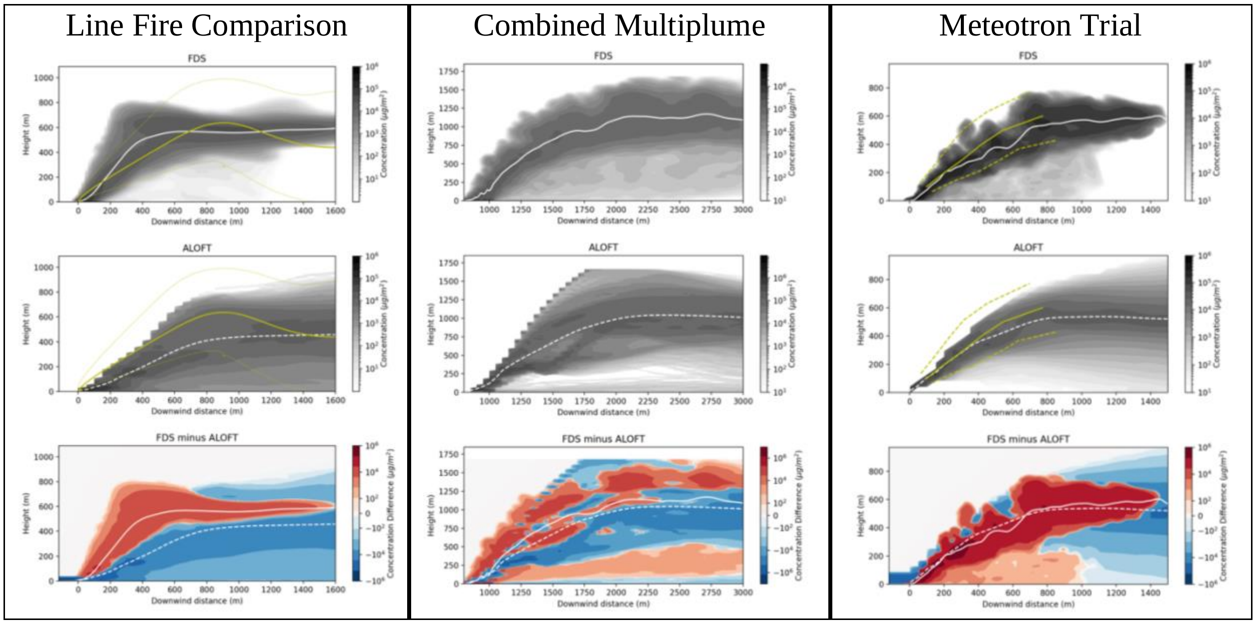

*Figure 6. Crosswind-integrated plume concentrations and centerlines. **Left column**: line fire with intensity of 500 kW/m in FDS (top), ALOFT-FT (middle) and MW94 plumes (top & middle, indicated by yellow lines). Centerlines are indicated by white solid or dashed lines. **Middle column**: Combined plume from five separate line fires in FDS (top) and ALOFT-FT (middle). **Right Column**: Comparison to 1971 trial of the Meteotron experiment. Observed plume extent shown in yellow lines. **Bottom row, all columns**: Differences between the FDS and ALOFT-FT simulated plumes. Red indicates regions in which the FDS concentration values are greater than those simulated by ALOFT-FT; blue indicates the opposite.*

Plume interaction was examined in a comparison of FDS and ALOFT-FT simulations of plumes from five line fires, each separated in the alongwind direction by 24 m (Figure 7). Plume shapes and centerlines were similar in both models, but crosswind-integrated concentrations differed considerably (Figure 6, middle column).

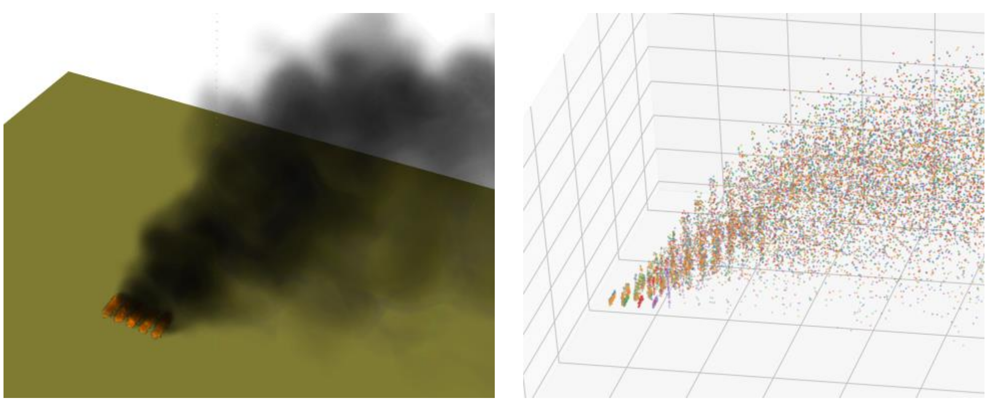

Figure 7. Multi-line fires in FDS (left) and ALOFT-FT (right) simulations. In both cases, the separate plumes merge at short distances above the fires, effectively forming a single plume.

In a separate set of simulations, the combined plumes from line fires separated by increasing downwind distances were simulated in ALOFT-FT (Figure 8). Results suggest that upwind lines may partially shield plumes from lines that are 1-2.5 fire line lengths downwind, allowing the downwind plumes to rise higher and increase the combined plume height in comparison to plumes from single lines. In addition, the interaction of plume vortices can also increase plume rise in downwind configurations (Trelles, et al. 1999). FDS simulations could be used to investigate this phenomenon in greater detail in future work.

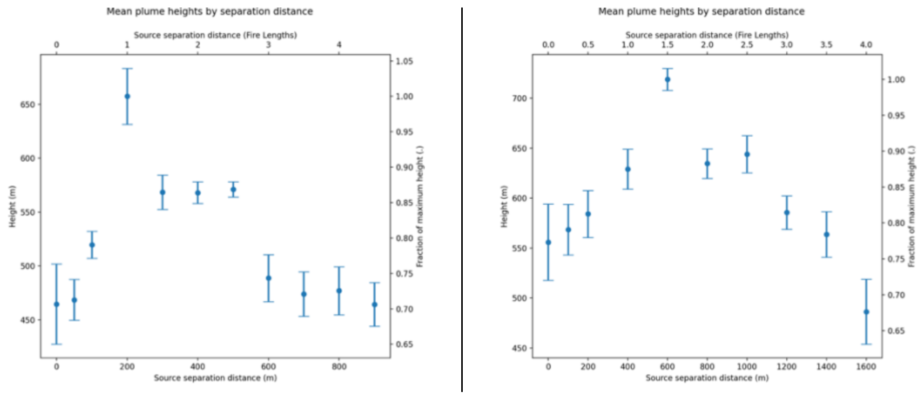

*Figure 8. Mean far-field centerline heights of the combined plumes from line fires. Standard deviations are shown as vertical error bars. Secondary axes show separation distance normalized by fire line length (upper x-axes) and the fractions of maximum height (right y-axes). **Left**: 200 m x 10 m static fire lines. **Right**: 400 m x 10 m static fire lines.*

Finally, plumes from FDS and ALOFT-FT were visually evaluated against plumes from the Meteotron plume experiment conducted in the 1970s (Benech 1976). An example of the results is shown in the right column of Figure 6. In some cases, both models matched the recorded plume extents (originally estimated visually by photogrammetry) reasonably well. It is not clear whether mismatched cases were due to simulation issues or to quality of meteorological data recorded in the experiment. In general, FDS plumes were spatially more similar to the Meteotron plumes (e.g., Figure 9), providing satisfactory matches to recorded plume profiles in four of six simulations.

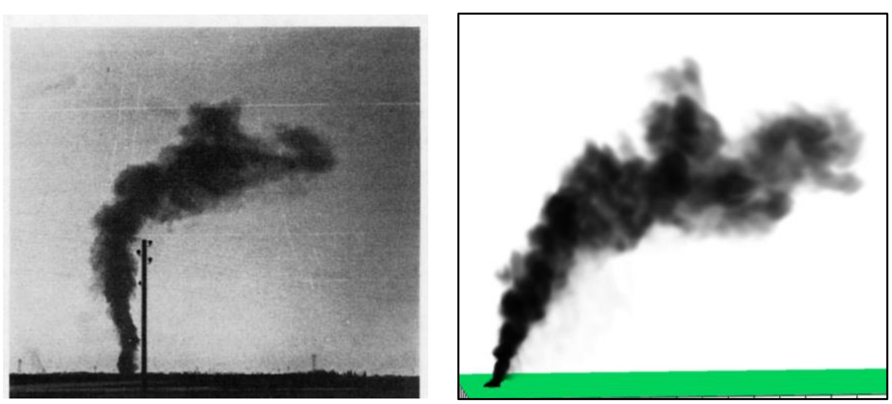

Figure 9. Left: a photograph of the April 1973 Meteotron plume (Benech 1976). Right: an FDS simulation of the experiment. Both images show the plume 300 s after ignition.

Computational costs vary considerably between the models. The MW94 and ALOFT-FT models provide results much faster than real time, while FDS is generally slower than real time (Table 1, p. 9). However, the physical fidelity and capabilities of FDS greatly exceed those of the other models.

Table 1: Computational cost of simulations. LS5 costs are not shown, they're similar to LS costs. The desktop computer used was purchased in 2019.

Model	Grid resolution	Computing hardware	Computing time	Computing cost, $/hr; total $	Comment
Fire behavior simulations (Figure 1 domain); 5 minutes were simulated					
WFDS-PB	5 to 20 cm vert. 25 cm horiz.	93 cpus AWS	418 RT	1.54; 55	standard for comparison
WFDS-LS	1 m	25 cpus Desktop	23 RT	0.62; 1	follows PB's fire behavior and consumption
WFDS-LS	2 m	25 cpus Desktop	3.4 RT	0.62; 0.15	follows PB's fire behavior
Smoke plume simulations in Figure 5 *domain; 15 mins were simulated*					
WFDS-LS	≥ 1 m	256 cpus AWS	123 RT	4.62; 132	standard for comparison
	≥ 8 m	20 cpus Desktop	3.6 RT	0.62; 0.56	matches standard; simple heat source
Smoke plume simulations, various scenarios					
FDS	≥ 1 m – 40 m	Laptop/Desktop 1 – 15 cpus	10 – 88 RT	N/A	plume comparisons
ALOFT-FT	10 – 100 m (y-z plane only; scales dynamically)	Laptop/Desktop 1 cpu	~1/100 – 1/400 RT	N/A	plume comparisons
MW94	~1000 pts along centerline	Laptop/Desktop 1 cpu	~1/15,000 RT	N/A	plume comparisons
KEY: cpus = physical cpus; AWS = Amazon Web Services; RT = factor to get real time cost: 4 RT means 1 min of simulated time takes 4 mins of computing time					

Implications for Future Research and Benefits

Overall, the results of this proof-of-concept study suggest that, depending on domain size and user needs, semi-routine CFD-based fire behavior and smoke plume simulations are within reach for use as prescribed-burn planning tools. The prescribed burn simulations (Fig. 3) clearly show the relevance of fire-atmosphere interaction captured with the CFD-based simulations. Such simulations are potentially within reach with a high-end desktop computer and definitely the case if cloud computing is available. For example, higher resolution simulations of fire behavior, in smaller computational domains, could be conducted with different candidate firing pattern options to obtain useful fire behavior predictions, HRR histories, and locations of higher likelihood of understory consumption. A representative HRRPUA could then be used for smoke plume simulations in larger computational domains. Or, for simulations focused on smoke plume development, approximations to the fire behavior could define the characteristics of the HRRPUA in the burn plot (i.e., spatial distribution and time history) to define coarse grid, faster turn-around, simulations. It is possible model runs with relatively quick turnaround times and qualitative accuracy could be used in prescribed burn training or to illustrate fire behavior relevant to fire safety.

Important issues to be addressed if this project is to move to the next stage include the following:

1. This study is largely based on model-to-model comparison for a limited range of scenarios. The range of scenarios needs to be expanded, as does comparison to experimental observations of fire behavior and smoke plume development. Currently, there is a dearth of reported observations for model evaluation use. A number of ongoing SERDP field experiments offer a possible source of relevant observations.
2. It is critical that beta users, who are experienced prescribed burn planners, are actively involved from the beginning of the project. This includes use of the models. Given the lack of observational data, those who are experienced in conducting prescribed burns will be the best resource for model assessment. This assessment includes the reliability of the models' predictions, in terms of practical application, and ease of use. It is also critical to success that the simulation team visit prescribed burn sites for direct observation and better understanding of the objectives and challenges of burn planning and operation.
3. The source code and program executables for Windows, Linux, and OSX should all be publicly available during the entire course of the project (note, WFDS and FDS source code and executables have always been publicly available). In addition, user and technical guides should be made available and regularly updated. This ensures transparency and supports a more collaborative advance of the modeling tools. Ideally, a public issue tracker and discussion group are used. These are practices currently followed by the FDS development team who would join us in a follow-on effort. FDS is a well-established model in the fire protection engineering community (e.g., from April 2020 – April 2021 there were 30,518 downloads). Work is well underway to incorporate the PB and level set capabilities of WFDS into FDS. If this project has a follow-on stage, FDS will replace WFDS.

Physics-based modeling of fire behavior and smoke plume development, how much is enough?
RC19-1132. W. Mell, A. Bova, T. Milac

Abstract

Introduction and Objectives

Over the last decade there has been a significant increase in the availability of affordable and capable computing power (e.g., Amazon Web Services cloud computing). As a result, there is a potential to use more advanced (i.e., greater physical fidelity) computational fluid dynamics (CFD) based fire behavior and smoke plume development models as tools for prescribed burn planning. There are two main questions addressed in this limited scope study from a model usability point view:

1. What is the lowest level of CFD-based model physical fidelity that results in predictions that are useful for the application in question (e.g., plume rise)?
2. How computationally expensive are the models considered here? For example, can they be run on a desktop computer or are cloud computing resources needed? Provide measures of computing time and cost in dollars.

Another objective is the development of a prototype tool for running simulations on Amazon Web Services (AWS).

Technical Approach

Predictions from four fire behavior and three smoke plume models were compared for a number of test scenarios. These models, in order of decreasing physical fidelity are: WFDS-PB, WFDS-LS, WFDS-LS5, WFDS-LS1 (for fire behavior) and FDS, ALOFT-FT, MW94 (for smoke plume development). Limited model validation, through comparisons to observations, were conducted. Given that the range of relevant observational studies needed for a more complete model validation does not currently exist, the highest physical fidelity models were used as a standard against which the lower fidelity models were compared in the test scenarios.

Results

Fire behavior focused simulations, for which qualitative results are sufficient, ran 2 - 3.4 times (depending on model fidelity) slower than real time in a 300 m x 300 m domain. Higher resolution simulations that predicted locations of understory consumption ran 23 times slower than real time. These simulations were run on a high-end desktop (25 cpus). For single line fires, all smoke plume models gave similar centerline heights. The simulations suggest that multiple, spreading, fires can be approximated by static fires and simulated on coarse grids, allowing a relatively fast computation. Plume interaction from multiple fires can affect plume height and requires CFD-based models, the simplest of which ran significantly faster than real time. A prototype user interface for running CFD-based simulations on AWS was demonstrated.

Benefits

Overall, the results of this proof-of-concept study suggest that, depending on domain size and user needs, semi-routine CFD-based fire behavior and smoke plume simulations are within reach for use as prescribed-burn planning tools. This is potentially the case with a high-end desktop computer and definitely the case if cloud computing is available. Model runs with relatively quick turnaround times and qualitative accuracy could be used in prescribed burn training or to illustrate fire behavior relevant to fire safety. More complete model evaluation is needed (through both model-to-model comparison and model comparison to observations). It is essential that further development of the modeling tools includes the collaboration of prescribed burn planners who are active beta testers. In addition, the model source code and executables need to be open source with readily available and regularly updated user guides. This ensures transparency and supports a more collaborative advance of the modeling tools.

Table of Contents

List of Tables

List of Figures

List of Acronyms

ALOFT-FT	A Large Oil Fire plume Trajectory – Flat Terrain. Two-dimensional smoke plume model with a simplified accounting of combustion heat release.
AWS	Amazon Web Services
CFD	Computational Fluid Dynamics
DoD	Department of Defense
FDS	Fire Dynamics Simulator from NIST
FARSITE	Fire front tracking model with no accounting of fire-atmosphere interaction.
HRRPUA	Heat Release Rate Per Unit Area, kW m^{-2}
HRR	Heat Release Rate, kW
LES	Large Eddy Simulation
LR	Atmosphere Lapse Rate, C km^{-1}
LS	Alternate notation for WFDS-LS
LS1	Alternate notation for WFDS-LS1
LS5	Alternate notation for WFDS-LS5
MW94	Mercer and Weber (1994) smoke plume model
NIST	National Institute of Standards and Technology
PB	Physics Based and alternate notation for WFDS-PB
SDI	Stand Density Index
TOA	Time Of Arrival of leading edge of fire front
USFS	United States Forest Service
WFDS	Wildland-urban interface Fire Dynamics Simulator model suite
WFDS-LS	WFDS using the level set with full fire-atmosphere coupling and an empirical formula for the head fire spread rate dependence on the local wind (i.e., there is no explicit modeling of the thermal degradation of vegetation).
WFDS-LS1	WFDS using the level set model with no fire-atmosphere interaction. Approach is consistent with, and can be made essentially identical to, the FARSITE model.
WFDS-LS5	WFDS using the level set model with partial fire-atmosphere coupling and a constant head fire spread rate.
WFDS-PB	WFDS using the full physics-based model for fire behavior

Keywords
Fire behavior model, CFD, WFDS, FDS, Smoke, Plumes

Acknowledgements

We thank Dr. Jason Ziegler and Prof. Chad Hoffman, of Colorado State University, for the information necessary to define the raised vegetation in the prescribed burn scenario simulations.

Technical Report

Objectives

There are two main questions addressed in this limited scope study, from a model usability point view:

1) What is the lowest level of CFD-based model physical fidelity that results in predictions that are useful for the application in question (e.g., fire line interaction, plume rise)?
2) How computationally expensive are the models considered here? For example, can they be run on a desktop computer or are cloud computing resources needed? Provide measures of computing time and cost in dollars

In more detail, we seek to answer these questions through the following approach:

1) For a prescribed burn scenario, assess how and to what degree the level of a model's physical fidelity influences predictions of relevant fire behavior and smoke plume characteristics.
2) Determine the computational resources required for the different levels of model fidelity considered.
3) Prototype the use of a cloud computing tool to implement a subset of the fire behavior and smoke plume models employed here.
4) Based on the information gathered, assess the physical fidelity requirements, and attendant computational costs, for simulating the fire and smoke behaviors of importance (e.g., fire line interaction or plume rise).
5) Assess if advancements in fire behavior and smoke modeling that support prescribed burn planning, through higher model physical fidelity, is possible at this time (given model complexity and computational cost) and, if so, provide a proposed path forward.

It is important to note that it is outside the scope of this project to validate the predictions of the models considered here or provide an evaluation of their use for prescribed burn planning. Instead, we focus on comparing models of different physical fidelity through simulations of idealized scenarios. In some cases, it is clear that a higher fidelity model captures a fire or smoke behavior that is important while a lower fidelity model does not. A more complete identification of what level of physical fidelity is needed for a given model application requires a larger effort that includes end users and appropriate observational data sets.

Background

Successful prescribed burn operations result in desired outcomes in terms of vegetation consumption and smoke transport. Firing operations are designed to create fire behavior that removes unwanted vegetation (e.g., invasive species) without harming (e.g., crown scorch) desired vegetation. In addition, to ensure public safety, the impact of smoke on downwind communities and roadways needs to stay within air quality and obscuration tolerances. Meeting these twin objectives is challenging, in part, because limiting fire intensity to avoid overconsumption of vegetation may also limit smoke plume rise and expose the public to hazardous smoke.

From the perspective of fully modeling the relevant physical processes, meeting the challenges described above requires the resolution of the fire-generated local heat fluxes (occurring over, approximately, centimeters) in a computational domain that is large enough to include the buoyancy-generated smoke plume rise (potentially 1000s of meters). High physical fidelity modeling of fire and buoyant flow requires a computational fluid dynamics (CFD) solver that incorporates sub models for the processes of gas-phase combustion, turbulence, thermal degradation of vegetation, and heat flux. With recent advances in numerical methods in CFD and readily available and affordable computational power (e.g., cloud computing), the next major advance in computer models to support prescribed burning will likely be built on CFD methods. The objective of this limited scope project is to assess how close we are to realizing this advance. We do this by comparing CFD-based modeling approaches that have different degrees of physical fidelity and associated computational cost.

Goodrick et al. (2013) and references therein, provides a review of wildland fire smoke modeling. The models they survey range from older Box (e.g. VALBOX) and Gaussian (e.g. VSMOKE) models, which by their limited physical basis clearly acknowledge the relatively primitive state of digital computing at the time of their invention, to full-physics (within the context of including processes relevant to atmosphere dynamics) models, such as ATHAM (Trentmann et al., 2001), the use of which require both more expertise and computational effort. More recently developed smoke models, such as the Puff model HYSPLIT or the particle model Daysmoke, use less restrictive assumptions in modeling the transport of smoke and particulates once airborne. This includes the presence and influence of multiple interacting plume cores. It is of interest to note that the numerical simulations of Trelles et al. (1999) predict that the nonlinear interactions of multiple plumes can lead to higher overall plume heights compared to a single plume created by the same heat output. This is inconsistent with predictions from Daysmoke which predict that the overall plume height decreases as the number of plume cores increases (Goodrick et al., 2013; Achtemeier et al., 2011). This difference in simulation results may be due to the higher physical fidelity of the modeling approach of Trelles et al. (1999), especially with regard to capturing the nonlinear interactions between plumes. None of the aforementioned models track the evolution of fire line(s) and cannot, therefore, account for the influence of the interaction of a spreading fire and the atmosphere on the development of smoke plumes. Consequently, the details of the near-fire plume structure and time evolution are not captured with the fidelity required for accurate fire growth and plume rise predictions which are important inputs to larger scale models (Simm, 2014).

A number of wildland fire smoke models have been developed that do model, with different degrees of physical fidelity, a spreading fire and the coupling of the fire-generated buoyant flow and the response of the atmosphere. These include WRF-SFIRE (Mandel et al., 2014), MesoNH-ForeFire (Filippi et al., 2009), Daysmoke-RabbitRules (Achtemeier et al., 2012), FIRETEC (Furman et al., 2020), QUIC-fire (Linn et al., 2020), WFDS-PB (Mell et al., 2007; Mell et al., 2009) and a recent modification of WFDS-LS (Bova et al., 2015). Figure 1 shows the smoke plume centerline height as a function of downwind distance from the simple scenario of a single static fire line, as predicted by a subset of these models (Mell and Linn, 2017). Note that among the models shown, only WFDS-PB and WFDS-LS employ CFD modeling approaches designed to capture the fine-scale, high-temperature and turbulent processes at the scale of the fire front, and only WFDS-PB and WFDS-LS explicitly model the gas-phase combustion process.

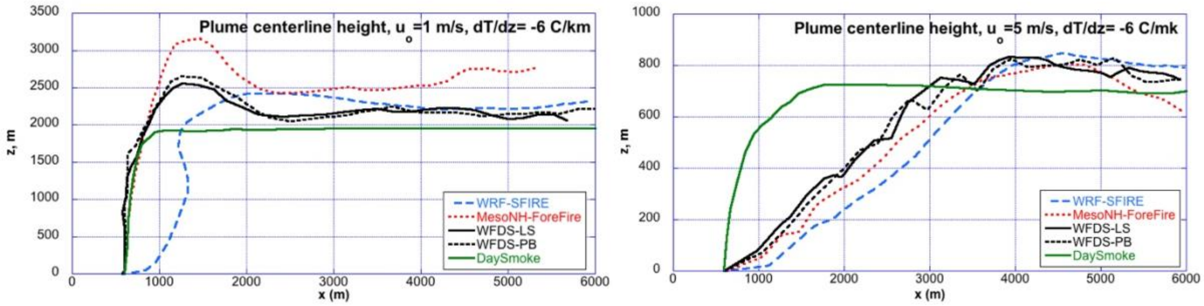

Figure 1: The smoke plume centerline height as a function of the downwind distance from an idealized single static fire line as predicted from five different models (Mell and Linn, 2017). Two different inflow wind speeds are shown: $u(z) = u_o(z/2)^{1/7}$ with u_o = 1 m/s (on the left) and u_o = 5 m/s (on the right). The source of heat is a 750 m long, 25 m deep, stationary fire line with a heat release rate per unit area of 2000 kW m^{-2}. The fire depth and heat release characteristics are based on fires observed during the International Crown Fire Modeling Experiments (Stocks et al. 2004).

Materials and Methods

This project compares results from numerical models that differ in their level of physical fidelity. No experiments in the field or laboratory were conducted. However, experiments previously conducted by others were used to evaluate the models. This model evaluation formed the basis for establishing some confidence in the models' performance and justification for extending the models to environmental scenarios not within the scope of the experiments (but relevant to a larger scale prescribed fire scenario). For example, we used laboratory experiments designed to identify thresholds in wind speed and shrub-crown base height below which sustained crown burning occurs (this is described in the Fire Behavior results section).

<u>*Fire behavior simulations*</u>

The WFDS (Wildland-urban interface Fire Dynamics Simulator) (Mell et al., 2007, 2009) model suited was used. WFDS builds upon the structure fire model FDS (Fire Dynamics Simulator) from NIST (National Institute of Standards and Technology). WFDS is designed to model three-dimensional, time dependent, buoyancy driven flow. We implement WFDS in the following four ways[1]:

- WFDS-PB, has the highest physical fidelity for fire behavior.
- WFDS with a level set based approach for simulating fire front propagation. In this approach the degradation of the surface vegetation is not explicitly modeled. The different levels of physical fidelity within the level set based approach are:

[1] In the following the short-hand denotation will be used: PB for WFDS-PB, LS1 for WFDS-LS1, LS5 for WFDS-LS5, LS for WFDS-LS.

- WFDS-LS1 (Bova et al. 2015). This has the lowest physical fidelity of all the fire behavior models considered. Wind speed and direction is constant. Bova et al. (2015) showed that with the use of the Rothermel (1972) surface head fire spread rate formula LS1 is consistent with FARSITE (Finney, 2004).
- WFDS-LS5. The interaction of fire generated winds and the surrounding atmosphere is explicitly model, but fire spread responds only to the direction of the local wind, neglecting the influence of the wind magnitude.
- WFDS-LS. This is WFDS-LS5 with the addition that the fire spread depends on the magnitude of the local wind.

PB has been described in detail in Mell et al. (2007), Mell et al. (2009), Perez-Ramirez et al. (2017), and Sánchez-Monroy et al. (2019). An overview of WFDS-PB is given here. PB is a comprehensive physics-based model in which all the recognized coupled physical processes driving wildland fire behavior are explicitly modeled. This includes convective and radiative heat transfer, gas phase combustion, buoyancy induced flow, and the thermal degradation (drying, pyrolysis, char oxidation) of vegetation. The model, which has been developed by the U.S. Forest Service and the National Institute of Standards and Technology (NIST), is an extension of the capabilities of the FDS (Fire Dynamics Simulator beta version 6.0), a structure fire behavior model developed by NIST. Computational fluid dynamics (CFD) methods are used to numerically solve the three-dimensional (or two-dimensional) time-dependent equations governing fluid motion, turbulent combustion, and heat transfer. A large-eddy simulation (LES) approach is used in the numerical model to solve the governing equations for momentum, mass and energy in the gas phase. A multiphase formulation to account for the exchange of mass, energy, and momentum between the gas phase and solid vegetation is used. The vegetation is assumed to be composed of fixed, thermally-thin fuel elements, approximated as point sources of mass, drag, heat release, and radiative absorption and emission. A three-stage thermal degradation model, coupled to the gas phase, is used to obtain the temperature of the vegetation: endothermic drying, endothermic pyrolysis, and exothermic char oxidation. An Arrhenius temperature dependent model provides the mass exchanges, due to drying, pyrolysis and char oxidation. Cylindrical vegetative fuel particles were assumed in order to compute the bulk drag force in the momentum conservation equation due to vegetation. The convective heat transfer coefficient is the maximum of the forced versus free coefficient for a cylinder in a crossflow. A single, 1-step chemical reaction is used to model the combustion of gaseous fuel generated from the pyrolysis of vegetation.

LS uses the same CFD solver and vegetation thermal degradation model for raised vegetation as PB. However, a level set based approach is used for fire in surface vegetation in (Bova et al., 2015). This approach was modified to include the generation of fuel gases along the fire perimeter. Thus, gas-phase combustion and heat transfer are modeled and drive the consumption of raised vegetation. The following are required in LS to model a fire spreading through surface vegetation:

1. Local spread rate of a head fire in the surface vegetation. This can be dependent on the local wind speed or can be a fixed value. The local spread rate, R, at a point on the fire perimeter is based on the local head fire spread rate modified according to orientation of the local wind and the orientation of the normal to the fire line. These two orientations

identify the location of the point in question on the fire perimeter (e.g., head versus flank fire). The direction of R is assumed to be normal to the fire line. The same assumptions in FARSITE (Finney, 2004) are used to determine the local spread rate (i.e., that the fire perimeter evolving from a point does so as an ellipse with a length-to-breadth ratio that depends on an effective wind speed).

2. Flame-base residence time, τ_d. This can be a prescribed by the user or be a function of the surface vegetation's surface-to-volume ratio, σ [1/m], following Anderson (1969), $\tau_d = 75600 / \sigma$ [s].

The level set based WFDS can be run with the local head fire spread rate in the surface vegetation computed from the Rothermel spread formula, a user defined constant value, or a formula derived from WFDS-PB simulations. A disadvantage of the Rothermel formula is that is requires a wind speed that is not influenced by the fire. This is due to its empirical basis (mostly wind tunnel experiments) in which the spread rate is determined as a function of the imposed wind speed. Fires evolving in light winds typical of prescribed burning conditions can be expected to influence the local winds and in turn influence themselves (e.g., fire line acceleration) and other proximate fire lines. Using the Rothermel model, which is tuned to ambient wind speeds, in conditions which have deviated from ambient due to the fire's influence is inconsistent. For this reason, for LS we use a head spread rate derived from WFDS-PB simulations. This spread rate depends on the net local winds (i.e., winds that are influence by the ambient and fire generated winds). The determination of this surface fire head spread rate is discussed below in Appendix 1. For LS5 we used a constant head fire spread rate determined from observations or higher fidelity WFDS simulations.

With the spread rate along the fire perimeter and flame-base residence time known, the depth of the flaming base (in the direction of spread) is $d = R\,\tau_d$ and the mass flux [kg/m^2/s] of fuel vapor is $m_F = (1 - \chi_{char})\, w / \tau_d$ (where χ_{char} is the char mass fraction and w is the dry fuel loading [kg/m^2]). This mass flux is used to inject fuel gas into the atmosphere which mixes with oxygen and combusts according to a subgrid combustion model (Mell et al., 2009).

Smoke plume simulations

ALOFT-FT (A Large Outdoor Fire plume Trajectory – Flat Terrain) was designed by NIST to model plume rise from *in situ* burning of oil spills from sea tankers (McGrattan et al., 1997). ALOFT-FT solves non-dimensionalized equations of conservation of momentum, mass and energy in two-dimensional, crosswind planes at specific downwind positions. Time-dependence is removed by the assumption of a constant mean transport wind speed, allowing for conversion of the along-wind coordinate (x-axis) to a temporal coordinate (McGrattan et al., 1997, p.18). This renders the model suitable for only constant wind speeds over relatively flat terrain (hence 'FT' in the model's name).

Stochastic Lagrangian particles are injected into the simulated velocity field, creating a representation of a three-dimensional smoke plume. Heat release rate, smoke production rate and fire area are prescribed but thermal degradation and combustion are not modeled. Plume concentrations are estimated based on the smoke production rate and spatial distribution of the Lagrangian particles.

The equations of conservation in ALOFT-FT are non-dimensionalized based on a length scale derived from HRR, wind speed and the Brunt-Väisälä frequency (which characterizes atmospheric stability). The implementation of ALOFT-FT is unusual in that the non-dimensionalized equations are employed in the source code (Fortran 77). However, this allows the code to execute quickly, performing simulations of plumes in large domains [O(10 km)] in less than 30 s on a mid-range laptop computer. Analysis of the results is somewhat complicated by the fact that domain height and crosswind dimension, but not the number of grid cells, are dynamically scaled during simulations if the plume approaches the top of the domain. This process may go through several iterations, effectively changing the resolution.

The original ALOFT-FT model simulates plumes from only elliptical sources and, although it will simulate multiple plumes, does not separately track each plume. We modified the source code (Fortran 77) so the model will track separate plume particles (to investigate plume interactions) and simulate linear heat sources. Unlike FDS and MW94, in ALOFT-FT the plume is injected in a vertical plane (i.e., not in a horizontal plane from an upwelling source) about three fire diameters or line widths downwind of the source at a height of about two fire diameters. In other words, the model assumes that the plume has already been bent somewhat before injection.

FDS (v. 6.7.5) was also used for smoke plume simulations to provide a means of evaluating ALOFT-FT against a model with higher physical fidelity. Both FDS and WFDS are publicly available. FDS has a more up to date code base and the capabilities of WFDS for fire in vegetation (both WFDS-PB and WFDS-LS) are being incorporated into FDS. It is expected that WFDS will be phased out and replaced by FDS within 1 to 2 years (see FDS (2021) and WFDS (2021) for source code, executables, and example input files).

To provide a greater range of physics capabilities for comparison in the smoke models, a simple plume model based on the work of Mercer and Weber (1994 & 2001) was implemented in Python 3.8. The model, herein referred to as "MW94," simulates a two-dimensional vertical cross section of a plume from a line fire. As in ALOFT-FT, heat release is prescribed but combustion is not explicitly modeled. Equations of mass, momentum and thermal energy conservation along the plume centerline (i.e., the plume is simulated with a top hat profile) are solved using the 'solve_ivp' function available in the open source SciPy package (v. 1.6.0). Smoke concentrations must be modeled separately, e.g., by a Gaussian distribution, and were not included in this study. Vertical wind and temperature profiles are prescribed, but simulated plumes are not coupled with wind nor will they interact with each other. To avoid the use of arbitrary parameters, the MW94 model was modified to incorporate adiabatic cooling, initial plume velocity and temperature based on fire line intensity (Appendix 3, p. 51).

Results and Discussion

In the sections on fire behavior results that follow, we first use two experiments of relevance for model validation. The PB, LS, and LS5 models are evaluated. The first experiment considered is a laboratory experiment designed to identify the wind speed and shrub crown base height thresholds above which a sustained shrub crown fire does not occur. The second experiment considered is a stand-scale grassland fire for which the footprint of entire fire front (e.g., heading and flanking fire fronts) was measured at four time points. PB and level set predictions of these experimental fires were found to agree sufficiently well with the observations to justify applying them to a prescribed burn scenario with grass surface vegetation in a forested area with under- and over-story vegetation (this is the subject of the last section on the results of model comparison focused on fire behavior).

Results from simulations of smoke plumes are discussed after the fire behavior sections. The first section describes a comparison of the performance of FDS, ALOFT-FT and MW94 in simulating plumes from line fires. Although FDS provides the greatest physical fidelity, it requires orders of magnitude more time for simulations than the other models. This section is followed by comparison of FDS and ALOFT-FT in simulating plumes from multiple line fires. Both models provide similar results for the same scenario. Sensitivity to the spacing of line fires is examined using ALOFT-FT. These simulations hint that spacing between fire lines may have a significant effect on plume height. Finally, an evaluation of FDS and ALOFT is performed by comparing plumes from both models to those generated in the Meteotron plume experiments conducted in the 1970s. Results from these simulations were mixed and demonstrate that conclusive evaluation is difficult without detailed plume information such as concentrations and complete plume profiles. Sensitivity studies, additional information and model results not shown in the main report section are available in the appendices.

Fire Behavior – Model Validation and Comparison using Laboratory Shrub-Crown Ignition Experiments

The experiments of Tachajapong et al. (2009) are used to evaluate both the PB and LS5 models. In these experiments a surface fire in an excelsior fuel bed (1.8 m long, 0.8 m wide, 0.1 m deep) spread towards a volume of chamise held above and spanning the 0.8 m wide surface fuel bed. The chamise volume had a 30 cm x 30 cm cross-section. The surface fire was ignited 1 m from the chamise. Wind conditions were no-wind and two different wind speeds (1.5 m/s and 1.8 m/s) imposed by a fan. For the no-wind condition, crown base height (the vertical distance from the top of the excelsior to the bottom of the chamise) were 20 cm, 30 cm, 40 cm. For the 1.5 m/s and 1.8 m/s wind speed cases the crown base height was 20 cm. The chamise was harvested shortly before the experiment in order to limit drying and simulate live fuel conditions.

The vegetation characteristics follow. The shrub crowns had a moisture of 84% (dry mass basis) and were composed of 0.259 kg of foliage (σ = 8000 1/m) and 0.23 kg of roundwood (σ = 1143 1/m). The excelsior moisture was 7%, had a loading of 0.313 kg/m^2, a fuel bed height of 10 cm, and σ = 4000 1/m. Both the excelsior and shrub crown vegetation were modeled using the fuel element approach in WFDS-PB (Mell et al., 2009) and Arrhenius kinetics (Perez-Ramirez et al., 2017).

Figure 2 shows images from the PB (on left) and LS5 (on right) simulations of the Tachajapong et al. (2009) experiment with a 1.5 m/s (3.3 mph) imposed wind (flowing from left to right) and a crown base height of 20 cm (8 inches). For this case there was sustained crown burning in both the experiments and the WFDS simulations. As stated previously, WFDS-PB explicitly models the presence of both the surface vegetation (excelsior) and raised vegetation (chamise) on the gas phase computational grid (as shown by their presence in the figure) and the physical processes involved in the vegetations' thermal degradation (drying, pyrolysis, and char oxidation). WFDS-LS5 does not explicitly model the surface vegetation and uses the experimentally observed spread rate. However, LS5 does explicitly model the raised vegetation.

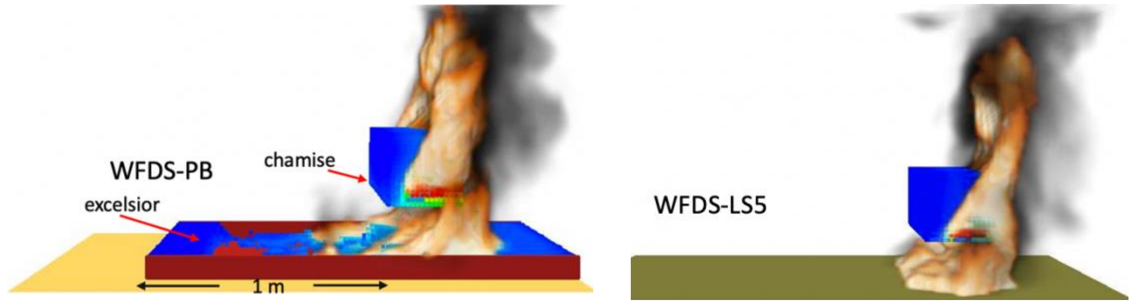

Figure 2: Snapshot of (55 s after ignition of excelsior fire) of WFDS-PB (on left) and WFDS-LS5 (on right) simulations of the Tachajapong et al. (2009) shrub crown fire initiation experimental case with a 1.5 m/s (3.3 mph) impose wind (flowing left to right) and a crown base height of 20 cm (8 inches). The flame surface is shown in orange, smoke in black, and vegetation temperature by colors with blue being the coolest (~ 20 C) and red the hottest (~1300 C). WFDS-LS5 does not explicitly model the presence of the surface vegetation.

The observed versus PB predicted rate of spread (cm /s) in the excelsior fuel were 1.9 ± 0.1 versus 2.0 for no wind; 3.3 ± 0.1 versus 3.7 for a 1.5 m/s wind; and 3.8 ± 0.2 versus 3.8 for a 1.8 m/s wind. In LS5, the observed rate of spread and flame residence time (τ_d = 7.9 s, 13.6 s, 15.8 s, for a 0 m/s, 1.5 m/s, 1.8 m/s wind, respectively) was used. Threshold values of the shrub-crown base height and imposed wind speed from the experiments and the PB and LS5 simulations are shown in Table 1. There is ambiguity regarding the identification of the outcome, whether experimental or simulated, of no sustained crown burning. The methodology for this is not reported in Tachajapong et al. (2009). In the WFDS simulations, an outcome was identified as no sustained crown burning when less that 20% of the foliage was consumed.

Table 1: Value of shrub crown base height and imposed wind speed at which no sustained crown burning occurred (i.e., shrub-crown ignition thresholds). Both the observed (from experiments) and predicted (from WFDS-PB and WFDS-LS5) values are shown.

Crown base height threshold No imposed wind			Wind speed threshold (crown base height = 20 cm = 8 inches		
Observed cm, inches	WFDS-PB	WFDS-LS5	Observed m/s, mph	WFDS-PB	WFDS-LS5
40, 16	60, 24	60, 24	1.8, 4	1.8, 4	1.8, 4

The results in Table 1 show that PB and LS5 predict the same crown base height and wind speed thresholds. Compared to the experiments, WFDS overpredicts the no-wind crown base threshold by 50% or 20 cm (8 inches). However, WFDS predictions of the wind threshold (with a fixed crown base height of 20 cm) agree with observed experimental value of 1.8 m/s (4 mph). Since the presence of wind is more realistic of prescribed fires these results provide some confidence that both PB and LS5 can predict the ignition of understory vegetation.

Fire Behavior – Model Validation and Comparison using a Stand-Scale Grassfire Experiment

Following the model validation study in Mell et al. (2009), we apply the current version of PB and LS to an Australian grassland experiment. The experiment in question is denoted C064. The grass properties were (Mell et al. 2009): 20 cm tall, moisture content of 6.3% (on a dry mass basis), surface-to-volume ratio of 9770 1/m, dry loading of 0.283 kg/m^2, dry bulk density of 1.35 kg/m^3, and a packing ratio of 0.0026. In the C064 field experiment, an initial 50 m long fire was created along the upwind border of the burn plot. Fire breaks upwind prevented backfire spread, but a head fire and extended flank fires formed and spread on a 104 m (windward direction) x 108 m burn plot. Photos were taken from a helicopter and georectified to provide the fire footprint at four different times. These fire footprints were compared to predictions from the PB and LS models in order to evaluate how well WFDS predicted the spread rate and the depth of the fire front along fire perimeter.

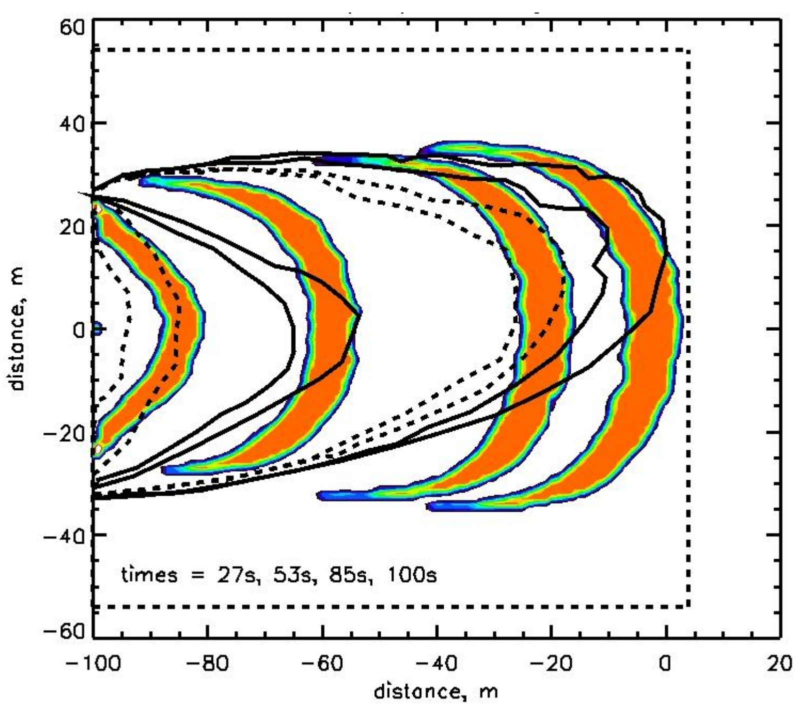

Figure 3: Observed (dashed or solid lines) and WFDS-PB predicted (color contours of mass loss rate, kg/s) footprints of the fire base at four times after the start of the ignition procedure in the AU grassland experiment C064 (Mell et al., 2009).

Results from PB simulations of the C064 experiment are shown in Figure 3. The observed edges (leading and trailing) of the fire footprint are denoted by dashed and solid lines. The PB predictions are shown by color contours of the mass loss rate. There was shift in wind direction during the experiment that resulted in the head fire not spreading directly downwind. Since only the magnitude of the wind was measured, we could not account for this shift in the simulations. This and other unmeasured atmospheric conditions may have contributed to the difference in fire perimeter shape. WFDS-PB did well-predict both the rate of spread and the depth of the head fire.

The PB computational grid was too coarse (1 m x 1 m x 1 m) to *explicitly* resolve the physical processes driving flank fire evolution. For this reason, the extended flank fires are not present in the PB results in Figure 3. This is a limitation of high-fidelity physics-based model such as PB for component processes that are explicitly modeled. We could run PB with finer meshes but at a higher (potentially insurmountable for larger domains) computational cost (e.g., number of cpus, amount of memory, and computational time). The LS model does not explicitly resolve the processes driving the thermal degradation of the surface vegetation and, therefore, can be run at coarser computational grids while retaining (at an approximation) the sub grid flank fires.

Fire footprint perimeters from LS simulations of the AU grassland experiment C064 are shown in Figure 4. Note, that unlike the LS5 mode considered above which assumed a constant head fire spread rate, the LS model uses a formula for the head fire spread rate as a function of the local wind speed. The determination of this formula is described in Appendix 1. It can be seen on the left side of Figure 4, that the flank fires do survive in LS simulations. The head fire depth is well-predicted by LS and the overall fire behavior (e.g., spread rate and head-fire depth) is very similar to the PB simulations. The "wiggles" along the head fire perimeter, especially at later times, are due to the local spread rate being dependent solely on the local wind behavior.

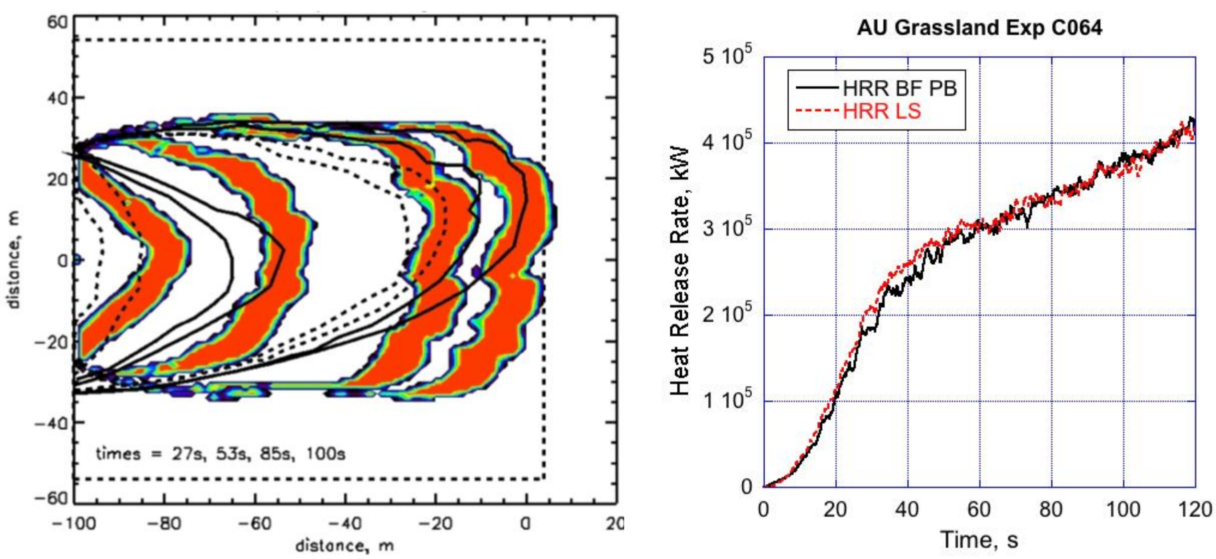

Figure 4: On the left are the fire footprints for the same case shown in Figure 3 for WFDS-PB, but here WFDS-LS predictions are shown by color contours of the heat release rate per unit area, kW/m^2. On the right is the time history of the HRR from WFDS-PB (black curve) and WFDS-LS (red dashed curve).

It is important to note that smoke plume rise for the C064 grassland fire simulations is driven by the overall heat release rate (HRR, kW) of the fire. The HRR is equal to the sum, along fire perimeter, of the local heat release rate per unit area (HRRPUA, kW/m^2) multiplied by the local area of the fire front. For many fires, the largest contribution to the HRR will be from the head fire because it contains most of the fire footprint area. This is confirmed by the HRR time history plots in Figure 4 (right side). The HRR from PB and LS agree closely with each other even though the flank fires are retained only in LS. The increase of the HRR up to about 30 s is due to the increasing size of the fire due to the ongoing ignition. After ignition is complete, the HRR continues to increase, largely due to the increase size of the head fire in the crosswind direction.

Fire Behavior – Model Comparison for a Prescribed Burn Scenario

While a more thorough investigation is needed, the model evaluation results of the last two sections provide some justification for the use of level set modeling approach in prescribed burn scenarios. For example, level set approaches shows promise for more computationally efficient (compared to PB) modeling of understory ignition, fire spread with extended fire lines in surface vegetation, and plume rise as controlled by the HRR of the fire. The computational cost of the different models will be discussed more fully below and is listed in Table 2.

In this section we apply PB and the level set models to a prescribed fire scenario that includes raised vegetation. The surface vegetation is grass. Both the understory and overstory vegetation characteristics are representative of southeastern US longleaf pine stands. The characteristics of the grass and the method used to determine the characteristics of the raised vegetation are described in Appendix 2.

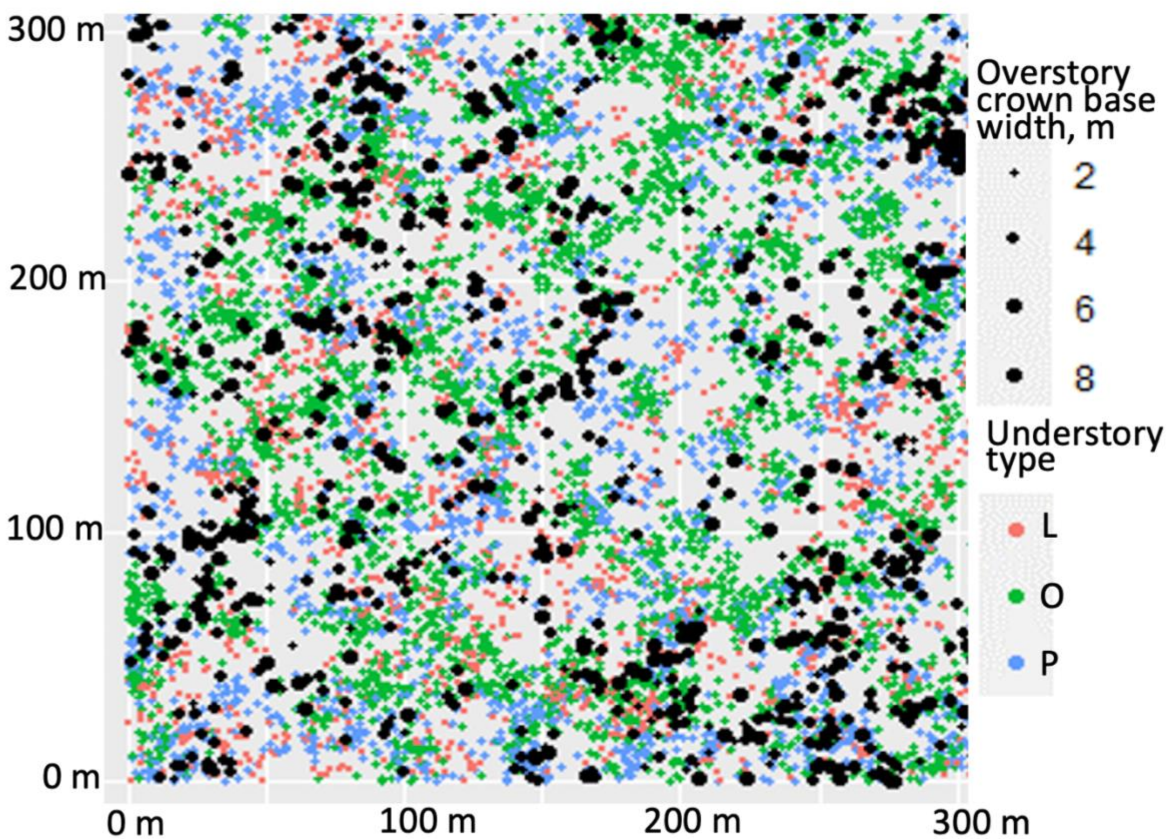

Figure 5: Distribution of raised vegetation used in the WFDS simulations. Black objects show location of longleaf pine and turkey oak overstory with the size of the object giving a measure of the crown base width (see legend). Colored objects denote the type of understory as shown in legend with L = longleaf pine, O = turkey oak, and P = persimmon.

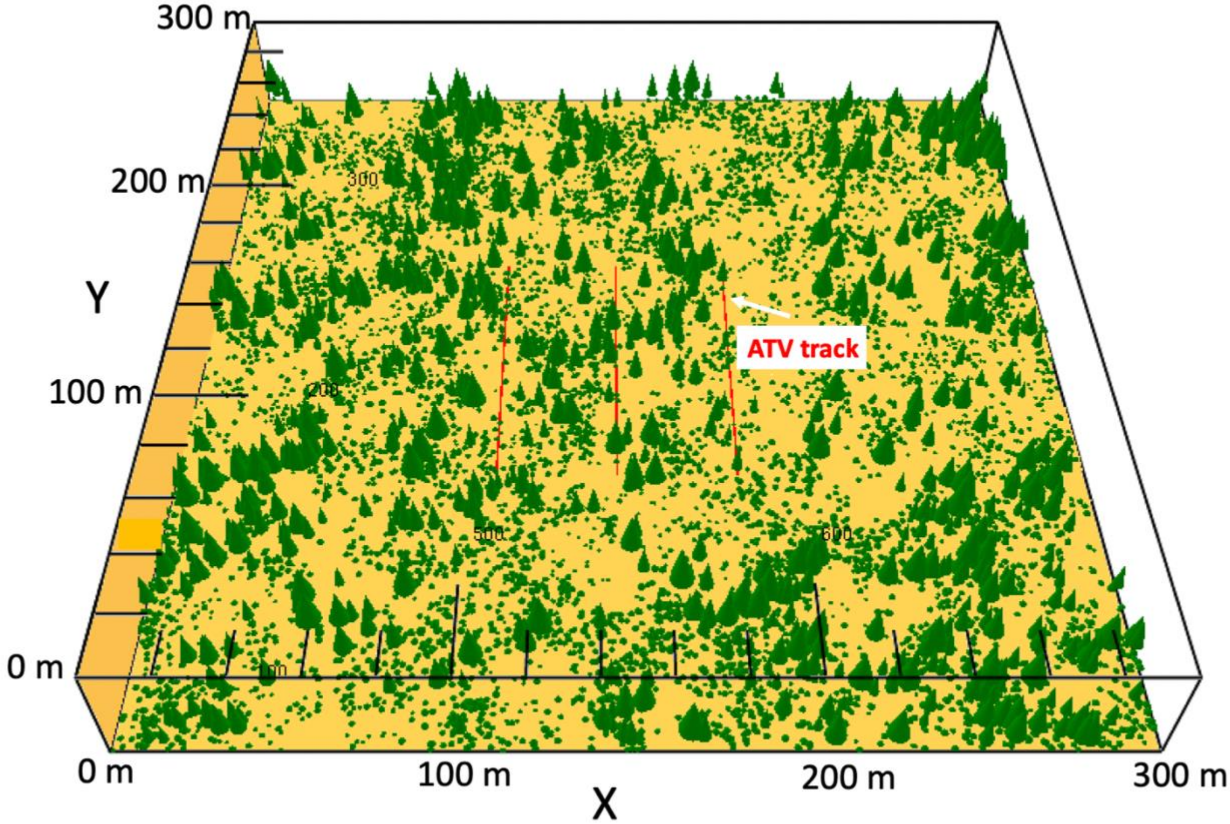

Figure 6: The 300 m x 300 m x 40 m computational domain used for comparing WFDS-PB and level set based predictions of a prescribed burn scenario. The vegetation is the same as was shown in Figure 5. The visualization tool Smokeview (designed for FDS and WFDS) is used. The locations of three simulated ATV ignition lines are shown in red.

Figure 5 and Figure 6 show the 9 ha (22 acre) scenario used for comparing, in a scenario similar to a prescribed burn, predictions from PB simulations with high spatial resolution to level set based simulations with a significantly coarser spatial resolution. In Figure 5 the locations of overstory trees (longleaf pine and turkey oak) are show as black objects whose size provides a measure of the crown width. Colors are used to locate the three types of understory: longleaf pine, turkey oak, and persimmon. In Figure 6 the software Smokeview, developed by NIST for FDS and WFDS, is used to show the overstory and understory vegetation as incorporated into WFDS.

The ignition lines were placed in the grass surface vegetation by simulating three ATVs spaced 40 m apart and traveling along the red lines in the positive Y direction in Figure 6. The ATVs all start at the same time (this can be easily changed) and travel at 1.5 m/s (3.5 mph) from Y=100 m to Y=200 m (328 feet). The ambient wind flows in the positive X direction with a speed of 2 m/s (4.5 mph) at an above ground height of 2 m (6.4 feet).

In the PB simulations, the highest spatial resolution was over the center 100 m x 100 m area which includes most of the burned area: vertical resolution of 5 cm (at ground level) and stretched to 20 cm (at 5 m above ground); horizontal resolution was 25 cm. Above and around this volume of higher resolution the resolution was coarser. Two different LS simulations were run: one with a resolution of 1 m throughout and another with a resolution of 2 m throughout the computational domain.

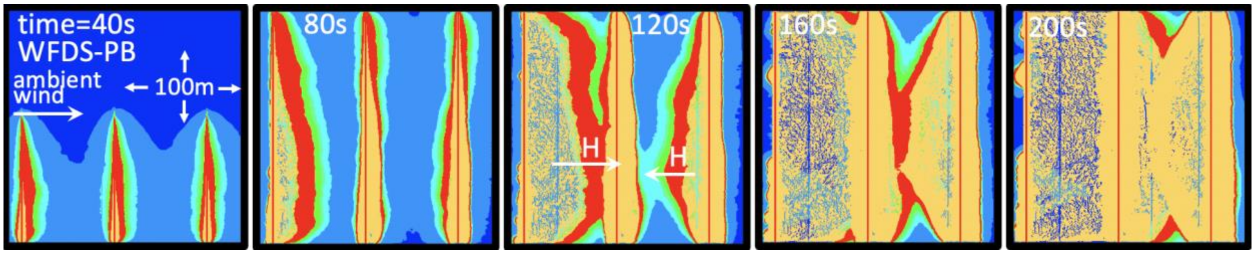

Figure 7: Color contours of the grass temperature at five times from the PB simulation of the prescribed burn scenario shown in Figure 6. Red denotes the location of the flaming base of the fire. The straight red lines are the simulated ATV tracks.

The time progression of the surface fires from the PB simulation is displayed in Figure 7. Only the 100 m x 100 m area that encompasses the ATV ignition lines is shown. The flaming base of the fire is colored red and times refer to the time since the start of ignition. Different fire behaviors (e.g., head versus back fire) are clearly seen.

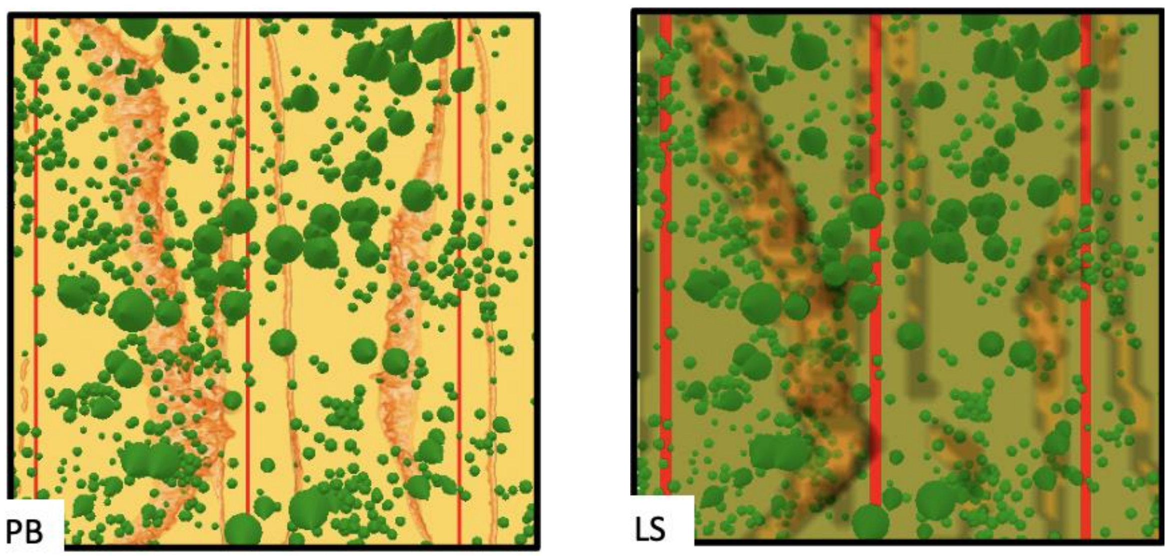

Figure 8: Comparison of simulated fire lines from WFDS-PB and WFDS-LS (2 m grid resolution) 84 s after start of ignition.

A comparison of fire behavior predictions from PB versus LS (2 m grid resolution) for the prescribed burn scenario described above is shown in Figure 8, which is a snapshot of the fire lines 84 s after the start of ignition. As in Figure 7, the 100 m x 100 m portion of the entire computational domain that includes the three simulated ATV ignition lines is shown. The relatively large head fire between the two left ignition lines is seen in both simulations. The leading portion of the head fire between the two left ignition lines spreads about 10% faster in the LS simulations. This head fire both blocks the ambient wind and generates its own wind which causes the fire spreading to the right (i.e., in the ambient wind direction) from the middle ignition line to spread as a backfire. This occurs in both the PB and LS simulations. Based on the direction of the ambient wind, the fire spreading to the left from the rightmost ignition line would be a backing fire. However, in both the PB and LS simulations this fire spreads as a head fire due to the strong entrainment of the upwind (relative to the ambient wind direction) fires – this is most easily seen in the PB results. Overall, LS predictions of fire behavior and fire location agree well with PB predictions.

An important question to ask in the context of this project is: What do we gain by using a CFD-based fire behavior model versus a model such as FARSITE (Finney, 2004; Bova et al., 2015) which is not CFD-based and runs much more quickly? The WFDS level set based model is capable of running without the use of CFD and can be implemented to produce fire lines that well-match those from FARSITE (Bova et al., 2015). As stated in the in the previous section, the level set based WFDS option that is consistent with FARSITE is denoted by LS1. Here, we implement the LS1 model using the direction of the ambient wind (left to right) and the value of the head fire spread rate (0.5 m/s, based on the LS simulations).

In Figure 9, predictions of the time of arrival (TOA) of the leading fire front from LS (on the right) and LS1 (on the left) are shown. The two models predict different TOA curves because of how they handle the interaction of the fire generated buoyant flow and the surrounding atmosphere. LS explicitly models the fire-atmosphere interaction. LS1, like FARSITE, does not model the fire-atmosphere interaction: the wind is constant in magnitude and direction throughout the domain. Relatively good agreement exists between the two approaches for the fire spreading between the left two ignition lines. This is because the fire in that area spreads as a head fire and the LS1 model was given a head fire spread rate based on the LS head fire spread rate in this region. In all other locations, however, the LS1 predictions are unrealistic because there was no accounting for the influence of the fire generated wind. The computational cost of these simulations is provided in Table 2 below in the fire behavior discussion section.

In particular, the fire progression between the right two ignition lines in the LS simulations (and in the PB simulations, see Figure 8) is a combination of backing and flanking fires spreading to the right and a head fire spreading to the left. These fires are labeled in Figure 9 (LS). The LS1 fire behavior is markedly different, spreading as predominantly as a head fire to the right throughout the plot. This is due to the neglection of fire generated wind in LS1. For example, in the LS simulations, the large head fire spreading between the two left ignition lines generates a right-to-left flow between the two right ignition lines.

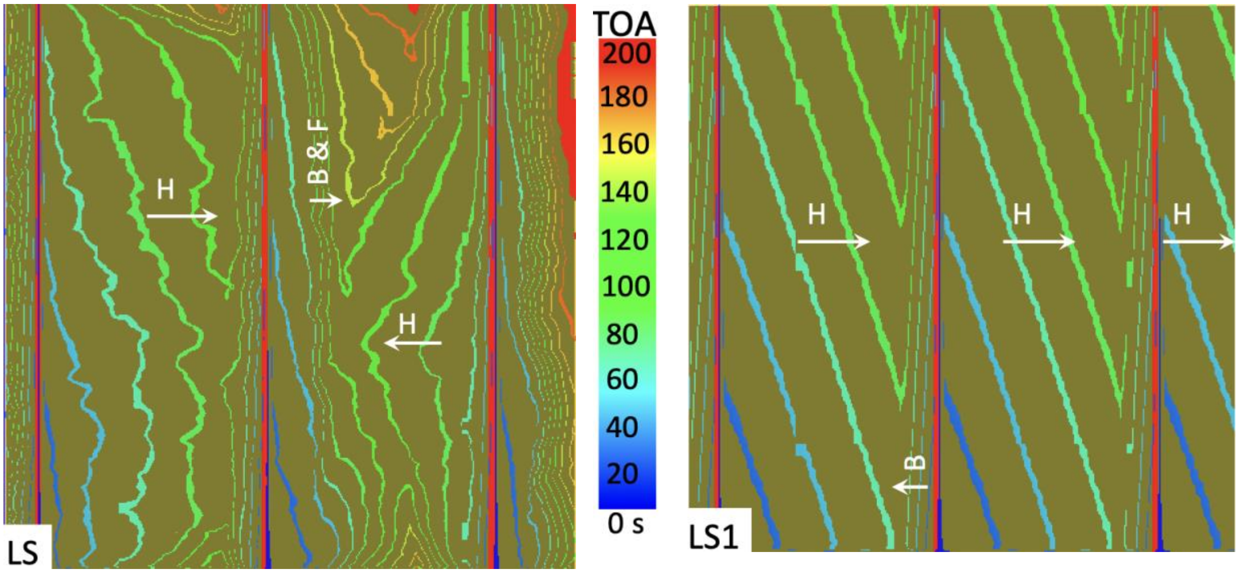

Figure 9: Surface fire time of arrival (TOA) contours in the center 100 m x 100 m area from simulations of the prescribed burn scenario shown in Figure 6 and Figure 8. The raised vegetation is not shown. The ambient wind flows left-to-right. The location of the leading edge of the fire front is plotted every 20 s (see legend). On the left are WFDS-LS predictions; on the right are predictions from the simplest level set implementation, WFDS-LS1, (consistent with FARSITE), both with a 1 m grid resolution. Some locations of head, back, and flank fire spread are identified by H, B, F, *respectively. Arrows show direction of fire spread.*

The differences in fire behavior between LS and LS1 clearly show a need for CFD-based simulations if predictions of the influence of the fire-atmosphere interaction and its effects are desired. For prescribed burn planning and firing pattern design, this prediction capability is needed in order to properly account for the interaction of backing, flanking, and heading fires. Note, that we have only conducted model comparisons here. More work is needed to determine how well PB or level set based models predict the formation and evolution of head, flank, and back fires resulting from various firing patterns, vegetation complexes, and atmosphere conditions.

Another, implementation of the level set based approach with a level of physical fidelity between LS1 and LS, is to account for the fire generated wind but simplify the spread rate calculation along the fire line by assuming a constant head fire spread rate. The local fire front spread rate is allowed to depend on the orientation of the fire line relative to the local wind direction (i.e., there is no dependence on the magnitude of the local wind). This implementation LS5 and avoids the need to develop a head fire spread rate formula that is a function of the local wind speed (such as is described in Appendix 1). This method also has the advantage of not having to develop a head fire rate of spread formula that accounts for the influence of different grid resolutions on the local wind.

The TOA and HRR for LS5 simulations of the prescribed burn scenario are shown in Figure 10. The TOA contour intervals (20 s) are the same as in LS and LS1 plots of Figure 9. As with the LS1 simulations, the head fire spread rate is assumed to be 0.5 m/s (based on LS results). While the LS5 fire spreads across the burn plot more quickly than LS, the influence of the fire generated winds is consistent with the more complete LS model and clearly more realistic than the LS1 predictions.

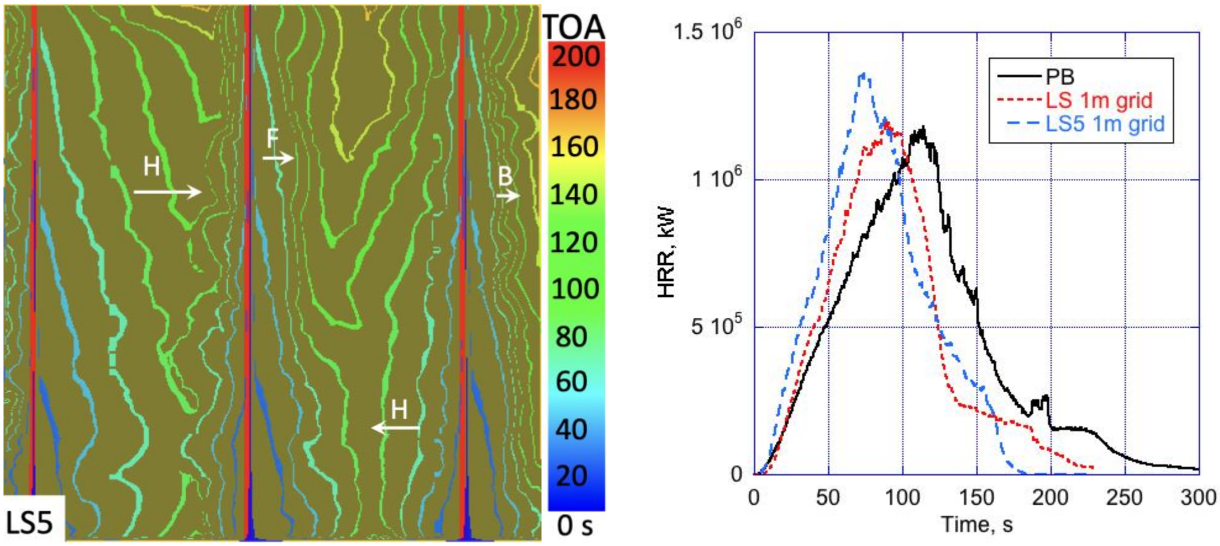

Figure 10: Time of arrival contours (on left) for the case in Figure 9 but using the level set implementation that is intermediate in physical fidelity, WFDS-LS5 (1m grid). Some locations of head, back, and flank fire spread are identified by H, B, F, *respectively. Arrows show direction of fire spread. On right is the HRR from the WFDS-LS5 (1m and 2m grid) and WFDS-PB simulations.*

The global heat release rate (HRR) from LS5 is plotted on the right in Figure 10 along with the HRR from the LS and PB models. As will be discussed more fully below, the HRR drives smoke plume rise.

A comparison of understory consumption predictions from PB and LS (1 m grid resolution) is shown in Figure 11 for the same area in Figure 8. The understory vegetation types are colored according to the degree of consumption: black is fully consumed, green is unconsumed (although some drying may have occurred). Overall, the locations of predicted consumption agree between the PB and LS models. It is important to note that these LS simulations required a finer grid resolution (1 m) compared to the 2 m grid LS simulations in Figure 8 for fire behavior comparisons. This is because in the LS simulations with a 2 m grid resolution too much of the understory was unresolved (not shown).

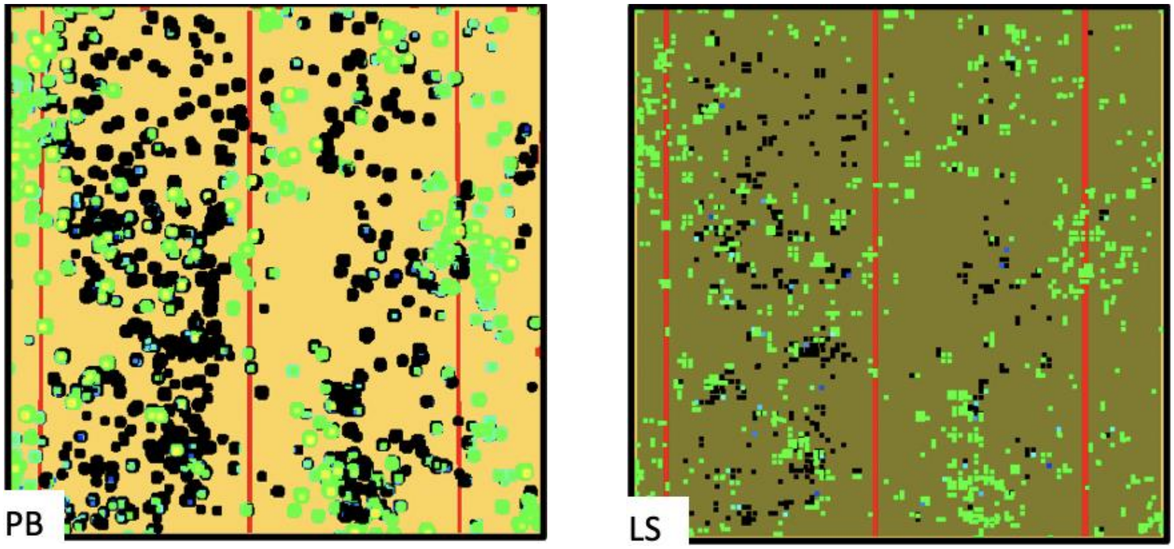

Figure 11: Comparison of the location of understory consumption from WFDS-PB and WFDS-LS (1 m grid resolution). Black denotes complete consumption; green denotes no consumption. The overstory is not shown.

The time histories of the global heat release (HRR) from the PB and the two LS simulations (1 m and 2 m grid resolution) are plotted in Figure 12. The PB and LS (1 m grid) cases have the same peak HRR. Because the LS head fire spreads about 10% faster than the PB (this can be seen in Figure 8) the LS HRR peaks sooner than the PB HRR. The peak HRR for the less resolved LS case (2 m grid) is about 20% smaller than the PB and more resolved LS case. Of particular interest is the well-behaved, smooth, character of the HRR rise and decay through the course of fire lines evolving in size and merging.

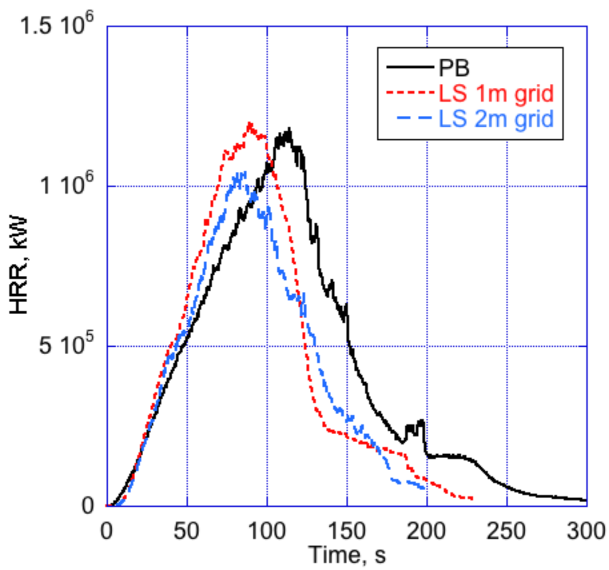

Figure 12: HRR history from the WFDS-PB and WFDS-LS prescribed burn scenario simulations.

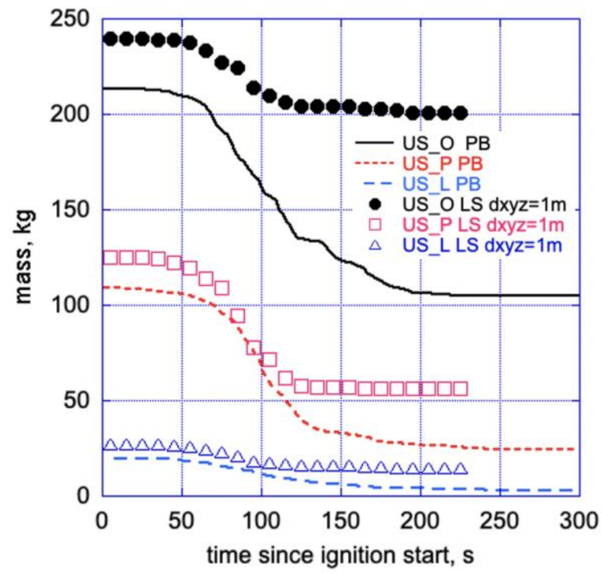

Figure 13: Time history of the dry mass in the understory components.

Figure 13 shows the time history of the total dry mass in each understory vegetation component from the LS simulation with 1 m grid resolution (symbols) and the PB simulation (lines). For comparison, the dry mass of the grass surface vegetation over the same 100 m x 100 m area is 7866 kg, which is about 20 times the total dry mass of the understory. The initial dry mass is larger in the LS case due to how the vegetation is resolved in the coarser resolution LS mesh. The method used assumed that if at least half the horizontal area of the cell had vegetation, then the whole cell had vegetation. This resulted in the LS having more mass than the PB case. There was less mass consumption in the LS case because the hot plume and resulting heat flux was less resolved. The method used to account for under resolved vegetation would be a focus area in a follow-on project.

In the prescribed burn scenario simulated here, the large majority of the HRR is from the burning of grass surface vegetation. This is shown in Figure 14 which has results from PB simulations for the case in which the understory and overstory are allowed to burn (i.e., the case considered above and shown as solid black curve) versus not allowed to burn (red short-dash curve). The difference between these two curves represents the contribution to the HRR from the burning (i.e., consumption) of the understory and overstory. Also plotted in Figure 14 (blue long-dash curve) is the HRR for a PB simulation with only the grass surface fuel (no understory or overstory vegetation is present). In this case, the peak HRR is larger because the fires spread more quickly (resulting in a larger flame base area) without the raised vegetation obstructing the wind (both the ambient and fire generated winds).

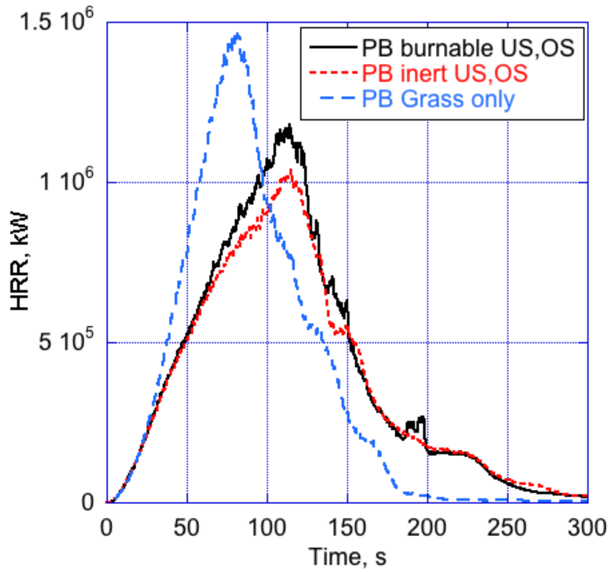

Figure 14: HRR history from WFDS-PB prescribed burn simulations with raised vegetation that can burn (black solid curve), raised vegetation that cannot burn (red short-dash), and no raised vegetation (only grass is present, blue long-dash).

WFDS-LS simulations with the two grid resolutions (1 m and 2 m) used previously were also applied to the three PB scenarios just considered. These are shown in Figure 15. Overall, the LS results are very similar to the PB results. The HRR reaches a larger peak value when only the grass surface vegetation is present. The cases with burnable and inert raised vegetation are more similar to each other in the LS simulations. This is most likely caused by the relatively under resolved heat fluxes in the LS simulations and reduced consumption of raised vegetation.

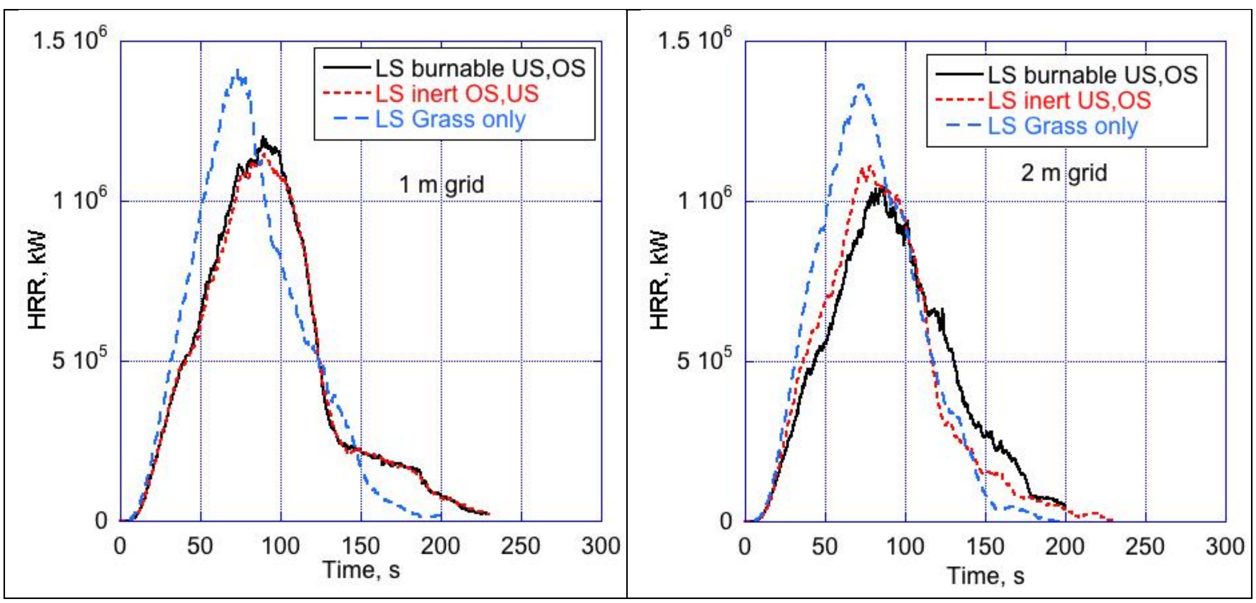

Figure 15: HRR from WFDS-LS prescribed burn simulations with raised vegetation that can burn (black solid curve), raised vegetation that cannot burn (red short-dash), and no raised vegetation (only grass is present, blue long-dash).

Influence of Fire Behavior on Smoke Plume Development

Comparison of the PB and level set based (LS and LS5) simulation results in the previous section established that they produce similar fire behavior characteristics that are relevant to smoke plume development (e.g., the location, size, and interaction of fire lines; and the global HRR time history). This suggests that we can use LS, and potentially LS5, to simulate smoke plume development on larger domains that are relevant to prescribed burn practices, but would be very computationally demanding when simulated with PB (a discussion on the computational costs of PB and level set approaches is given in the next section). For this reason, we now turn to a simulation scenario focused more on smoke plume development than fire behavior.

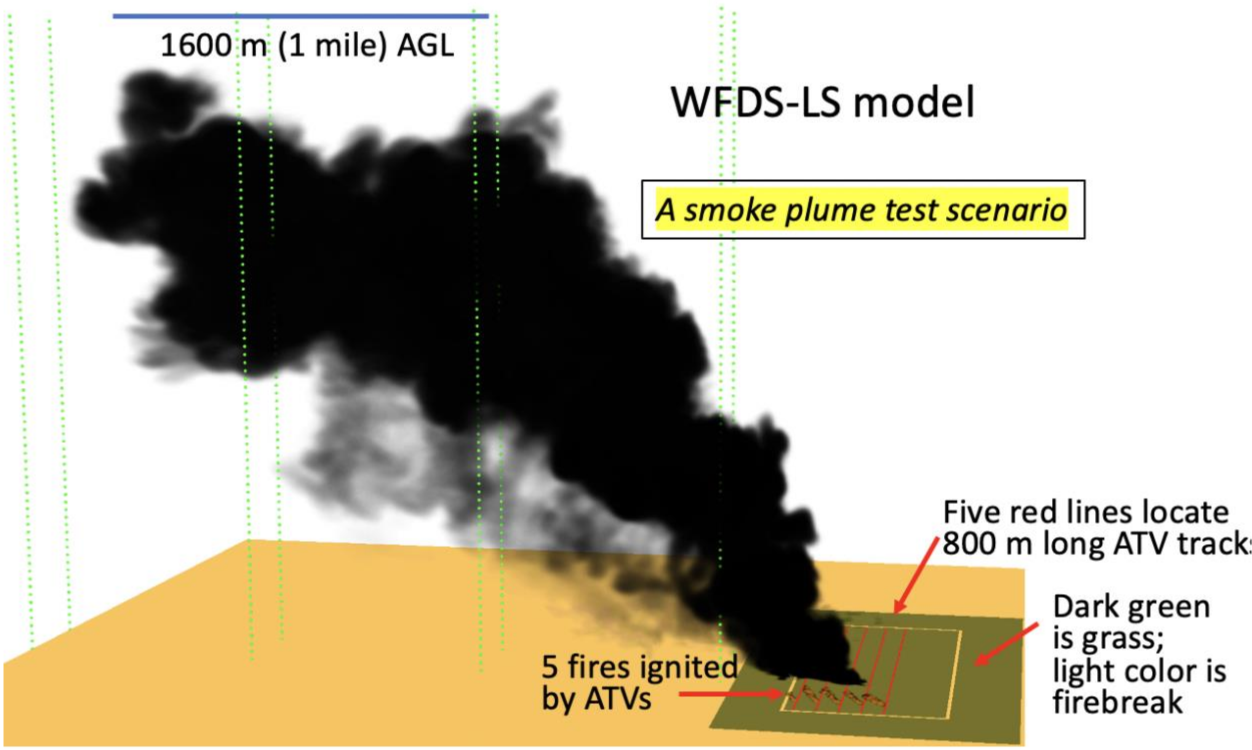

Figure 16: A smoke plume test scenario using WFDS-LS. The green dotted vertical lines are locations where the smoke concentration is output.

The image in Figure 16 shows a snapshot from a LS smoke plume test scenario simulation. The overall computational domain size is 3200 m (2 miles) long (windward direction), 2400 m (1.5 miles) wide, 1600 m (1 mile) tall. Only grass surface vegetation is considered and is the dark green area (32 ha, 80 acres). Note that in the previous section it was shown that the HRR, which drives plume rise, was dominated by the fire in the surface vegetation. For this reason, not including the raised vegetation in these smoke plume simulations is unlikely to have significant influence on the conclusions of this scoping study. Five ATVs, traveling 1.56 m/s (3.5 mph) ignite strip head fires along 800 m (0.5 mile) tracks shown as red lines. The ambient wind, U, flows right to left at 2 m/s (4.5 mph). The vertical wind profile follows $U(z) = 2\ (z / 2)^{1/7}$ in m/s where z is the height above ground in meters. The lapse rate of the atmosphere is LR = -6 C/km.

The HRR time history from LS simulations of the Figure 16 scenario is shown on the left in Figure 17. Two different grid resolutions are used: 1 m and 8 m. In both cases, the HRR has a quasi-steady value for most of the burn history due to the fires spreading with a quasi-steady spread rate and footprint size. The 8 m grid HRR is about 5% less than the 1 m grid case, during quasi-steady burning. This quasi-steady behavior of the global HRR suggest we can simplify the model for the fire generated heat release rate per unit area (HRRPUA). For example, we can use the five quasi-steady spreading fires seen in Figure 16 to define the location, footprint area, and HRRPUA of five static burners. The ramp up and ramp down of the HRR generated by the five static burners can be made the same as the HRR for 1 m grid case in Figure 17. This was done for an 8 m grid and the smoke profiles for the 1 m grid case (with spreading fires) and the 8 m grid case (with five static fires) are plotted in Figure 17 (on the right). There is good agreement between the simpler, and computationally cheaper, 8 m grid case and the 1 m grid.

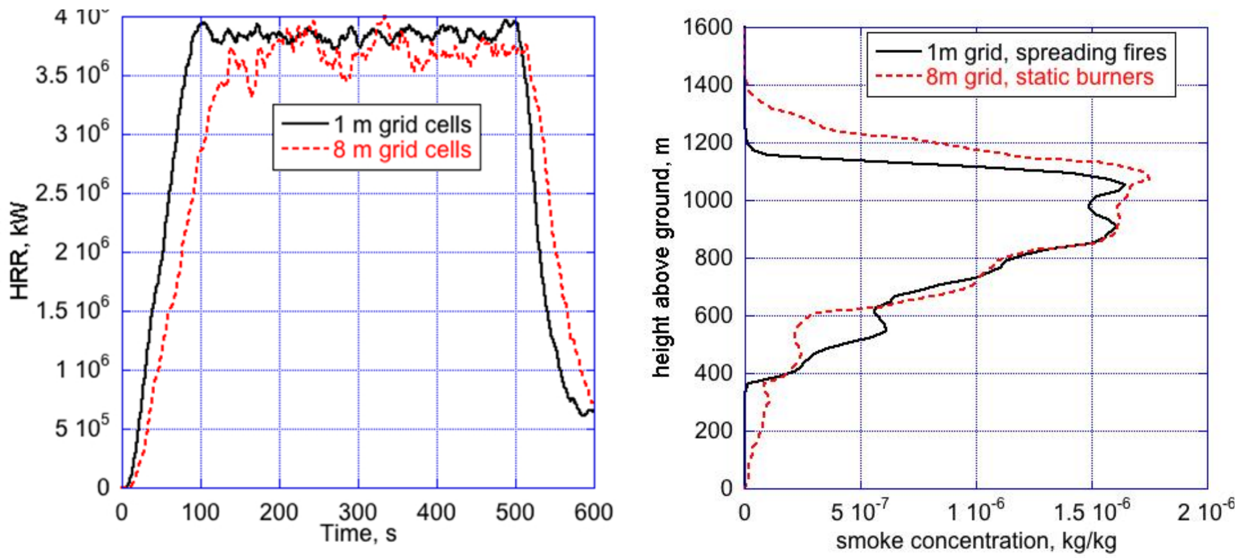

Figure 17: On the left are HRR time histories from WFDS-LS simulations of the smoke plume scenario shown in Figure 16 using two grid resolutions, 1 m and 8 m. On the right are 30 second time averaged smoke concentration profiles 2 km downwind of the middle of the burn plot shown in Figure 16 (see text for details).

The good agreement of smoke plume profiles in Figure 17 between the more highly resolved LS simulation with spreading fires and the coarser grid WFDS simulation with static burners suggests that we can investigate the performance of different smoke plume models with a simplified representation of the fire (i.e., using static burners) without loss of applicability to prescribed burns. This is the approach we take in the Smoke Plume simulation section that follows. More work is needed to investigate the generality of this assumption.

Fire Behavior – Summary and Discussion

The results in the previous sections on fire behavior established a degree of confidence in the capability of both the PB and LS models. The PB and LS5 models reproduced experimentally observed fire behavior characteristics relevant to the ignition of shrubs and the PB and LS model predictions agreed with observations of surface fires in grass. We next moved up in scale to consider a scenario more representative of a prescribed burn in order to compare results from the PB and LS models.

In the prescribed burn scenario, the simplest level set based approach, LS1, produced unrealistic results due to its lack of accounting for fire generated winds and highlighted the need for CFD-based simulations. The LS and LS5 predictions of fire behavior agree qualitatively with PB simulations. LS predictions of understory consumption, with a 1 m grid resolution, qualitatively matched the PB locations of consumption. Quantitatively, LS under predicted the amount of understory mass consumed, compared to PB. While the LS results are promising, more investigation is needed to fully assess the capability of LS as a prescribed burn planning tool relevant to meeting fuel treatment and burn severity objectives.

In a larger computational domain, suitable for simulating the rise and establishment of the smoke plume, relatively coarse resolution WFDS-LS simulations (grid cells ≥ 8 m) compared well with finer resolutions simulations (grid cells ≥ 1 m). This implied that simulations focused on smoke plume require less grid resolution than simulations focused on fire behavior. In fact, using a static burner to approximate the moving heat source generated by spreading fires produced a nearly identical plume profile with a significantly coarser grid.

Table 2: Computational cost of the WFDS-PB and WFDS-LS simulations considered in the previous sections.

Model	Grid resolution	Computing hardware	Computing time	Computing cost, \$/hr; total \$
Cost of fire behavior simulations (Figure 6 domain); 5 minutes were simulated				
WFDS-PB	5 cm to 20 cm vertical 25 cm horizontal	93 vcpus AWS	418 RT	1.54; 55
WFDS-LS	1 m in all directions	25 vcpus Desktop	23 RT	0.62; 1, see text
WFDS-LS	2 m in all directions	25 vcpus Desktop	3.4 RT	0.62; 0.15, see text
WFDS-LS5	1 m in all directions	25 vcpus Desktop	21 RT	0.63; 0.91
WFDS-LS5	2 m in all directions	25 vcpus Desktop	2 RT	0.62; 0.09
WFDS-LS1	1 m in all directions	1 vcpu Desktop	1/17 RT	minimal
Cost of smoke plume simulations (Figure 16 domain); 15 mins were simulated				
WFDS-LS	≥ 1 m	256 vcpus AWS	123 RT	4.62; 132
	≥ 8 m	20 vcpus Desktop	3.6 RT	0.62; 0.56
vcpus = virtual cpus; AWS = Amazon Web Services computer; RT = factor to get real time cost: 4 RT means 1 min of simulated time takes 4 mins of computing time				

Table 2 provides measures of computational cost for the PB and level set based simulations of fire behavior and smoke plume development. The cost is characterized using three measures: 1) the computing resources needed (vcpus and platform [AWS versus a high-end Desktop computer]); 2) computing time; 3) cost in dollars per hour of compute time and total cost of the simulation in dollars. The desktop computer was purchased in 2019 and has 32 vcpus and 160 GB of memory. The computer cost $10,400 (this includes $730 for 128 GB of third-party memory and does not include the cost of the monitor). The AWS runs used Amazon's Elastic Compute Cloud EC2. Only the cheaper AWS spot instances were used for this project. To aid cost comparison across simulations, estimates of the AWS costs for the cases run on the desktop computer are provided.

Based on the cost summary of the fire behavior simulations in Table 2, the LS model is significantly cheaper than the PB model. In terms of dollars, the total cost of the PB fire behavior run was $55 on AWS while the desktop LS run cost $1 (on a 1 m grid) and $0.12 (on a 2 m grid) (these were simulations of about 5 minutes real time). However, LS did not run faster than real time. The fastest case (2m grid) ran 3.4 times slower than real time (i.e., simulating 5 minutes of fire behavior took 5*3.4 = 17 minutes of computing time on a desktop computer.

Smoke Plumes – Line Fire Comparisons

In this comparison, separate simulations of 200 m long, 10 m deep line fires with a HRRPUA of 50 and 200 kW/m^2, respectively, were performed using FDS and ALOFT-FT (Figure 18). Fires with equivalent fireline intensities (500 and 2000 kW/m) were also simulated using the MW94 model. Soot emission rates were the same in FDS and ALOFT-FT (concentrations were not calculated in MW94). A vertical temperature profile derived from a burn in the Meteotron simulation set (see below) was used in all three models. In the ALOFT-FT simulation, angles of vertical and crosswind dispersion from center were 10° and 15°, respectively, corresponding to a weakly stable atmosphere (McGrattan et al. 1997).

Vertical profiles of the horizontal wind speed, $U(z)$, in FDS and MW94 were prescribed as a power law profile,

$$U(z) = 1\tfrac{m}{s}\left(\frac{z}{10\ m}\right)^{1/7},$$

where z is the height above ground level (AGL). Wind in FDS was simulated using the 'wall of wind' technique, in which the upwind boundary condition is essentially a blower with the prescribed wind profile (McGrattan, et al. 2020). ALOFT-FT uses only a single constant wind speed. In this case it was prescribed as the transport wind speed of 1.6 m/s, which is the mean speed given by the above equation from ground level to the approximate plume heights (600-800 m).

ALOFT-FT and the MW94 model generate time-averaged plumes. For this comparison set, the smoke concentrations of the FDS-generated plumes were averaged over the final 300 s of a 900 s simulation. Python 3.8 scripts were created to read, analyze and plot data from all three models. Concentration data from multi-mesh simulations in FDS can be difficult to recreate spatially when meshes are of different resolution and spatial configurations. To create images such as those found in Figure 19, values from each FDS mesh were interpolated to a single, uniform mesh using the ‘RegularGridInterpolator’ function from SciPy 1.6.0. From visual inspection, this does not appear to have a significant effect on the data if the interpolated cells are not too large.

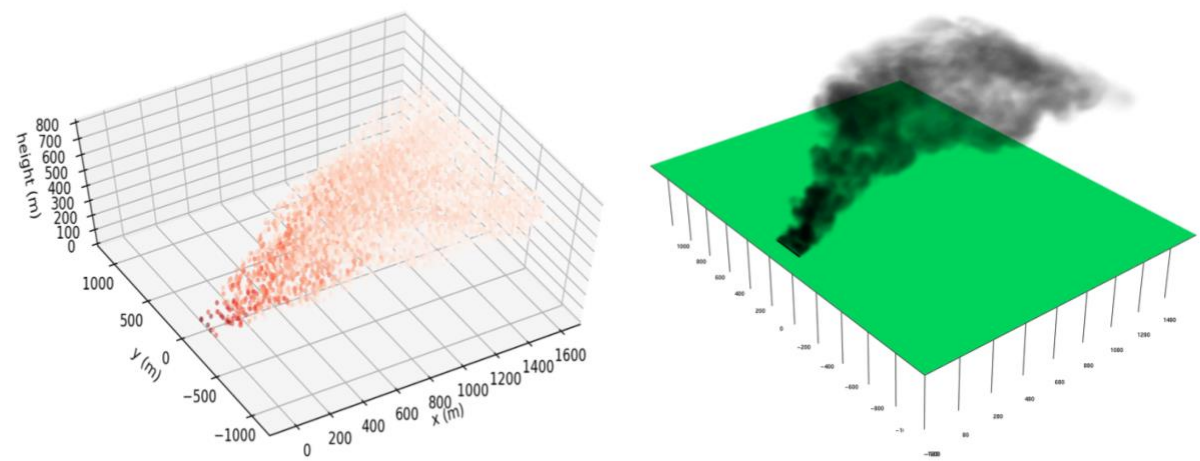

Figure 18. 3D Plumes from line fire simulations. Left: ALOFT-FT, Right: FDS.

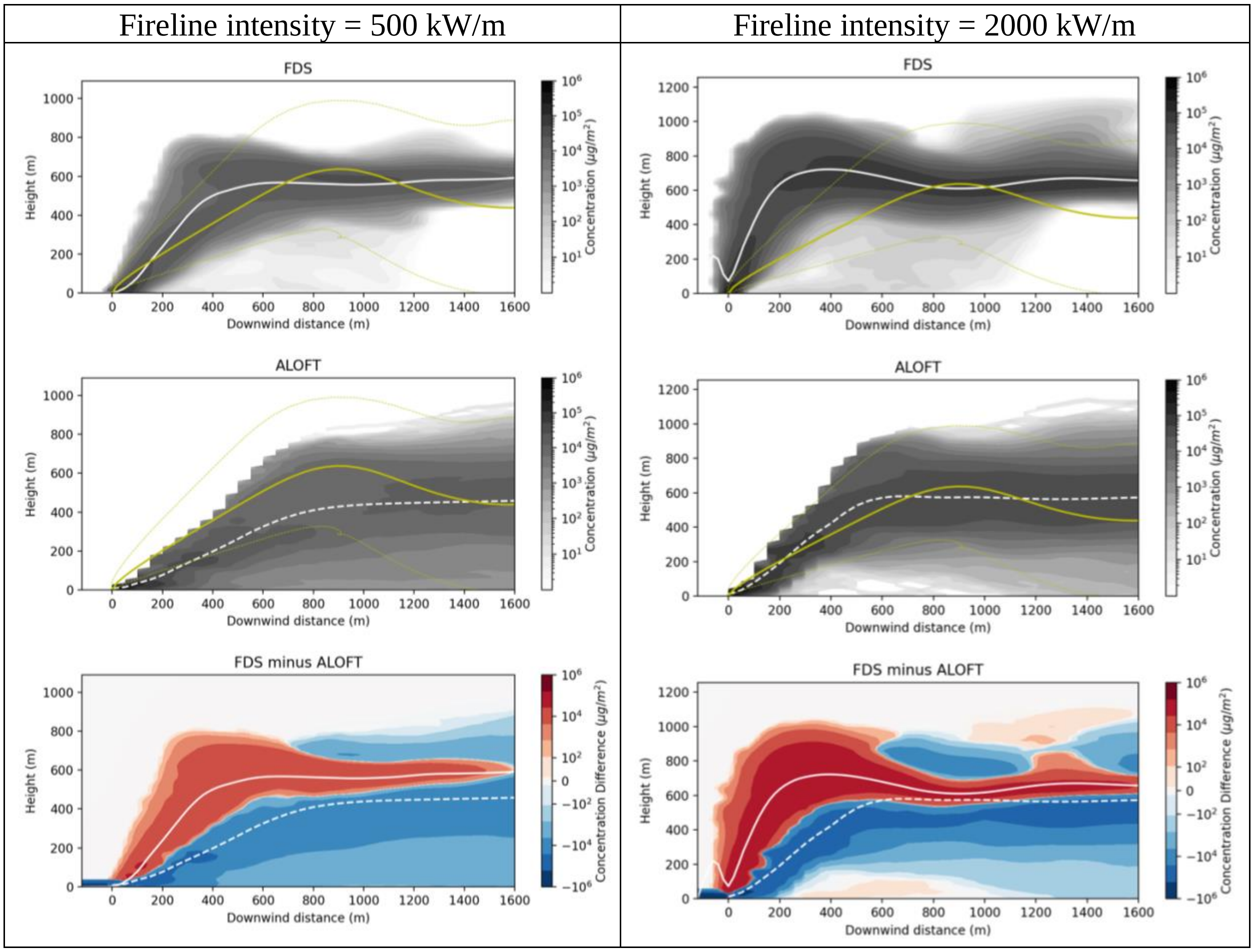

*Figure 19. Crosswind-integrated plume concentrations from line fires with intensities of 500 kW/m (**left column**) and 2000 kW/m (**right** column). Centerlines are indicated by white solid or dashed lines. MW94 plumes are indicated by yellow lines. **Top row**: FDS plumes with MW94 plumes. **Middle row**: ALOFT-FT plumes with MW94 plumes. **Bottom row**: Differences between the FDS and ALOFT-FT simulated plumes. Red indicates regions in which the FDS concentrations are greater than those simulated by ALOFT-FT; blue indicates the opposite.*

Results are summarized in Figure 19 and Figure 20 (the stepped appearance of windward portions of the ALOFT-FT plumes is an artefact of coarse resolution in the alongwind direction). Figure 19 indicates that plume centerlines from the FDS and MW94 models are more closely matched in the lower intensity simulations than in those at higher intensity, while the opposite is true for the ALOFT-FT model. Plumes from the MW94 and ALOFT-FT simulations bend more with the wind than does the plume from FDS. In ALOFT-FT this occurs because it is assumed in the model that the plume is already bent (plumes are injected in a vertical plane), and because a single transport (mean) wind speed is prescribed, resulting in higher windspeeds near the ground than would occur with a standard profile. These assumptions enhance execution speed but may also be a disadvantage in low-wind simulations.

The differences between soot concentration profiles are significant due in part to the differences in plume shape and height (Figure 19, bottom). As shown in Figure 20, the FDS and ALOFT-FT plumes spread significantly in the crosswind direction. Crosswind spread far downwind is much greater in ALOFT-FT than in FDS (Figure 20, bottom panels). This may in part be due to the fact that ALOFT-FT solves momentum and energy equations in y-z (crosswind-vertical) planes only.

A key consideration of these comparisons is the computational time needed to simulate the plumes (

Table 3). The most complex and physically accurate model, FDS, is also the most computationally expensive, requiring about 10 times the ‘real time’ (900 s) in this case to adequately simulate a three-dimensional plume. As mentioned, while ALOFT-FT produces a three-dimensional plume, it is actually solving for the flow field in only two dimensions (crosswind and vertical) at 50 discrete along-wind distances and, unlike FDS, does not simulate combustion and fluid dynamics at the source. For these reasons, as well as others, ALOFT-FT performs simulations far faster than FDS but with less physical fidelity. The MW94 model solves a relatively simple set of six coupled differential equations at a relatively to provide plume centerline and width but not concentration, allowing it to simulate a plume in less than one second.

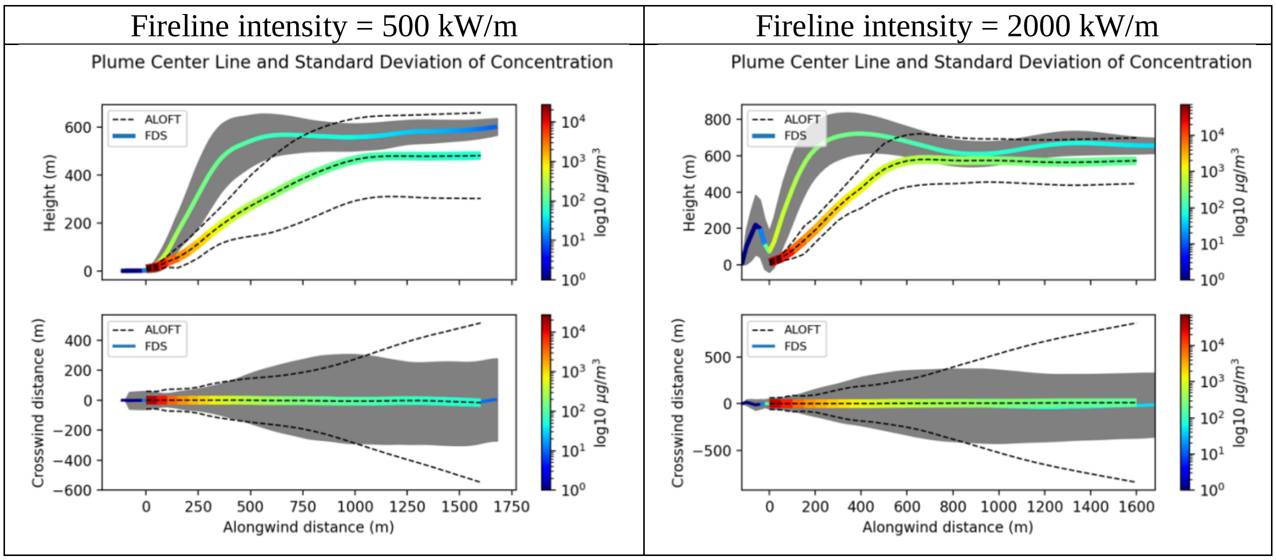

*Figure 20. Plume centerlines and standard deviations of concentration in the FDS and ALOFT-FT simulations. Centerlines are colored by concentration (centerlines overlap in the bottom panel). Areas of one standard deviation of concentration from the centerline values are shown as gray shaded areas (FDS) and dashed lines (ALOFT-FT). **Top panels**: Vertical section of plumes. **Bottom panels**: Bird’s eye view showing crosswind spread of FDS and ALOFT-FT plumes.*

Table 3. Mesh parameters and cpu times of line fire simulations ('RT' = Real Time).

Model	FDS	ALOFT-FT	MW94
Number of grid cells	1.14×10^6 (13 meshes in parallel)	64,500 (y-z plane only)	1,000 (points along plume centerline)
Typical CPU time	8,931 s (~10 x RT)	7.6 s (1/118 x RT)	0.06 s (1/15,000 x RT)

Smoke Plumes – Plume Interactions of Multiple Fire Lines

To compare simulations of multi-plume interaction, five static 24 m x 96 m fire lines, positioned 24 m apart in the alongwind direction, were simulated in ALOFT-FT and FDS (MW94 was omitted as simulated plumes do not interact). The HRRPUA was 312.5 kW/m^2 (HRR = 720 MW) in both models, with a smoke (soot) emission rate of 3.47×10^{-4} kg/m^2/s. The vertical wind speed profile in FDS was prescribed as

$$U(z) = 1.9\frac{m}{s}\left(\frac{z}{2\ m}\right)^{1/7}.$$

A constant vertical temperature profile of -6 °C/km was used in both simulations. Angles of dispersion in the ALOFT-FT model were 25° and 10° in the crosswind and vertical directions, respectively.

Centerline heights and plume extents from the FDS and ALOFT-FT simulations matched much more closely in this comparison case (Figure 22 and Figure 23) than in the line fire simulations above. This may in part be due to ALOFT-FT providing more realistic results when HRR is greater (as in *in situ* oil spill burns). In addition, although the sources are line fires, the plumes merge quickly and act more similarly to a plume from a pool or mass fire. Although the crosswind-integrated concentrations differ in detail (Figure 22), they are similar in magnitude (Figure 24).

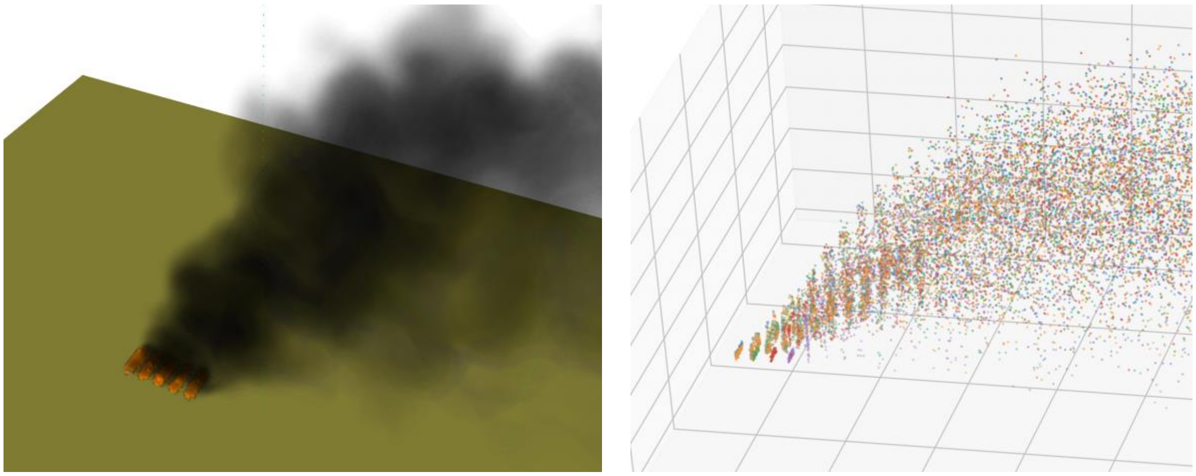

Figure 21. Five simultaneous line fires in FDS (left) and ALOFT-FT (right) simulations. In both cases, the separate plumes merge at short distances above the fires, effectively forming a single plume.

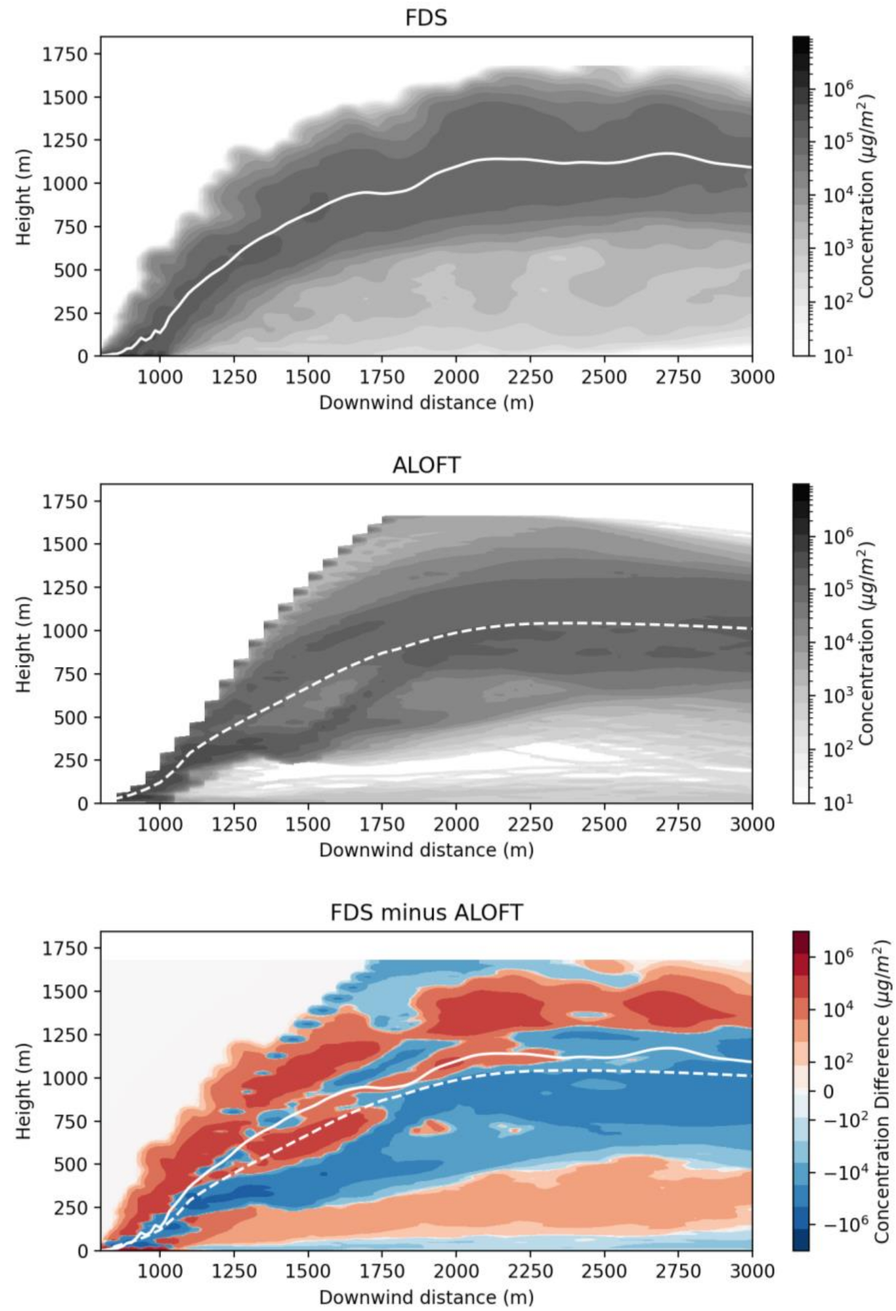

Figure 22. Crosswind-integrated plume concentrations from five line fires. Centerlines are indicated by white solid or dashed lines. Top: FDS plume with MW94 plume (yellow lines). Middle: ALOFT-FT plume with MW94 plume (yellow). Bottom: Difference between the FDS and ALOFT-FT simulated plumes. Red indicates regions in which the FDS concentration values are greater than those simulated by ALOFT-FT; blue indicates the opposite.

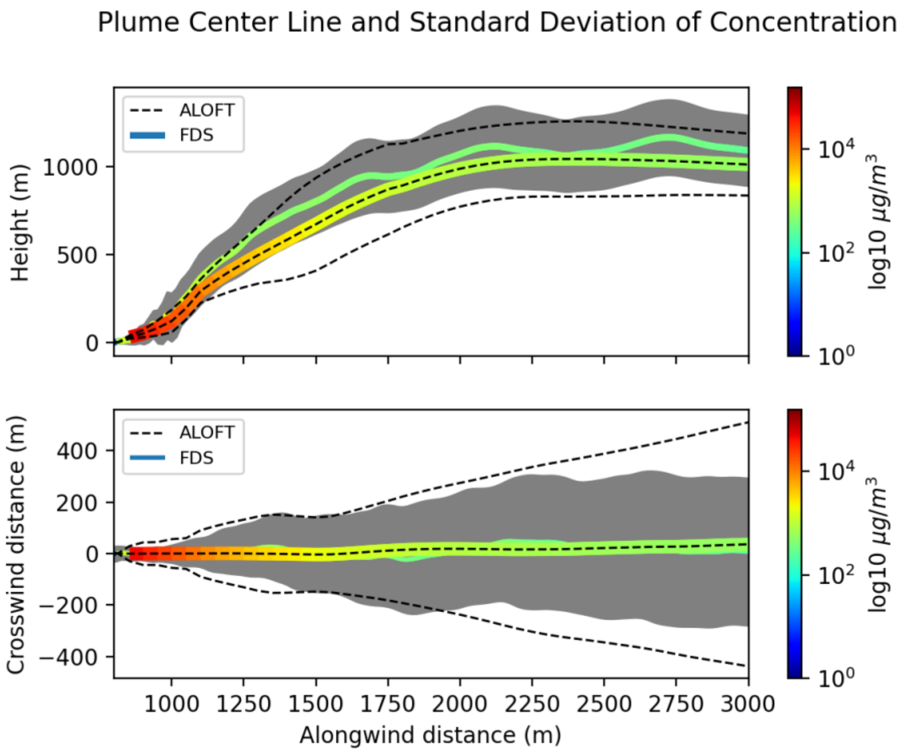

Figure 23. Plume centerlines and standard deviations of concentration in the FDS and ALOFT-FT simulations. Centerlines are colored by concentration (centerlines overlap in the bottom panel). Locations of one standard deviation of concentration from the centerline values are shown as gray shaded areas (FDS) and dashed lines (ALOFT-FT). ***Top****: Vertical section of plumes.* ***Bottom****: Plan view showing crosswind spread of FDS and ALOFT-FT plumes.*

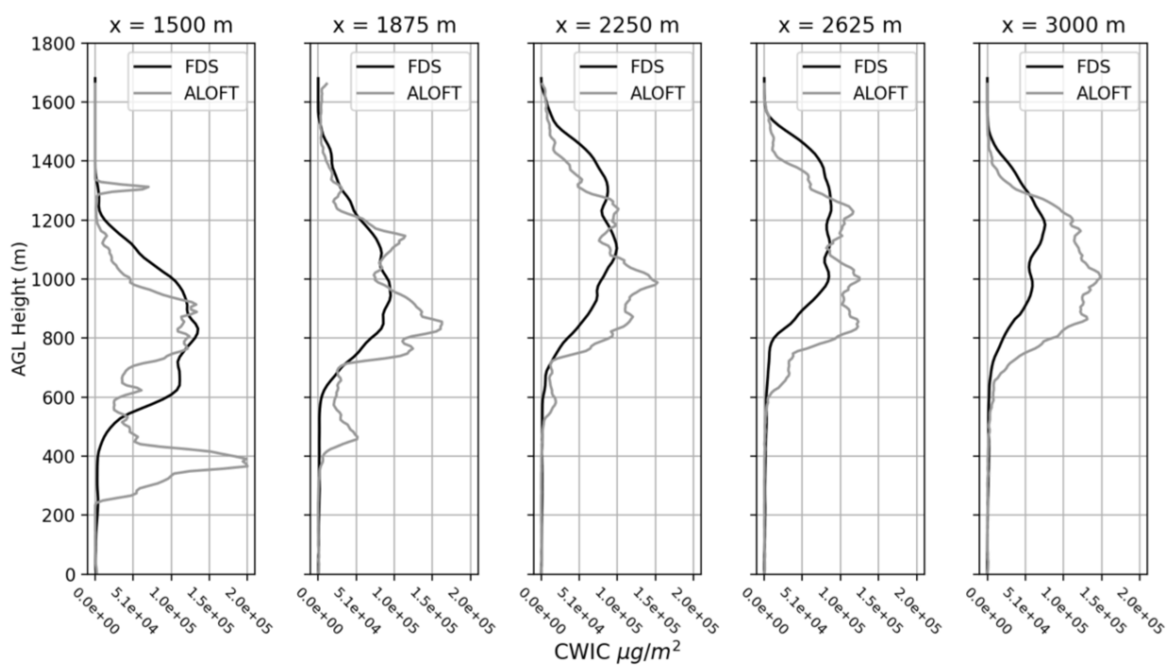

Figure 24. Vertical profiles of crosswind-integrated smoke (soot) concentrations at five downwind locations.

Smoke Plumes – Fireline Separation Distance and Plume Interaction

To explore the effect of source separation distance on plumes downwind of each other, plumes from two static line fires separated by increasing downwind distances were modeled in separate ALOFT-FT simulations. Heat release rate per unit area was 200 kW/m^2 in all simulations, and a vertical temperature profile of -6 °C/km was prescribed. Crosswind and vertical angles of dispersion were 15° and 10°, respectively.

Two sets of simulations with the same HRRPUA but with fire line lengths of 200 m and 400 m, respectively, were created. In the first trial of each set, a single source of double width (approximating two abutting line fires) was simulated. In the remaining trials, one line remained at the original source location while the second line was positioned downwind. Separation distances of 100 m to 1600 m were simulated (Figure 25).

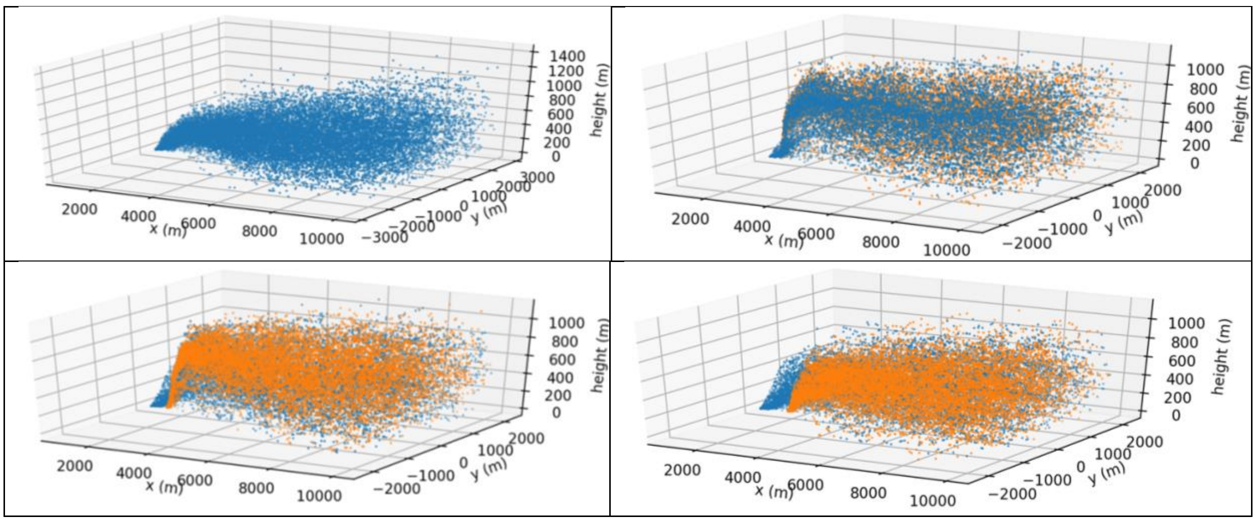

Figure 25. Examples of plume interaction simulations in ALOFT-FT. Plumes separated by 0 m (top left), 200 m (top right), 500 m (lower left) and 900 m (lower right) in the alongwind direction. Lagrangian particles representing the smoke are colored blue for the upwind fire and orange for the downwind fire.

Mean heights of crosswind-integrated centerlines of the *combined* plumes from both simulation sets are plotted against separation distance in Figure 26. In both sets, there is a noticeable increase in combined plume height when the sources are separated by 1 to 2.5 fire line lengths. This may be because the interaction of plume vortices in downwind configurations can increase plume rise (Trelles, et al. 1999), and because the upwind plume partially shields the downwind plume from the wind, causing more vertical rise in the downwind plumes and increasing the combined plume height. In future work, FDS could be used to examine this phenomenon in more detail.

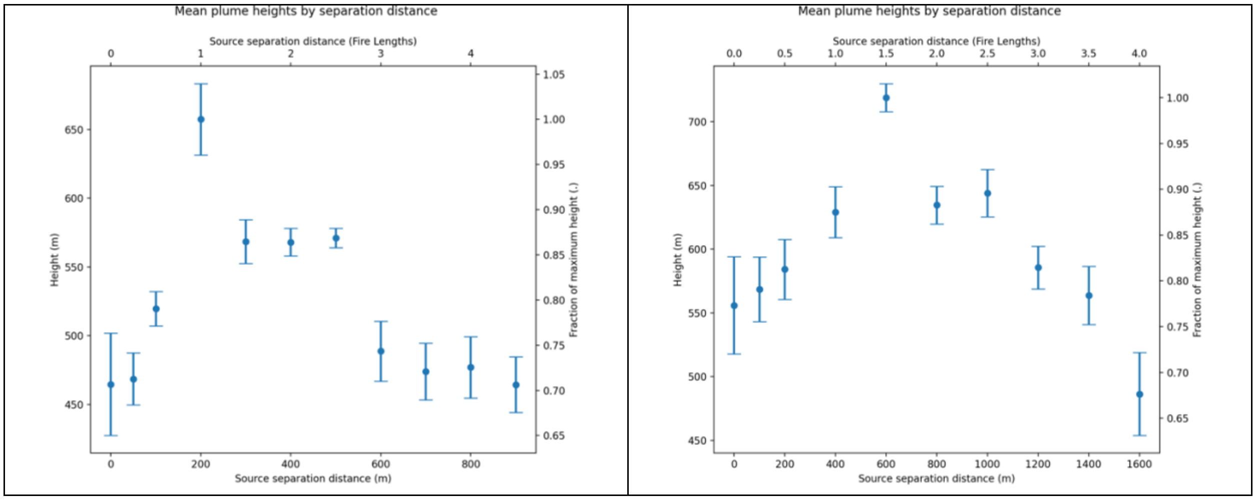

Figure 26. Mean far-field centerline heights of the combined plumes. Standard deviations are shown as vertical error bars. Secondary axes show separation distance normalized by fire line length (upper x-axes) and the fractions of maximum height (right y-axes). Left: 200 m x 10 m static fire lines. Right: 400 m x 10 m static fire lines.

Smoke Plumes – Meteotron Experiments

The results above were from comparisons between models only. To compare the performance of ALOFT-FT and FDS to actual plume experiments, we used data from the well-documented Meteotron experiment performed in France in the 1970's (Benech 1976). In each trial of the experiment, a hexagonal array of oil jet burners, operating for 300 s to 600 s at a combined power of about 600 MW, produced thick smoke plumes in relatively low wind conditions. Temperature and wind speed profiles of the plumes and atmosphere were recorded for each experiment, and photogrammetric techniques were used to estimate plume dimensions (Benech 1976).

Of the eleven trials detailed in Benech (1976), five were chosen for simulations based on the atmospheric temperature profiles (near adiabatic). Temperature profiles in the simulatons were derived from the vertical profiles of temperature *gradients* provided by Benech (1976) for each trial (temperatures were not given). Vertical wind speed profiles, but not wind directions, were provided. In the simulations it was assumed that wind directions did not vary with height.

The spatial configuration of the hexagonal array of burners used in the Meteotron experiments was modeled in FDS (Figure 27). Each burner was assigned a HRR of 6186 kW, yielding a total power of 600 MW. The detailed array was used in each FDS simulation (Figure 27 and Figure 28), but it was determined that a circular burner with an equivalent radius and HRRPUA generates plumes that are virtually indistinguishable from those produced by the detailed array (Appendix 5, p. 55).

The mesh around and above the burner array was refined to a resolution of 1 m to capture the dynamics near the burners and was nested within coarser meshes of 4 m and 8 m, as shown in

Figure 28. This mesh configuration was used for each simulation, although sensitivity tests suggest that a coarser uniform grid could provide similar results in less time (Appendix 6, 57).

A nudging technique, in which simulation parameters are gently driven towards prescribed values, was used instead of the wall-of-wind method employed in the line fire simulations (Appendix 8, p. 62). Unlike the wall-of-wind method, this allows FDS to simulate customized vertical profiles of wind speed (instead of a power law profile) as well as temperature. Plumes in the FDS simulations were generated over the same time periods as the experiments (300 s or 600 s) to ensure that the plume extents and shapes matched as closely as possible.

Corresponding ALOFT-FT simulations were performed using the original algorithm (without line fire modification) with a circular source area of about 3400 m^2. Transport wind speed in each simulation was prescribed as the mean wind speed in the mixed layer based on the data in Benech 1976. Crosswind and vertical angles of dispersion were assumed to be 15° and 10° in all cases.

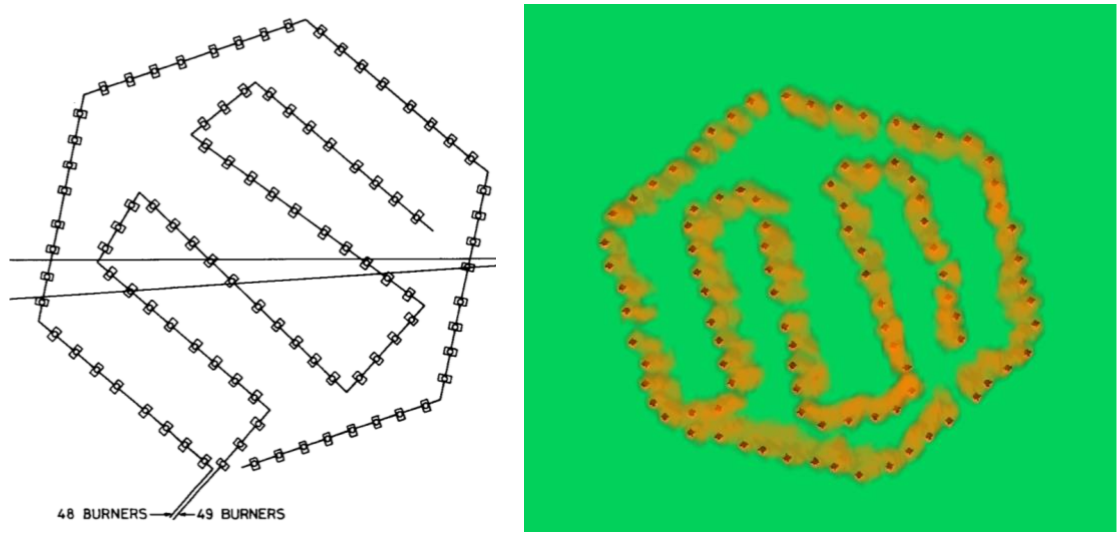

Figure 27. Hexagonal burner array used in the Meteotron experiments. ***Left****: schematic of the array (from Benech 1976).* ***Right****: plan view of an active burner array in FDS.*

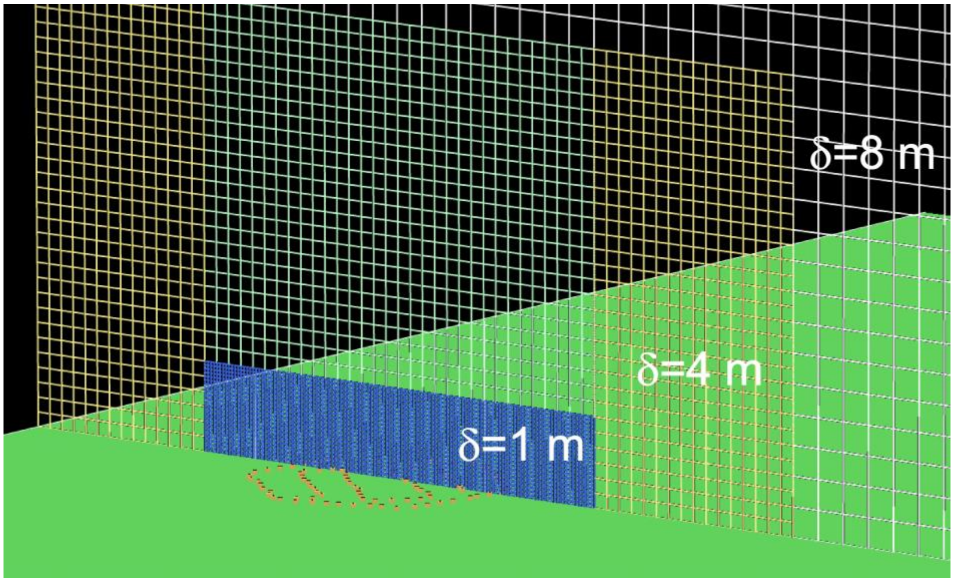

Figure 28. Vertical cross section of computational meshes used in the Meteotron simulations. The burner array is shown at the bottom of the finest mesh (blue grid). Mesh cell sizes are indicated in the image.

Two simulation sets are shown as examples below. Results from the remaining simulations are given in Appendix 7 (p. 59). Plume extents given in Benech 1976 were estimated at the end of the trial times (300 or 600 s), therefore only the concentration fields at the last time step of the FDS simulations were used to generate the contour plots shown below. ALOFT-FT provides only time-averaged solutions, resulting in concentration contours that appear smoother than those from FDS simulations.

The first example illustrates simulations of the Meteotron trial on October 1, 1971 (Figure 29). A wind speed of 4 m/s was prescribed in ALOFT-FT. The same temperature profile was used in both simulations. Soot concentration data were not recorded in Benech 1976 and so are not a consideration in these comparisons, but the contours provide a rough guide to plume width in the ALOFT-FT and FDS simulations. In this set, the simulated plumes from both ALOFT-FT and FDS match closely with the estimated plume radius and centerline shown in yellow.

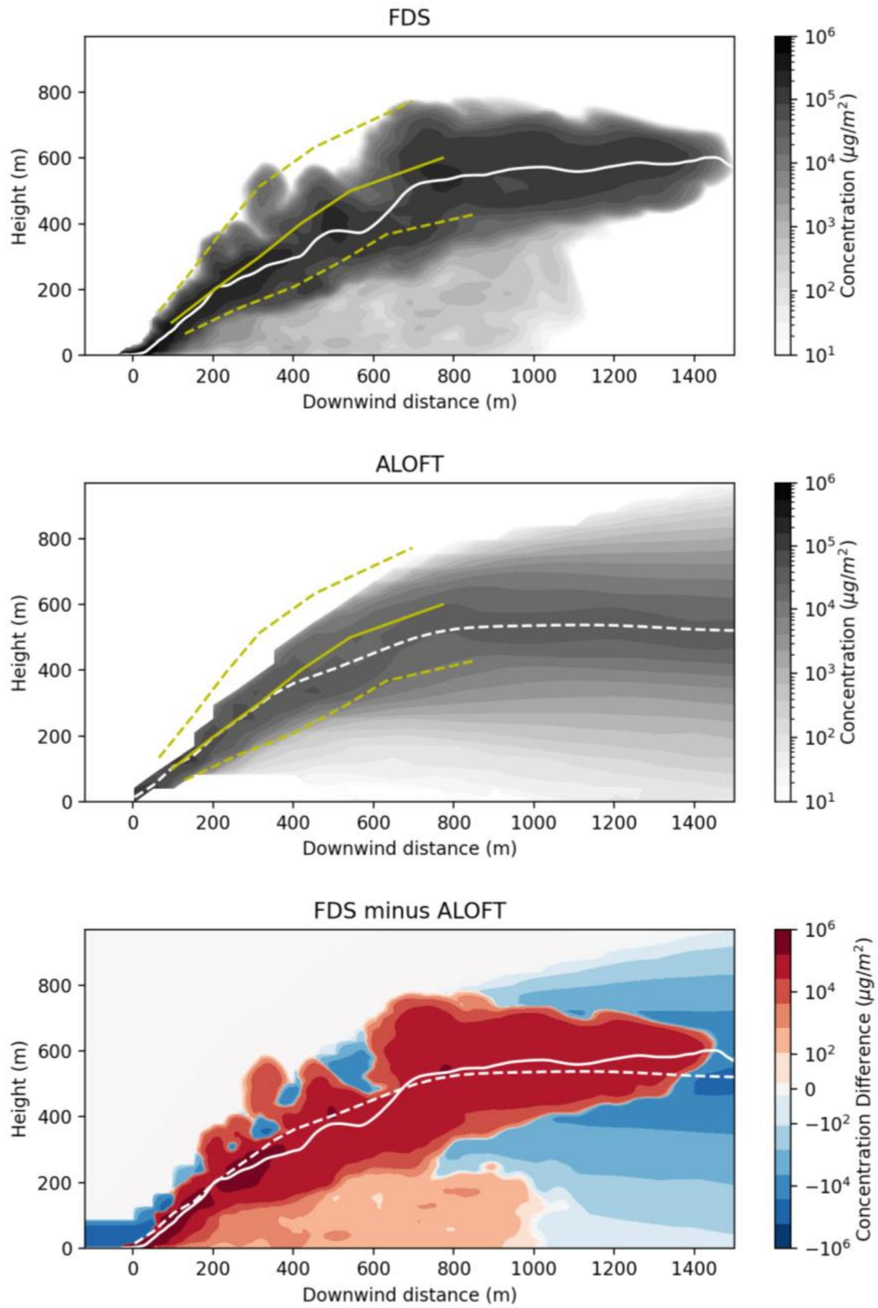

Figure 29. Crosswind-integrated concentration contours from FDS (top) and ALOFT-FT (middle) simulations of the October 1971 Meteotron experiment. The extent of the plume as estimated from photogrammetry is shown in yellow. In most of the experiments, only a portion of the plume extent was estimated. Bottom: difference in CWIC between the FDS and ALOFT-FT simulated plumes.

The second example displays simulations of the April 4, 1973 trial (Figure 31). A mean wind speed of 2 m/s was used in the ALOFT-FT simulation. Although the plume center line heights are within about 100 m of the experimental estimate, the plume extents do not match the experiment data well in either simulation. In the Meteotron trials, temperature and wind speed soundings were taken roughly two hours apart with one before and one after plume generation, (Benech 1976), so it is possible that wind speeds were lower at the time of the trial than those recorded in the experiment. An FDS simulation with a lower wind speed in the mixed layer (~1 m/s) matched the recorded plume extent more closely (Appendix 7, Figure 48). Despite the mismatch of the exact profiles, the FDS plume shows a remarkable similarity to a photograph of the corresponding plume from Benech 1976 (Figure 30).

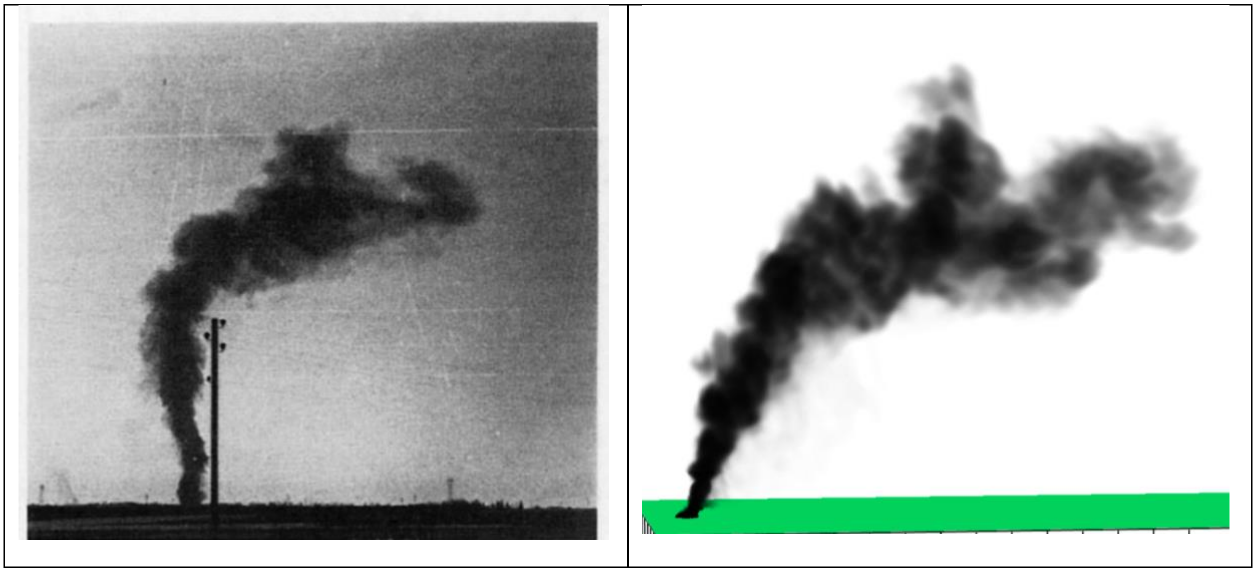

Figure 30. Left: a photograph of the April 1973 Meteotron plume (Benech 1976). Right: an FDS simulation of the experiment. Both images show the plume 300 s after ignition.

In four of the six simulations (the October 71, July 1973, October 1973 and the modified April 1973 trials), FDS provides acceptable matches to the recorded plume extents (Appendix 7, p.59). Plumes from ALOFT-FT show poorer correspondence, especially in the near field, due in part to poor alongwind resolution and the tendency toward greater bending of the plumes.

While the FDS results are encouraging, only partial vertical spatial profiles were used in this comparison. Crosswind profiles and concentrations, or concentration surrogates such as visibility, were not recorded in the experiments.

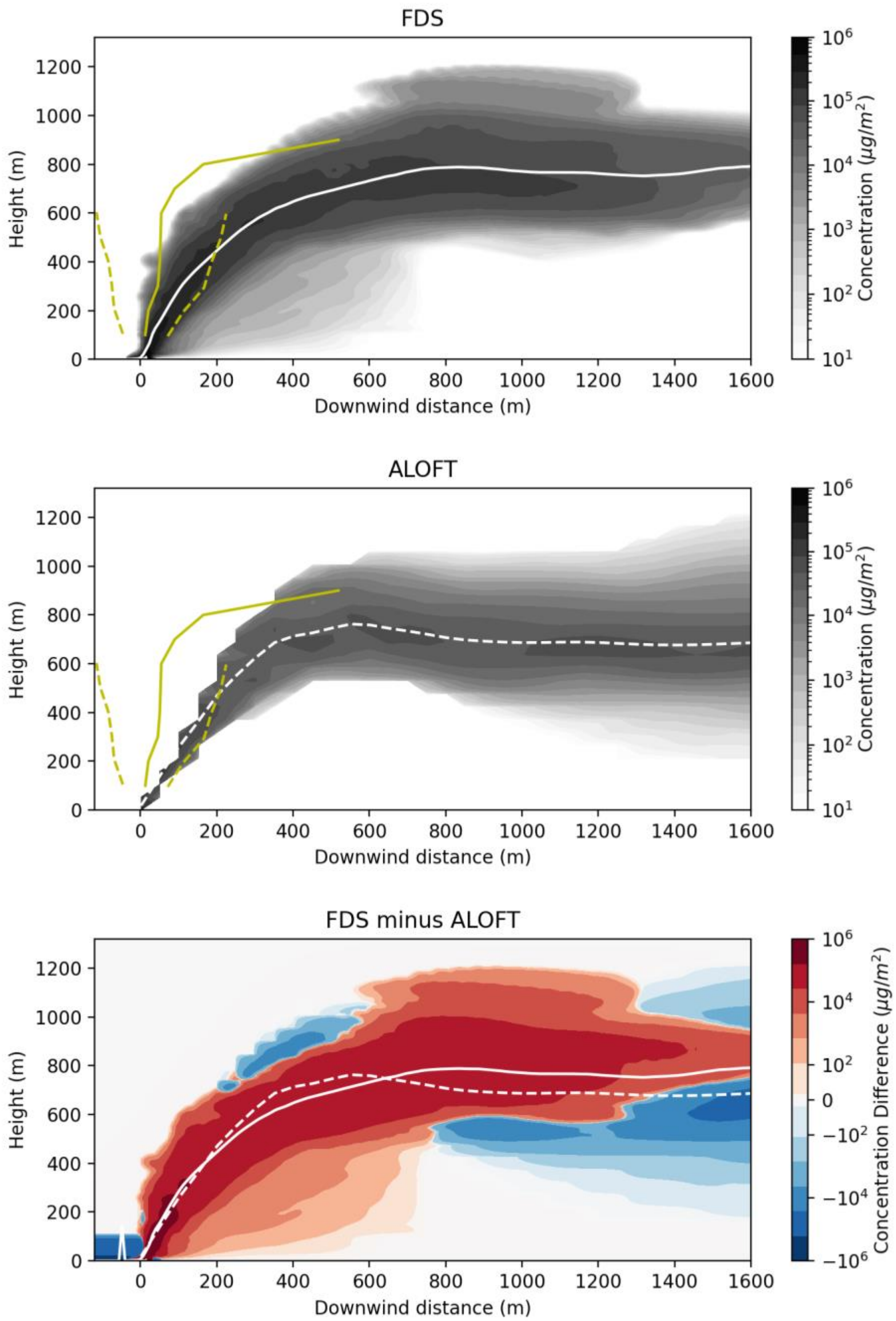

Figure 31. Vertical crosswind-integrated concentration contours from FDS (top) and ALOFT-FT (middle) simulations of the April 1973 Meteotron experiment. The extent of the plume as estimated from photogrammetry is shown in yellow. In most of the experiments, only a portion of the plume extent was estimated. Bottom: difference in CWIC between the FDS and ALOFT-FT simulated plumes. *Results from simulations of the same trial at a lower wind speed are given in Appendix 7, p.59.*

As in previous cases, FDS took considerably longer than real time to execute the Meteotron simulations (Table 4). However, as noted in Appendix 6 (p. 57), reducing the resolution of the simulations by increasing the cells sizes uniformly to 10 m would speed up the simulations by roughly a factor of 10 without much impact on the results. Execution times for ALOFT-FT are much faster than real time (Table 4), but the resulting plumes were not as similar to the corresponding Meteotron trials due in part to poor alongwind resolution, especially in the near field.

Table 4. Mesh parameters and execution times of Meteotron simulations ('RT' = Real Time).

Model	**FDS**	**ALOFT-FT**	**MW94**
Number of grid cells	4.8 x10^6 (15 meshes or vcpus)	40,000 (y-z plane only)	N/A
CPU time	26,100 - 54,140 s (84-88 x RT)	1.28-1.62 s (1/242 – 1/376 x RT)	N/A

Smoke Plumes Summary and Discussion

Not surprisingly, FDS—the model with the greatest physical fidelity—provides the most realistic plumes but also requires far more computational resources than ALOFT-FT and MW94.

The results of the plume interaction simulations using ALOFT-FT, in which fire line separation enhances plume height, are intriguing and lend at least some support to the work of Trelles, et al. (1999). Although ALOFT-FT compares well with FDS in some cases, it would have to be significantly modified to simulate moving fires with geometries other than simple lines or ellipses. It is not clear whether such modifications would significantly increase execution time. Further simulations of this phenomenon could be performed in FDS in a follow-on project.

The results from simulations of the Meteotron experiment were mixed, and it is not clear if this is due to deficiencies in the models, the meteorological data from the experiments, or a combination of both. Regardless, FDS was able to produce plumes with strong resemblances to those produced in the experiment (e.g., Figure 30).

The choice of plume model depends in large part on the needs of the user. For example, results suggest that the MW94 model could provide rapid estimates of mean plume extent and centerline height from a single line fire that are likely to be better than estimates using rule-of-thumb methods. For exploring near-field plume effects and investigating plumes from moving and interacting fires, FDS is the best option if computational resources are available. With significant modification, the ALOFT-FT model may provide a good balance between the speed of MW94 and the physical fidelity of FDS.

Cloud Computing

The computational resources required to simulate a prescribed burn can vary considerably. A cloud service like Amazon Web Services (AWS) allows one to launch an appropriate computing resource ranging in power from a laptop to a cluster supercomputer.

For this limited-scope project, we created an application to make the submission of FDS/WFDS simulations of a prescribed burn to AWS as seamless as possible. A snapshot of this application's graphical user interface is shown in Figure 32. A five-minute video presentation of the run tool, which was part of this project's February 2021 progress report, is available [here](). The key functions of the application include the following.

- Starts one or more AWS instances, on-demand (fixed price) or spot (bid price).
- Organizes the instances launched into a parallel computing cluster.
- Uploads to AWS the input and executable files needed to execute the simulations of the prescribed burn.
- Monitors the state of the instances launched.
- Stores the results of the simulation to persistent storage (Amazon S3).
- Notifies the user on completion of the simulation.
- Shuts down the instances.

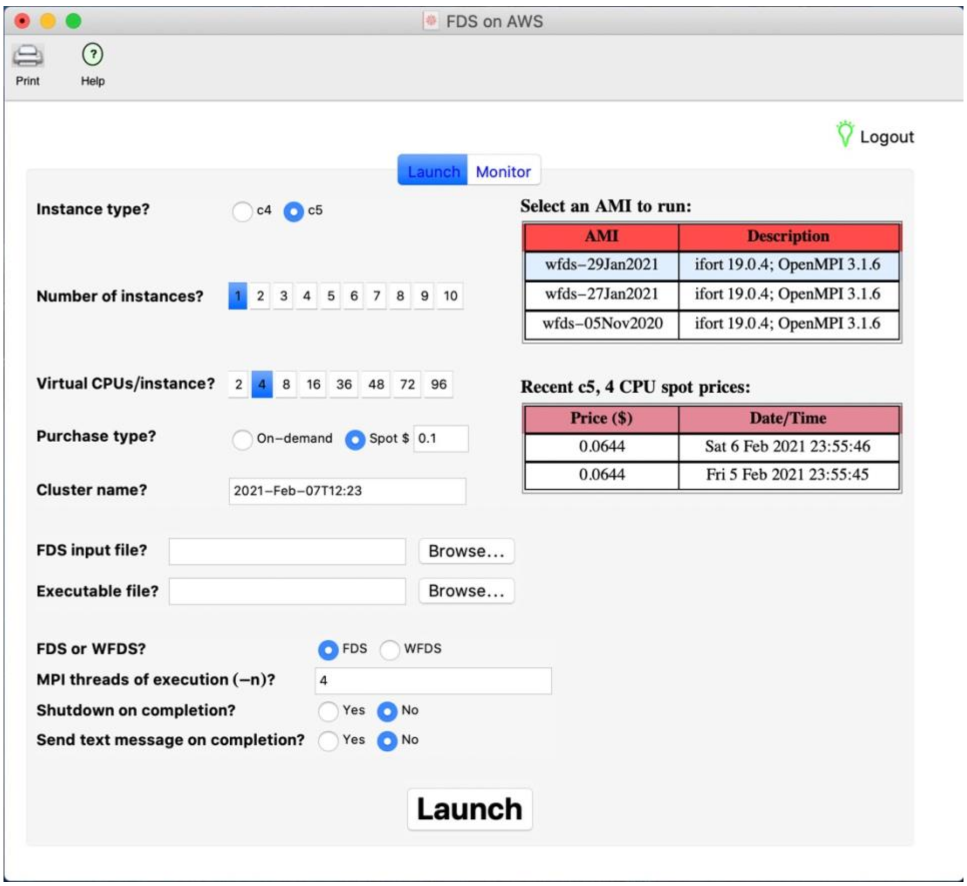

Figure 32: A screenshot of the prototype graphical user interface that allow a user to run WFDS or FDS on Amazon Web Service computers.

Were this limited-scope project to be extended, we propose to deliver a trio of tools (apps) with which to plan and assess the impact of prescribed burns.

- **Burn builder app**: To simulate a burn scenario with FDS requires the construction of an input file. This file describes terrain, built features, vegetation, wind, the ignition plan and other aspects of a prospective burn. Assembling such an input file by hand is complex and error-prone. We would build an interactive, visual interface to facilitate this task.

- **Burn model execution app**: The burn scenario described by an FDS input file requires sometimes substantial computational resources to execute. The software we have created in this limited-scope project manages the mechanics of this process using the AWS cloud service. It is largely complete and would only need to be integrated with the other apps proposed.
- **Burn model assessment app**: An FDS simulation can generate a massive amount of data describing the evolution of smoke, fire lines, temperatures and air velocities over the course of a simulated burn. The assessment app would provide purpose-built visualizations and report generators specific to assessing and approving prescribed burns.

For our team to make this suite of apps useful and accessible, it would be essential to structure an extended project so that we are able to obtain design input and on-going critiques of our work from burn managers and other SERDP stakeholders who have agreed to be beta testers of the overall modeling product.

Implications for Future Research and Benefits

Conclusions regarding fire behavior modeling of the scenarios considered here

- Comparison of the LS and LS1 models highlight the need for CFD-based modeling to simulate dynamic fire behavior, including the formation and interaction of head, flank, and back fires during a prescribed fire (see Figure 9).
- PB simulations required computational grids that are sufficiently fine to resolve the explicitly modeled processes driving the smaller flank and back fires. As a result, PB simulations are likely to be too computationally expensive for routine prescribed-fire simulations: runtime is 418 RT and significant computational resources are required (93 cpus on AWS, see Table 2)
- LS simulations are able to replicated PB surface fire(s) behavior using a range of grid resolutions. As a result, they are significantly cheaper than PB simulations. Depending on the desired degree of agreement with PB predictions, LS simulations are within reach of use with a high-end desktop and certainly with the use of AWS.
- LS fire behavior simulations, with a 1 m grid, qualitatively agree with PB predictions of the location of understory consumption and have a runtime cost of 23 RT with 25 cpus on a desktop computer. These were run on small domains relative to simulations focused on smoke plumes.
- LS simulations focused on obtaining the HRR history to support smoke plume predictions require less grid resolution. For example, LS simulations with 2 m grid produced HRR time histories that were close to PB predictions and had a runtime cost of 3.4 RT with 25 cpus (on a desktop) compared to 418 RT and 93 cpus for PB (see Table 2).
- LS5 simulations have the advantage of not requiring a head-fire spread rate formula that depends on the local wind speed. Instead, an expected constant head fire rate of spread is used. The influence of the fire-generated winds on fire behavior is more approximated. What the LS5 approach loses in accuracy may be made up in ease of use, especially for

qualitative predictions regarding the influence of fire generated winds on dynamic fire behavior (see Figure 10). LS5 ran faster than LS: 2 RT compared to 3.4 RT.

- The HRR obtains a near constant value for fires spreading in a quasi-steady manner (i.e., sufficiently constant spread rate and fire footprint area). This HRR, and an approximation of the moving fires as static burners, can be used for a relatively coarse grid smoke plume simulation at a significant savings in computational cost (see Figure 17 and Table 2).

Conclusions regarding smoke plume modeling

Three models of different complexity were used to simulate smoke plumes in a variety of scenarios. The most complex model, FDS, required far more computational resources than the ALOFT-FT and MW94 models, but also provided greater physical fidelity (e.g., Figure 30). Intercomparison of models, while instructive, is of limited value compared to evaluation of plume models against empirical data. Unfortunately, complete empirical datasets for smoke plumes (plume shape, concentrations, contemporaneous meteorological data, etc.) at the scales modeled in this study are scarce.

The physics required for plume modeling depends on user needs. For example, for simple estimates of plume centerline height from a single line source, the MW94 model (as well as other models that were not evaluated, such as the Briggs plume rise equation (Lareau and Clements, 2017)) can provide reasonable, or at least operationally functional, estimates much faster than real time. The MW94 model is limited to single idealized line fires, however, and requires empirical relations to model plume concentrations (e.g., a Gaussian distribution) and temperatures, which limits the applicability of the model for other purposes.

The ALOFT-FT model provides faster-than-real-time estimates of plume geometries in three dimensions and over large scales [O(10 km)], that compare favorably with FDS simulations and empirical data. It is limited, though, by its inability to model moving smoke sources and, in its current form, source geometries other than ellipses or lines. In addition, it is appropriate only for relatively flat terrain and cannot incorporate changes in wind speed and direction with height. It is not clear whether these limitations could be addressed without significantly increasing processing time. Regardless, any future development would require completely rewriting the code in a different language or modern Fortran format.

In addition to featuring combustion physics, FDS incorporates far more atmospheric physics than either MW94 or ALOFT-FT, and it can simulate moving fires with changing geometries over complex terrain. However, simulations at appropriate resolution (~10 m, depending on domain size) will generally not be able to provide operational (faster than real time) results, at least in the current version. Further research into appropriate relaxation times is required to optimize the nudging method for simulation of smoke plumes. Future work will include evaluation of FDS smoke plumes against more recent experimental data.

Implications for future research

Overall, the results of this proof-of-concept study suggest that semi-routine CFD-based fire behavior and smoke plume simulations are within reach for use as prescribed-burn planning tools. The prescribed burn simulations (Fig. 9) clearly show the relevance of fire-atmosphere interaction captured with the CFD-based simulations. Such simulations are potentially within reach with a high-end desktop computer and definitely the case if cloud computing is available. For example, higher resolution simulations of fire behavior, in smaller computational domains, could be conducted with different candidate firing patterns to obtain useful fire behavior predictions, HRR histories, and locations of higher likelihood of understory consumption. A representative HRRPUA could then be used for smoke plume simulations in larger computational domains. Or, for simulations focused on smoke plume development, approximations to the fire behavior could define the characteristics of the HRRPUA in the burn plot (i.e., spatial distribution and time history) using coarse grid, faster turn-around, simulations. It is possible model runs with relatively quick turnaround times and qualitative accuracy could be used in prescribed burn training or to illustrate fire behavior relevant to fire safety.

Important issues to be addressed in a follow-on effort include the following:

1. This study is largely based on model-to-model comparison for a limited range of scenarios. The range of scenarios needs to be expanded, as does comparison to experimental observations of fire behavior and smoke plume development. Currently, there is a dearth of reported observations for model evaluation use. A number of ongoing SERDP field experiments offer a possible avenue toward meeting this challenge. One particular application is the ability to model the likelihood of residual smoke (i.e., smoke that is not lofted) given atmospheric and canopy conditions and firing patterns.
2. It is critical that beta users are experienced prescribed burn planners and are actively involved from the beginning of the project. This includes use of the models. Given the lack of observational data, those who are experienced in conducting prescribed burns will be the best resource for model assessment. This assessment includes the reliability of the models' predictions, in terms of practical application, and ease of use. It is also critical to success that the simulation team visit prescribed burn sites for direct observation and better understanding of the objectives and challenges of burn planning and operation.
3. The source code and program executables for Windows, Linux, and OSX should all be publicly available during the entire course of the project (note, WFDS and FDS source code and executables are publicly available). User and technical guides will be available and regularly updated. This ensures transparency and supports a more collaborative advance of the modeling tools. Ideally, a public issue tracker and discussion group are used. These are practices currently followed by the FDS development team who would join us in a follow-on effort. FDS is a well-established model in the fire protection engineering community (e.g., from April 2020 – April 2021 FDS there were 30,518 downloads of FDS). Much of the WFDS level set model capability has been incorporated into FDS. This work is continuing. If this project has a follow-on stage, WFDS will be replaced by FDS.

Literature Cited

Achtemeier GL, Goodrick SA, Liu Y, Garcia-Menendez F, Yongtao H, Odman MT (2011) Modeling smoke plume-rise and dispersion from southern United States prescribed burns with Daysmoke. *Atmosphere*, **2**:358-388.

Achtemeier GL, Goodrick SA, Liu Y (2012) Modeling multiple-core updraft plume rise for an aerial ignition prescribed burn by coupling Daysmoke with a cellular atomic fire model. *Atmosphere*, **3**: 352-376

Anderson HE (1969) Heat transfer and fire spread. *USDA Forest Service Research Paper* INT-69, Intermountain Forest and Range Experiment Station, Odgden, Utah

Berg EE, Hamrick JL (1994) Spatial and genetic structure of two sandhills oaks: *Quercus laevis* and *Quercus margaretta* (Fagaceae). *American J. of Botany*, **81(1)**: 7-14

Benech B (1976) Experimental Study of an artificial convective plume initiated from the ground. *Journal of Applied Meteorology*, **15**:127-137.

Bova AS, Mell WE, Hoffman CM (2015) A comparison of level set and marker methods for the simulation of wildand fire front propagation. *International Journal of Wildland Fire*, **25**:229-241

Coen JL, Stavros EN, Fites-Kaufman JA (2018) Deconstructing the King megafire. *Ecological Applications*, **28**(6):1565-1580.

FDS (Fire Dynamics Simulator) (2021) https://pages.nist.gov/fds-smv

Filippi JB, Bosseur F, Mari C, Lac C, Le Moigne P, Cuenot B, Veynante D, Cariolle D, Balbi J-H. (2009) coupled atmosphere-wildland fire modeling. *Journal of Advances in Modeling Earth Systems*, **1**: 11.

Finney MA (2004) FARSITE: Fire Area Simulator-Model, development and applications. *Paper RMRS-RP-4*, USDA Forest Service, Rocky Mountain Research Station, Fort Collins, CO.

Furman JH, Linn RR, Williams BW, Winterkamp J (2020) Using a Computational Fluid Dynamic Model to Guide Wildland Fire Management. *Final Report ESTCP Project RC-201303*, April 2019. https://www.serdp-estcp.org/content/download/51368/505456/file/RC-201303%20Final%20Report.pdf

Goodrick SL, Achtemeier GL, Larkin NK, Liu Y, Strand TM (2013) Modeling smoke transport rom wildland fires: a review. *International Journal of wildland fire*, **22**:83-94.

Hudak AT, Bright BC, Pokswinski SM, Loudermilk EL, O'Brien JJ, Hornsby BS, Klauberg C, Silva DA (2106) Mapping forest structure and composition from low-density LiDAR for informed forest, fuel, and fire management at Eglin Air Force Base, Florida, USA. *Canadian J. of Remote Sensing*, **42**: 411-427.

Keyser EK (2020) Southern (SN) Variant Overview – Forest Vegetation Simulator. Internal Rep. Fort Collins, CO: U. S. Department of Agriculture, Forest Service, Forest Management Service Center. 82p. (revised November 2, 2020) https://www.fs.fed.us/fmsc/ftp/fvs/docs/overviews/FVSsn_Overview.pdf

Lareau, NP and Clements, CB (2017) The Mean and Turbulent Properties of a Wildfire Convective Plume. Journal of Applied Meteorology and Climatology **56**:2289-2299. DOI: 10.1175/JAMC-D-16-0384.1

McGrattan, KB, Baum, HR, Walton, DW, Trelles, J (1997) Smoke plume trajectory from in situ burning of crude oil in Alaska—field experiments and modeling of complex terrain. NISTIR 5958. National Institute of Standards and Technology. https://nvlpubs.nist.gov/nistpubs/Legacy/IR/nistir5958.pdf (last accessed March 23, 2021)

McGrattan, KB, Hostikka, S, Floyd, J, McDermott, R, Vanella, M (2020) Fire dynamics simulator user's guide. NIST Special Publication 1019 (6th ed., Revision: FDS6.7.5-0-g71f025606, http://dx.doi.org/10.6028/NIST.SP.1019).

Mandel J, Amram S, Beezly JD, Kelman B, Kochanski AK, Kondratenko VY, Lynn BH (2014) Recent advances and applications of WRF-SFIRE. *Natural Hazards and Earth System Science*, **14**: 2829-2845.

Mell WE and Linn RR (2017) FIRETEC and WFDS modeling of fire behavior and smoke in support of FASMEE. *Final report, JFSP project 16-4-05-1*, 2017. https://www.firescience.gov/projects/16-4-05-1/project/16-4-05-1_final_report.pdf

Mell WE, Maranghides A, McDermott R, Manzello SL (2009) Numerical simulation and experiments of burning Douglas fir trees. *Combustion and Flame*, **156**:2023-2041.

Mell WE, Jenkins MA, Gould J, Cheney P (2007) A physics-based model for grassland fires. *International Journal of Wildland Fire*, **16**: 1-27.

Mercer GN and Weber, RO (1994) Plumes above line fires in a cross wind. Int J. Wildland Fire **4**(4):201-207.

Mercer GN and Weber, RO (2001) Fire Plumes *in* Johnson, EA & Miyanishi, K (eds.), Forest fires: Behavior and ecological effects. Academic Press, San Diego, California.

Ninemets U, Ellsworth DS, Lukjanova A, Tobias M (2002) Dependence of needle architecture and chemical composition on canopy light availability in three North American Pinus species with contrasting needle length. *Tree Physiology*, **22**, 747-761.

Perez-Ramirez Y, Santoni PA, Tramoni JB, Bosseur F, Mell WE (2017) Examination of WFDS in modeling spreading fires in a furniture calorimeter. *Fire Technology*, **53**:1795-1832.

Quintiere, JG (2006) Fundamentals of fire phenomena. John Wiley & Sons, Ltd.

Rothermel RC (1972) A mathematical model for predicting fire spread in wildland fuels. USDA Forest Service. Intermountain Forest and Range Experiment Station, *Research Paper INT-114* (Ogden, UT) https://www.fs.usda.gov/treesearch/pubs/32533

Sánchez-Monroy X, Mell W, Torres-Arenas J, Butler BW (2019) Fire spread upslope: Numerical simulation of laboratory experiments. *Fire Safety Journal*, **108**.

SDI (2021) Stand density index, *Wikipedia*, https://en.wikipedia.org/wiki/Stand_density_index

Simm L (2014) State of smoke plume dispersion modeling for wildland fire planning. In State of Fire Behavior Models and their Application to Ecosystem and Smoke Management Issues, Special Session Summary Report, *Smoke Symposium, IAWF*, College Park, Maryland, October 24, 2013. Authors: SJ Pritchard, RD Ottmar.

Scott JH, Burgan RE (2005) Standard Fire Behavior Fuel Models: A comprehensive set for use with Rothermel's surface fire spread model. *USDA Rocky Mountain Research Station, General Tech. Report RMRS-GTR-153*

Stocks BJ, Alexander ME, Lanoville RA (2004) Overview the international ground fire modeling experiment (ICFME). Canadian Journal of Forest research, **34**:1543-1547.

Sun R, Jenkins MA, Krueger SK, Mell W, Cheney JJ (2006) An evaluation of fire-plume properties simulated with the fire dynamics simulator the apprentice (FDS) and the Clark couple of wildfire model. *Canadian Journal of Forest Research*, **36**:2894-2908.

Tachajapong W, Lazono J, Mahalingham S, Zhou X, Weise DR (2009) Experimental and numerical modeling of shrub crown fire initiation. *Combustion Science and Technology*, **181**:618-740.

Trelles J, McGrattan KB, Baum HR (1999) Smoke dispersion from multiple fire plumes. *AIAA Journal*, **37**(12):1588-1601.

Trentmann J, Andreae MO, Graf H-F, Hobbs PV, Ottmar RD, Trautmann T (2002) Simulation of a biomass-burning plume: Comparison of model results with observation. *Journal Geophysical Research*, **107**(D2):AAC 5-1 to 5-15.

WFDS (Wildland-urban interface Fire Dynamics Simulator) (2021)
https://github.com/ruddymell/wfds9977

Appendix 1: Development of a head fire rate of spread formula using WFDS-PB

WFDS is not the only CFD based model that uses a simplified representation of a spreading fire to locate and couple a fire's heat release rate to the surrounding flow dynamics. For example, WRF-SFIRE (Mandel et al., 2014) is a model focused on atmospheric physics with a level set based representation of a spreading fire that uses the Rothermel (1972) surface fire spread rate formula. Similarly, the CAWFE model (Coen et al., 2018) is another atmosphere-physics model that uses a tracer method to move a fire line according to the Rothermel (1972) surface fire spread model.

It is possible to implement WFDS or FDS with the level set approach and the Rothermel (1972) surface fire spread equation. There is, however, an inconsistency – or at least a complication – with the use of the Rothermel model in a CFD-based fire behavior model. The Rothermel spread rate equation requires the ambient wind as input. That is, the wind unaffected by the presence of the fire. Strictly speaking, this would require running the CFD model without a fire in order to obtain the predicted ambient wind for input to the model when a fire is present. This is not done. Instead, the Rothermel model is given a wind value based on the simulation with the fire present. The reason for this approach stems from the desire to include, however inconsistently, the influence of the fire generated wind on fire behavior. This allows for some accounting of important fire dynamics due to the influence of fire generated winds, such as acceleration of a fire up a drainage.

In this project we implemented the level set based model for surface fire spread (WFDS-LS) with a surface fire spread rate formula derived from the more complete physics-based model WFDS-PB. This formula accounts for the influence of fire generated winds and, therefore, the approach does not have the inconsistency present when the Rothermel surface fire spread rate formula is used.

This Appendix describes the method used to derive the WFDS-PB based surface fire spread rate formula. This was done for Australian grass because that allowed us to use the Australian grassland experiments (see the section: Model Validation and Comparison using a Stand-Scale Grassfire Experiment) to evaluate the approach.

A head fire rate of spread formula was obtained from WFDS-PB simulations of fire spreading in grass with properties from experiment C064 (see Mell et al., 2007; and the section here on Stand-Scale Grassfire experiment) to create a database of "observations". Five different ambient wind speeds (at 2.5 m above ground) were used: 1.5, 2.5, 3.75, 5.5, 7.5 m/s. Each wind speed case was run with three different lengths of the ignition: 10, 20, 48 m. Ignition occurred from the middle of the line out, as in the field experiment (Mell et al., 2007). The spatial resolution of the simulations was 0.5 m. The boundary fuel model of WFDS-PB was used. Results from the case with a 2.5 m/s wind and a 20 m ignition line are shown in Figure 33. Both the fire footprint is shown (on the left plot) and the location of the leading edge and width and depth of head fire (on the right plot). The time average of the spread rate of the head fire and the local horizontal wind speed normal to the head fire was computed for each case. Different averaging windows, both in the sense of duration and the size of the area near the leading edge of the head fire, were tested.

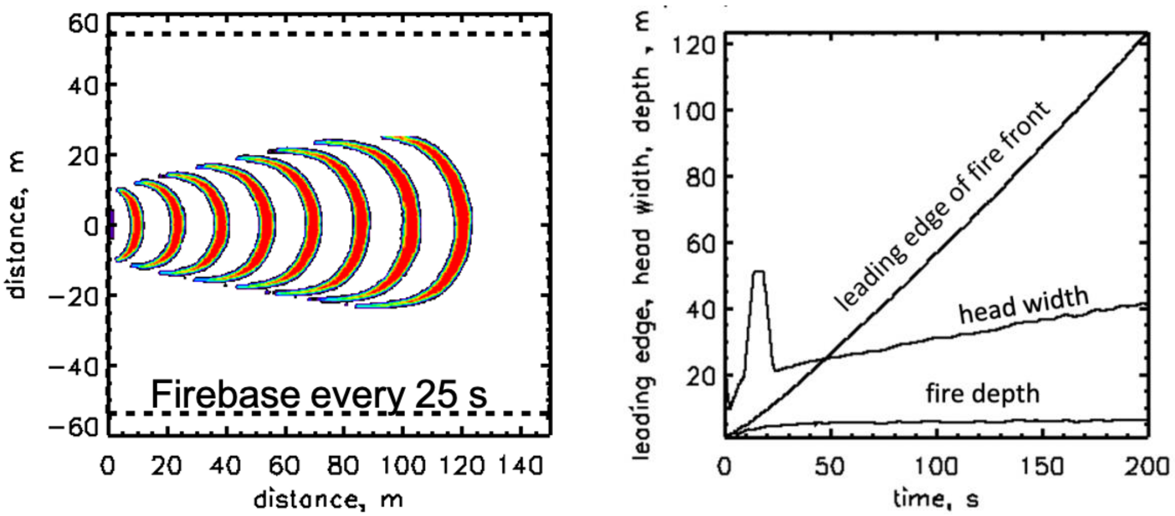

Figure 33: An example case from the WFDS-PB simulation database created to derive a formula for the head fire rate of spread as a function of the local net wind. In this case the ambient wind is 2.5 m/s (2 m above the ground) and the ignition fire line is 20 m long.

The derived local head fire spread rates from WFDS-PB simulations of fires spreading from a 10 m long ignition line are shown as colored points in Figure 34. Five ambient winds were used as shown in the figure's legend and identified by specific colors. As the ambient wind increases, the head fire spread rate increases. Note that there is overlap between cases of different wind speeds. This is due, in part, to the spread rate increasing as the head-width of the fire increases (Mell et al., 2007). As a fire's head-width increases, the HRR increases (see Figure 4 and associated discussion) generating stronger fire induced winds. These fire induced winds are especially relevant to the spread rate when the ambient wind speed is relatively low. This results in a lower ambient wind speed case overlapping (at its higher rate of spread values when the head width is larger) with the next higher ambient wind speed case (at its lower rate of spread values when it head width is smaller). The other source of overlap, especially for the larger ambient wind cases, is noise in the computation of the spread rate and local wind speed values and depends on the windows used in the time and space averaging.

The final formula for the head fire spread rate as a function of the local wind can be obtained by fitting a line (in this case a second order polynomial) through the points in Figure 34. The solid line in Figure 34 is

$$RoS = 0.098 + 0.063U + 0.004U^2 \text{ m/s},$$

where U is the local averaged wind speed normal to the fire front. This was computed using a 10 s time average and a spatial window that covered the fire base plus one head width downwind in the windward direction and 1 m to each side of the centerline in the crosswind direction.

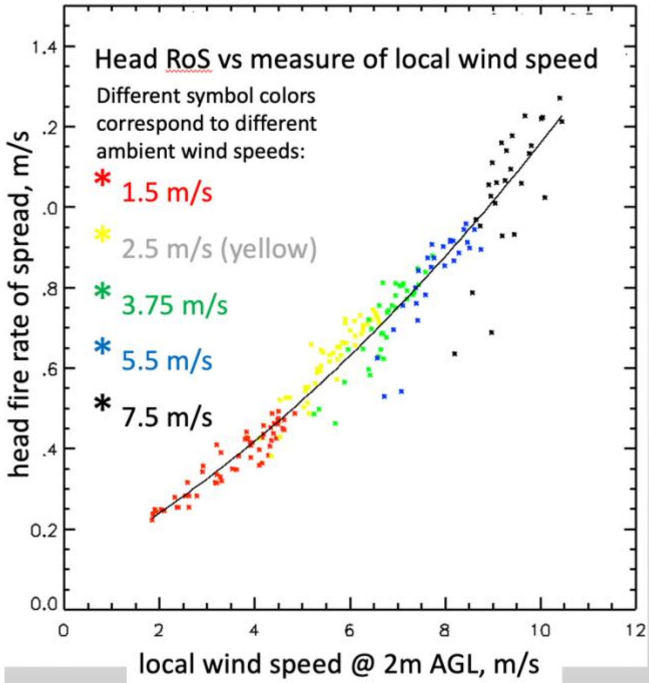

Figure 34: The local head fire rate of spread (RoS) plotted against the local horizontal wind speed normal to the leading edge of the head fire. Derived from five WFDS-PB simulations (each with a different ambient wind as denoted by the different colors) of a grassfire with a 10 m long ignition line

In order to test the use of the above head fire rate of spread formula within the WFDS CFD model, a number of WFDS-LS and WFDS-PB simulations with only head fires were conducted and compared. For example, simulations were performed with grass strips of 6 m, 12 m, and 24 m crosswind dimension with a 2.5 m/s (at 2 m above ground) ambient wind speed (see Figure 35).

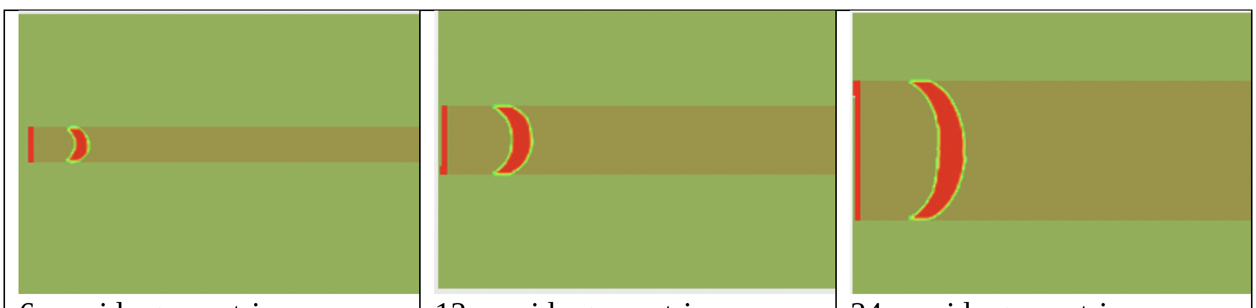

6 m wide grass strip	12 m wide grass strip	24 m wide grass strip

Figure 35: Configuration of grass-strip test cases to compare WFDS-PB and WFDS-LS. Ambient with of 2.6 m/s (2 m AGL) flow left to right.

The HRR time histories from the PB and LS simulations of the grass-strip fire cases in Figure 35 are shown in Figure 36. Overall, there is good agreement between the PB and LS HRR. Some disagreement exists due to the longer time it takes for the fire to establish itself in the PB simulations. The spread rates of the fires are in Table 5. There is good agreement between the PB and LS simulations. In particular, note that the spread rate increases as the width of the grass strip increases due to the increased local wind speed generated by the larger HRR.

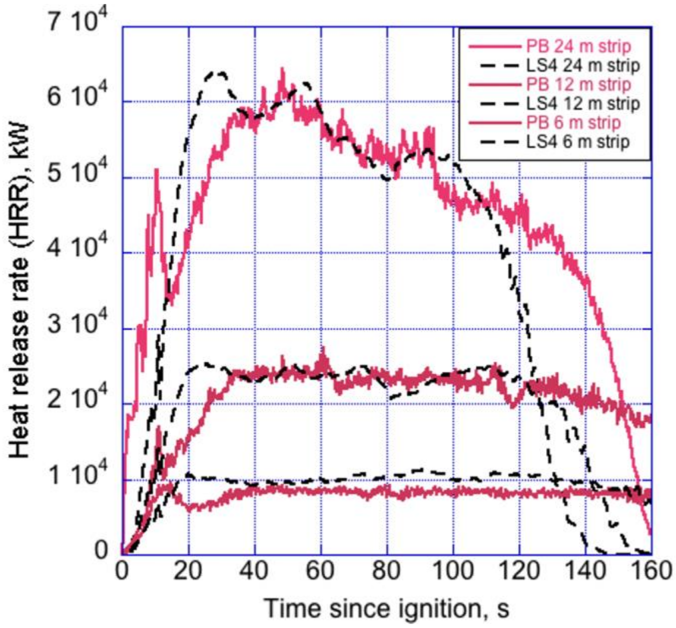

Figure 36: HRR for WFDS-PB (red line) and WFDS-LS (dashed black line) simulations of the grass-strip fire test cases shown in Figure 35. The higher magnitude HRR histories are for the wider grass strips.

Table 5: Rate of spread values for the WFDS-PB and WFDS-LS simulations of the grass-strip fire cases in Figure 35.

Rate of spread in the grass strip fires, m/s		
	WFDS-PB	WFDS-LS
6 m wide	0.34	0.40
12 m wide	0.49	0.50
24 m wide	0.60	0.60

Appendix 2: Characteristics of raised vegetation in the prescribed burn scenario[2]

Table 6 lists the physical properties of the vegetation. Both the understory and overstory vegetation characteristics are representative of southeastern longleaf pine stands. Some properties (e.g., the Oak and Persimmon surface-to-volume ratios and particle densities and the bulk density of all raised vegetation) are assumed based on best estimates. Note that the focus of the effort is to compare the WFDS-PB and WFDS-LS results in the context of a prescribed burn scenario. Vegetation characteristics can easily be changed if more appropriate values are available for a particular scenario.

[2] We thank Dr. Justin Ziegler and Prof. Chad Hoffman of Colorado State University for the development of the raised vegetation.

The overstory is longleaf pine and turkey oak with stocking rates based on Hudak et al. (2016) who report the average rate for Eglin Air Force Base. Understory stocking rates are based on the stems/acre reported in Appendix B of Furman et al. (2020). Tree locations are based on spatial patterns reported in Berg and Hamrick (1994) and Hudak et al. (2016) for oaks and pines, respectively. We applied the model of oak spatial patterns to simulate persimmon locations because no referential studies for persimmon were found.

Overstory and understory tree heights were determined by sampling a uniform distribution of height using ranges reported in Appendix B of Furman et al. (2020). From the tree height (HT) the diameter at breast height (DBH), crown ratio (CR) [from which the crown base height can be derived], and the width of crown base (CW) for each tree was determined (in US customary units):

1. DBH = { $\log_{10}$[(HT-4.5)/P2] / (-P3) }^(1/P4) from Eq. 4.1.1 in Keyser (2020), where the variables P# are species dependent.
2. CR = d_o + (d_1*$\log_{10}$(RELSDI)) Eq. 4.3.1.6 in Keyser (2020), where the variables $d_\#$ are species dependent.
    a. The relative stand density index, RELSDI = (10*(Stand SDI / Max SDI)).
    b. The Stand SDI is computed from $\log_{10}$(Stand SDI) = $\log_{10}$(N) + 1.604 $\log_{10}$(D) – 1.065 (see SDI, 2021), where N is the number of trees per acre and D = DBH of the tree of average basal area.
    c. Maximum SDI (Max SDI) is species dependent and can be found in Table 3.5.1 in Keyser (2020).
3. CW is determined from Eq. 4.4.1 in Keyser (2020):
    a. For DBH >= 5 inches: CW = a_1 + a_2 DBH + (a_3 DBH^2) + a_4 CR + a_5 HI
    b. For DBH < 5inches: CW = [a_1 + a_2 5 + a_3 25 + a_4 CR + a_5 HI]*DBH / 5

    Where HI in the Hopkins index = (elevation – 887)/100) + (latitude – 39.54) – 1.25*(longitude + 82.52) [Eglin AFB location is used here) and a_1 – a_5 are coefficients in tables 4.4.1 and 4.4.2 of Keyser (2020).

Table 6: Physical properties of vegetation in forested stand prescribed burn simulations.

Longleaf pine overstory (OL) & understory (UL) Turkey Oak understory (OO) & understory (UO) Persimmon understory (P)		**Source**
surface-to-volume ratio, 1/m	4831 (OL, UL), 3940 (OO,UO), 3940 (P)	Ninemets et al. 2002 (OL, UL)) assumed (O), assumed (P)
moisture, %	170 (OL,OO), 200 (UL,UO), 133 (P)	assumed
particle density, kg/m^3	485 (OL,UL), 514 (OO,UO), 514 (P)	Ninemets et al. 2002 (OL, UL) assumed (O), assumed (P)
bulk density, kg/m^3	0.25 (OL,UL,OO,UO,P)	see text above
crown dimensions	varies	see text above
overstory height range, m	11.3 – 23.2 (OL)	Furman et al. (2020) Appendix B

	7.3 – 11.6 (OO)	
understory height range, m; stems/acre	1.5 – 3.5; 165 (UL) 2 – 4.5; 398 (UO) 1.5 – 2; 223 (P)	Furman et al. (2020) Appendix B
Grass		
surface-to-volume ratio, 1/m	6582	GR6 fuel, Scott and Burgan (2005)
moisture, %	6	assumed
particle density, kg/m^3	512	GR6 fuel, Scott and Burgan (2005)
height, m	0.46	GR6 fuel, Scott and Burgan (2005)
bulk density, kg/m^3	1.71	GR6 fuel, Scott and Burgan (2005)
loading, kg/m^2	0.82	GR6 fuel, Scott and Burgan (2005)

Appendix 3: Amendments to the MW94 model

In the original MW94 model, the initial half width, vertical velocity and plume temperature are prescribed along with an ambient temperature and a vertical profile of wind velocity. Rather than use arbitrary values for the plume parameters, we added an equation for initial vertical velocity, w_i, based on fire line intensity (adapted from Quintiere 2006, p. 307):

$$w_i = \sqrt{g z_c}\ \text{, where } z_c = \left(\frac{I}{\rho_\infty c_p T_\infty \sqrt{g}}\right)^{2/3}.$$

The characteristic length scale, z_c, is a function of fireline intensity, I (kW/m). Ambient air density, specific heat and temperature are denoted as ρ_∞, c_p and T_∞, respectively, and g is the gravitational constant.

Assuming a top-hat profile, initial *mean* plume temperature was estimated based solely on dimensional considerations and adapted from Quintiere (2006, p. 307) as:

$$T_i = \frac{I}{\rho_\infty c_p 2 b_i w_i}$$

Where $2b_i$ is the depth of the fire line.

Changes in simulated plume temperature occur solely through entrainment in the original version. To account for the effects of atmospheric stability (temperature lapse rate) on the plume, the model was modified to include adiabatic changes in plume temperature (Figure 37).

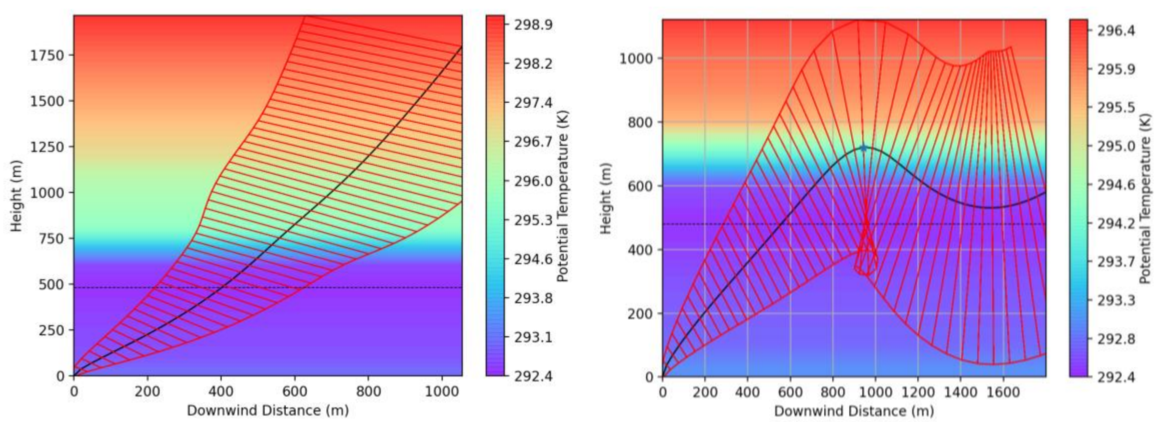

Figure 37. Plumes from MW94 model. The dotted horizontal line in both panels indicates the beginning of a temperature inversion above a mixed layer. Air temperature is indicated by the background colors in the plots. On the left is a plume from the original model before the effects of atmospheric stability are accounted for. On the right, using the same plume parameters, the plume from the modified model penetrates the temperature inversion and then oscillates around an equilibrium level. (Temperature and height scales differ between panels.)

Appendix 4: Sensitivity tests of ALOFT-FT

Input parameters to the original ALOFT-FT model include (circular) burning area, HRRPUA, vertical temperature profile (lapse rate) and transport wind speed. The number of computational grid cells and angles of standard deviation of wind are also prescribed for the crosswind (y-axis) and vertical (z-axis) directions. To investigate the sensitivity of the simulations to key parameters, a set of simulations was performed with four key variables of three different values (Table 7) in a factorial set of combinations, resulting in 81 simulations. A dry adiabatic lapse rate was prescribed up to a height of 1000 m and was capped by a strong temperature inversion in each simulation.

The output from each simulation was analyzed to determine the plume centerline height from the center of mass of the crosswind-integrated concentration. The mean centerline heights of the plume far downwind of the source and the minimum of mean plume concentrations downwind of the source were regressed against the key parameters. Far field concentrations were recorded 20 km from the source in all simulations.

P-values and correlation coefficients from multivariate linear regressions of the key parameters suggest that firepower flux and transport wind speed are the most significant parameters influencing plume height (Figure 38 and Table 8), while the standard deviations of vertical (and by correlation, horizontal) dispersion have the greatest influence on far field plume concentrations (Figure 39 and Table 9).

Table 7. Parameter values in sensitivity test of ALOFT-FT. Each set of parameters was combined factorially. Vertical standard deviation of wind is 2/3 of the crosswind deviation (McGrattan et al., 1997), and the number of vertical cells was arbitrarily set to half the number of the horizontal cells (horizontal dispersion is generally much greater than vertical dispersion in the model).

Wind Speed (m/s)	st dev of wind (m/s) (Crosswind / Vertical)	Number of cells (Crosswind / Vertical)	HRRPUA (kW/m^2)
2	0.5 / 0.33	100 / 50	100
5	0.8 / 0.53	160 / 80	500
10	1.1 / 0.73	200 / 100	1000

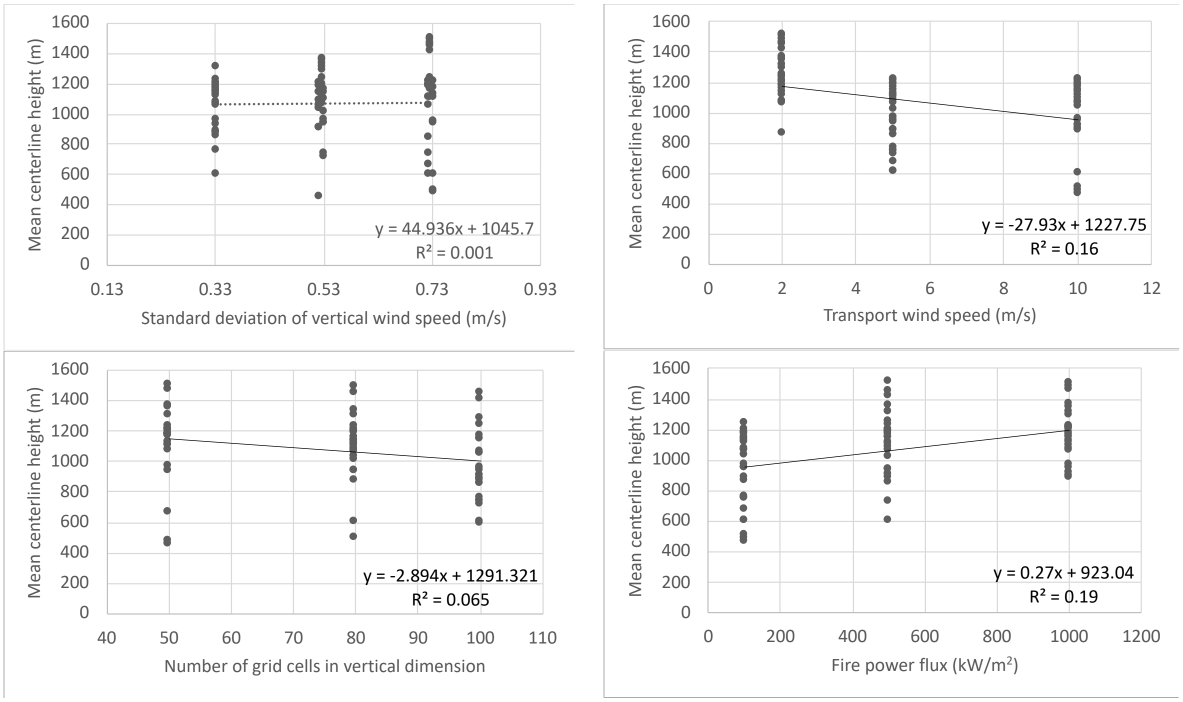

Figure 38. Effect of key parameters on mean plume centerline height (m)

Table 8. Multivariate linear regression of key parameters against plume centerline height

Regression Statistics	
Multiple R	0.64
R Square	0.41
Adjusted R Square	0.38
Standard Error	186.02
Observations	81

ANOVA

	df	*SS*	*MS*	*F*	*Significance F*
Regression	4	1806775.4	451693.85	13.0541123	3.85385E-08
Residual	76	2629725.55	34601.652		
Total	80	4436500.95			

	Coefficients	*Standard Error*	*t Stat*	*P-value*	*Lower 95%*	*Upper 95%*	*Lower 95.0%*	*Upper 95.0%*
Intercept	1278.62	114.39	11.18	1.03E-17	1050.79	1506.45	1050.79	1506.45
Fire power flux (kW/m^2)	0.27	0.06	4.89	5.47E-06	0.16	0.39	0.16	0.39
Wind speed (m/s)	-27.94	6.26	-4.46	2.79E-05	-40.41	-15.46	-40.41	-15.46
Number of vertical cells	-2.89	1.01	-2.88	5.21E-03	-4.90	-0.89	-4.90	-0.89
stdev vertical wind speed	46.45	127.76	0.36	7.17E-01	-208.00	300.91	-208.00	300.91

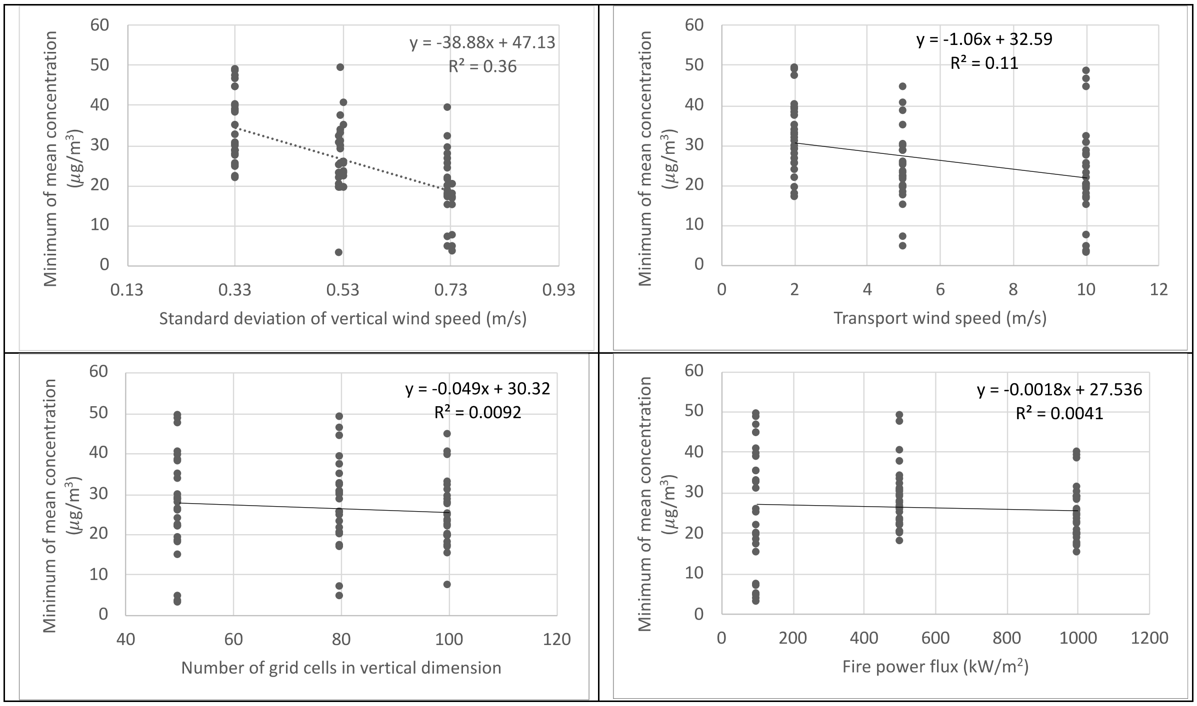

Figure 39. Effect of key parameters on mean far field plume concentration (µg/m²)

Table 9. Multivariate linear regression of key parameters against far field plume concentration

Regression Statistics	
Multiple R	0.69
R Square	0.48
Adjusted R Square	0.45
Standard Error	7.83
Observations	81

ANOVA

	df	*SS*	*MS*	*F*	*Significance F*
Regression	4	4310.75	1077.69	17.60	0.00
Residual	76	4654.54	61.24		
Total	80	8965.29			

	Coefficients	*Standard Error*	*t Stat*	*P-value*	*Lower 95%*	*Upper 95%*	*Lower 95.0%*	*Upper 95.0%*
Intercept	57.83	4.81	12.02	3.01E-19	48.24	67.41	48.24	67.41
fire_power_kW	0.00	0.00	-0.77	4.42E-01	0.00	0.00	0.00	0.00
U_m/s	-1.06	0.26	-4.02	1.38E-04	-1.58	-0.53	-1.58	-0.53
nz	-0.05	0.04	-1.16	2.50E-01	-0.13	0.04	-0.13	0.04
sd vertical	-38.82	5.38	-7.22	3.34E-10	-49.52	-28.11	-49.52	-28.11

Appendix 5: FDS Meteotron Simulations – Burner Array vs. Equivalent Circular Burner

Simulations of plumes from the detailed Meteotron burner array and an equivalent circular burner were compared to assess the need for resolving the separate burners in FDS. The area of the circular burner was equivalent to that of the original array (3400 m^2) and had a HRRPUA of 176.48 kW/m^2 to provide a total power of 600 MW (Benech 1976). All other conditions (wind speed, mesh resolution, etc.) were identical in both simulations. Simulated time was 1200 s in both simulations. Concentrations were averaged over the final 600 s of simulated time for the purpose of comparison.

Results are summarized in Figure 40, Figure 41 and Figure 42. The differences between time-averaged plumes from both simulations are not significant in terms of the typical variations between smoke simulations and in terms of air quality predictions.

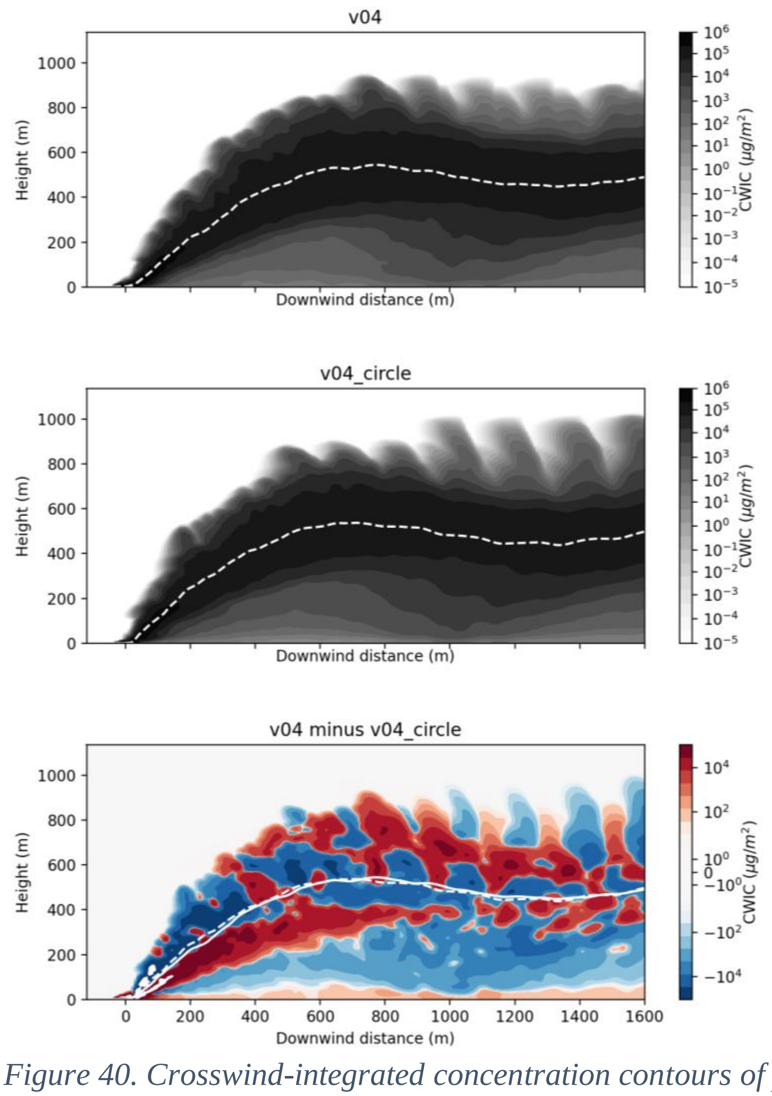

Figure 40. Crosswind-integrated concentration contours of plumes from the original burner array (top) and equivalent circular burner (middle). Bottom: differences between the detailed and circular burner concentrations. The largest variations are only about 20% of the maximum values of CWIC.

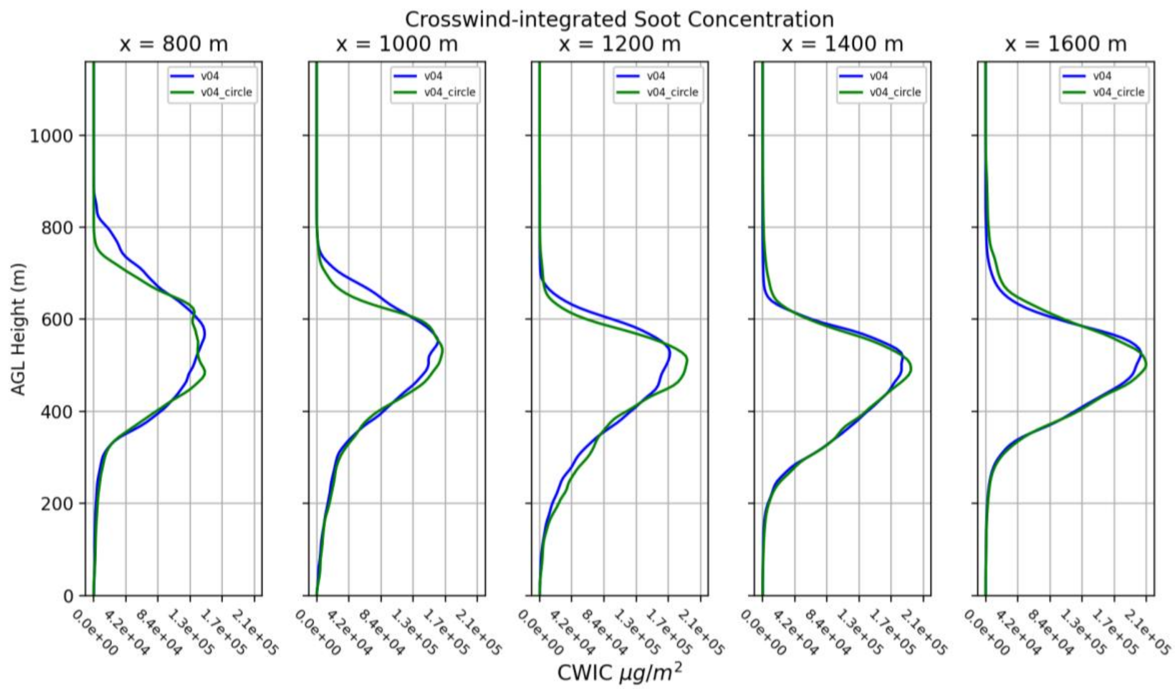

Figure 41. Crosswind-integrated concentrations of plumes from the original burner (blue) and circular burner (red) at specific downwind locations.

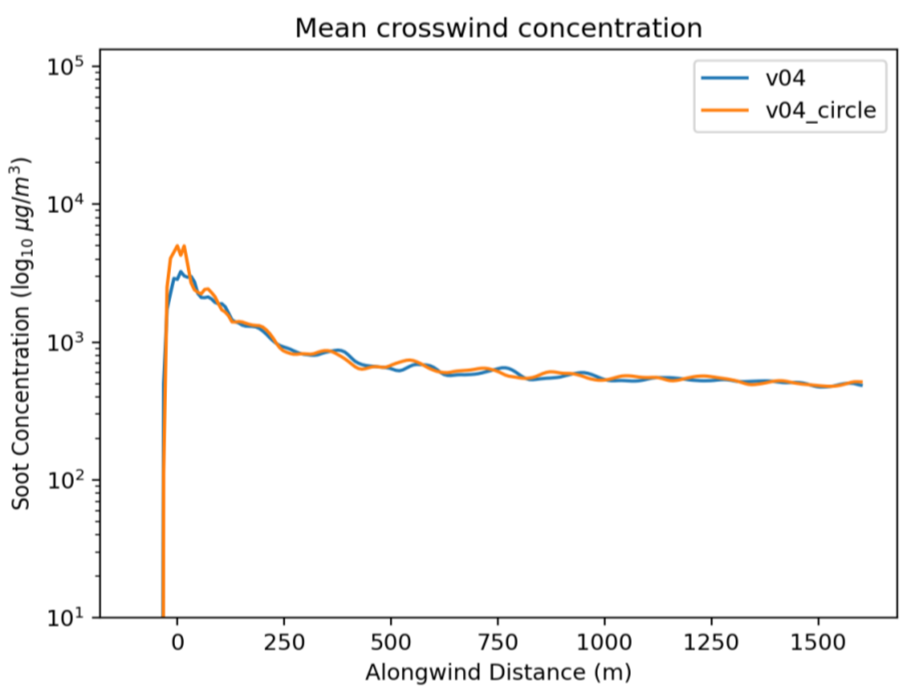

Figure 42. Mean crosswind concentrations are almost identical between the detailed (blue) and circular (orange) burner simulations.

Appendix 6: Sensitivity of FDS Meteotron Plumes to Mesh Resolution

FDS simulations of the April 1973 Meteotron trial were repeated over a range of grid cell sizes to explore the effect of mesh resolution on the simulated plumes. The cell sizes in the original simulation varied from 1 m near the burner to 8 m further from the source (Figure 28). Grid cell sizes were uniform throughout the domain of the comparison simulations. To avoid issues with resolution of the burner array, a single circular source of equivalent HRRPUA was used in the comparison simulations.

As shown in Figure 43 and Figure 44, plume appearances and concentration values depart noticeably from those in the original simulation when grid cell sizes are greater than 10 m. Larger grid cells essentially increase diffusion of the plume as smoke is mixed into larger cells. The 10 m simulation executed about 11 times faster than the original (Table 10). This suggests that 10 m cell sizes, for plumes at this scale (~2 km), might provide a good balance between accuracy and execution time in FDS.

Table 10. Cell sizes and execution times of the April 1973 Meteotron simulations.

Resolution	Original	8 m	10 m	20 m	40 m
CPU time (s) (# meshes)	34249 (15)	3153 (5)	3053 (5)	27 (2)	19 (1)

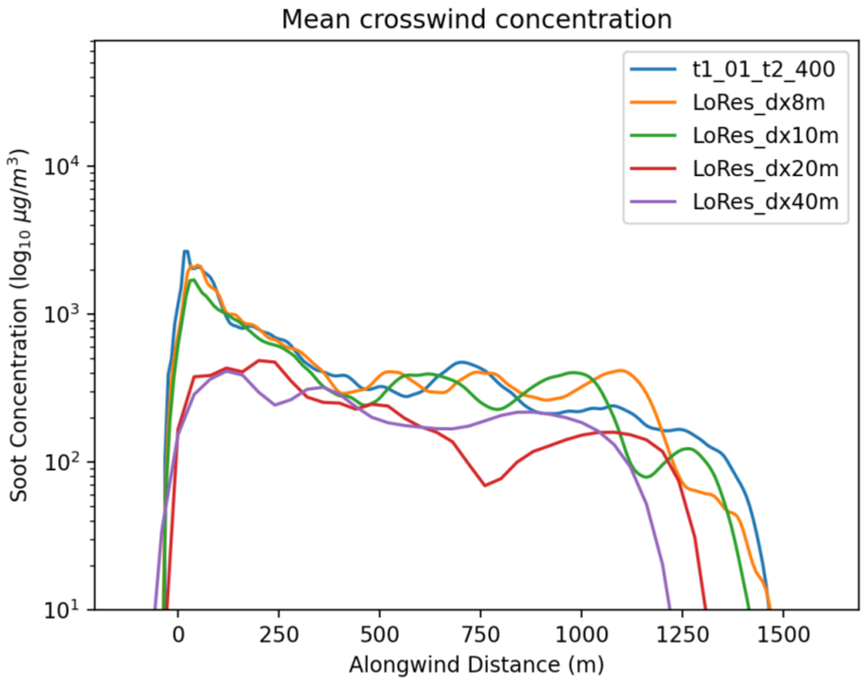

Figure 43. Alongwind concentration profiles. Grid cell sizes greater than 10 m produce lower concentrations than the original higher resolution simulation.

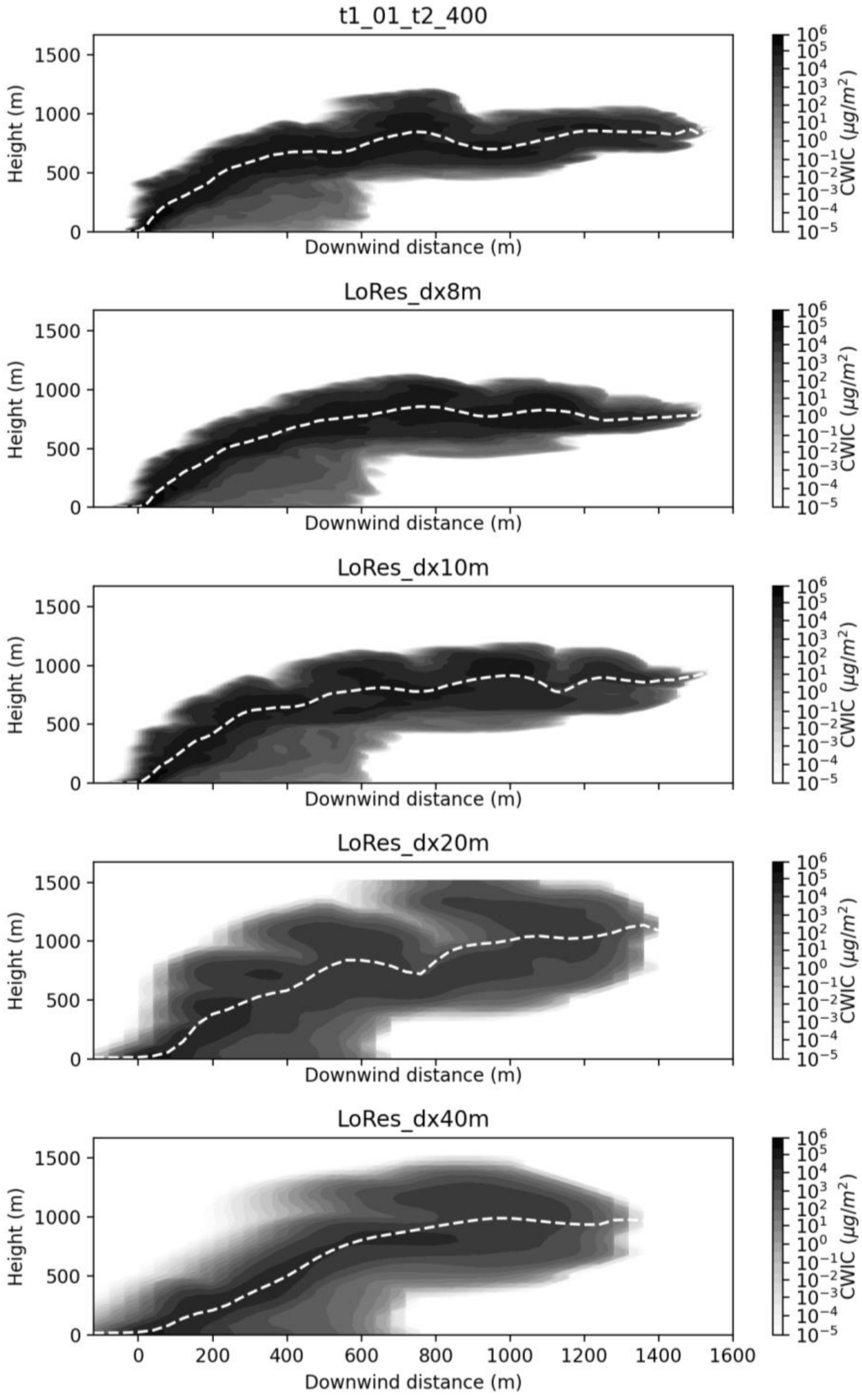

Figure 44. Concentration contour plots from FDS simulations of the April 1973 Meteotron plume experiment. Grid cells sizes increase from top to bottom in the figure.

Appendix 7: Results from Other Meteotron Simulations

Contours of crosswind-integrated concentrations from simulations not presented in the main body of the report are shown below.

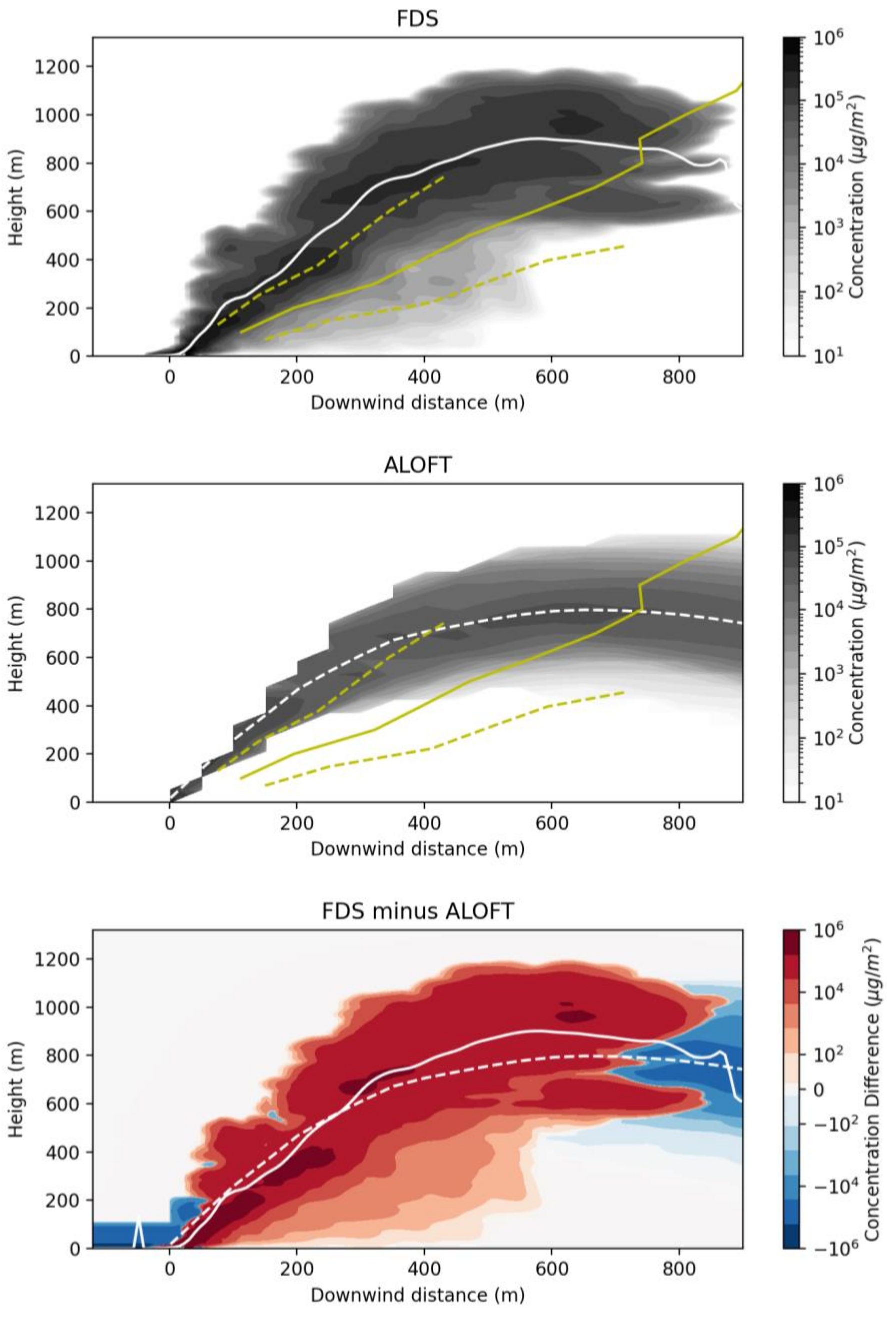

Figure 45. Crosswind-integrated concentration contours from FDS (top) and ALOFT-FT (bottom) simulations of the ***February 1973*** *Meteotron experiment. The extent of the plume as estimated from photogrammetry is shown in yellow. Bottom: difference in CWIC between the FDS and ALOFT-FT simulated plumes.*

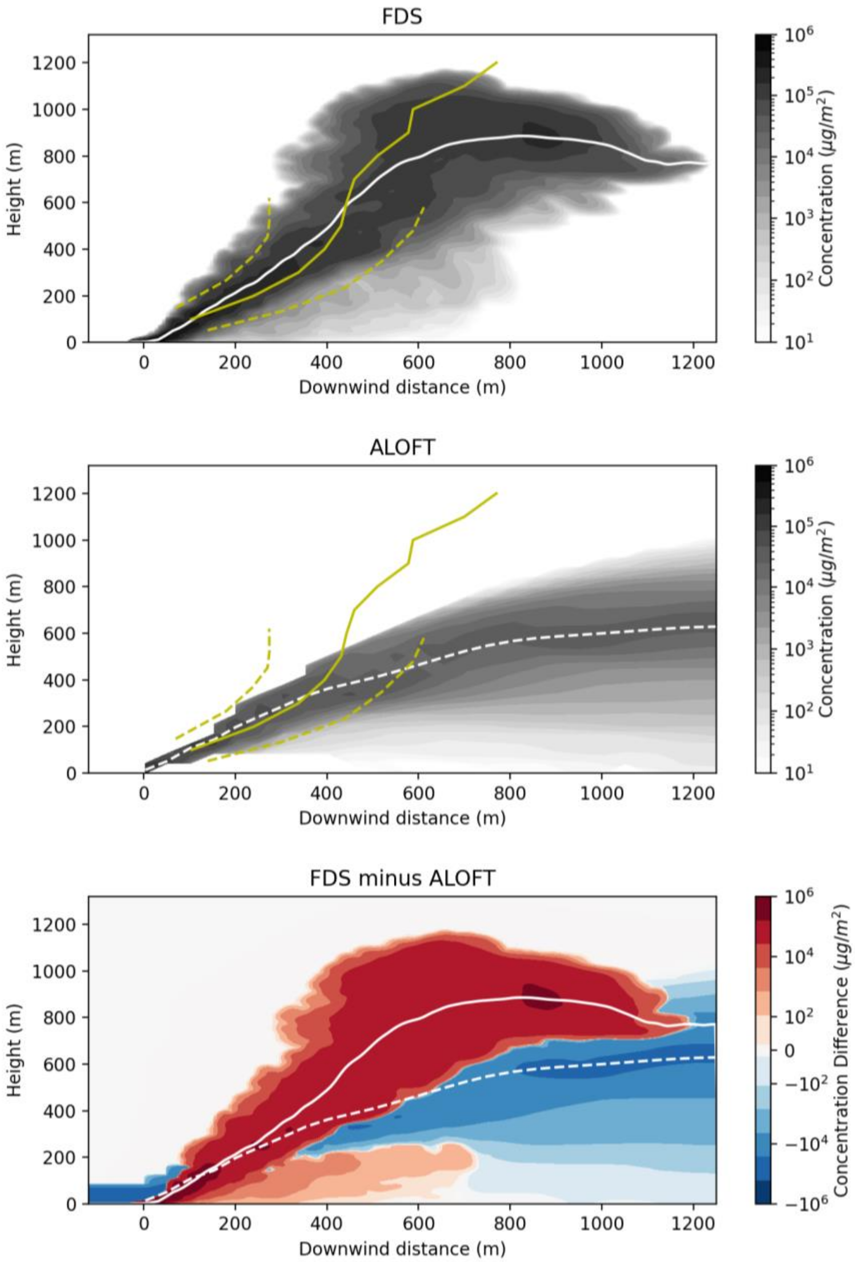

Figure 46. Crosswind-integrated concentration contours from FDS (top) and ALOFT-FT (bottom) simulations of the ***July 1973*** *Meteotron experiment. The extent of the plume as estimated from photogrammetry is shown in yellow. Bottom: difference in CWIC between the FDS and ALOFT-FT simulated plumes.*

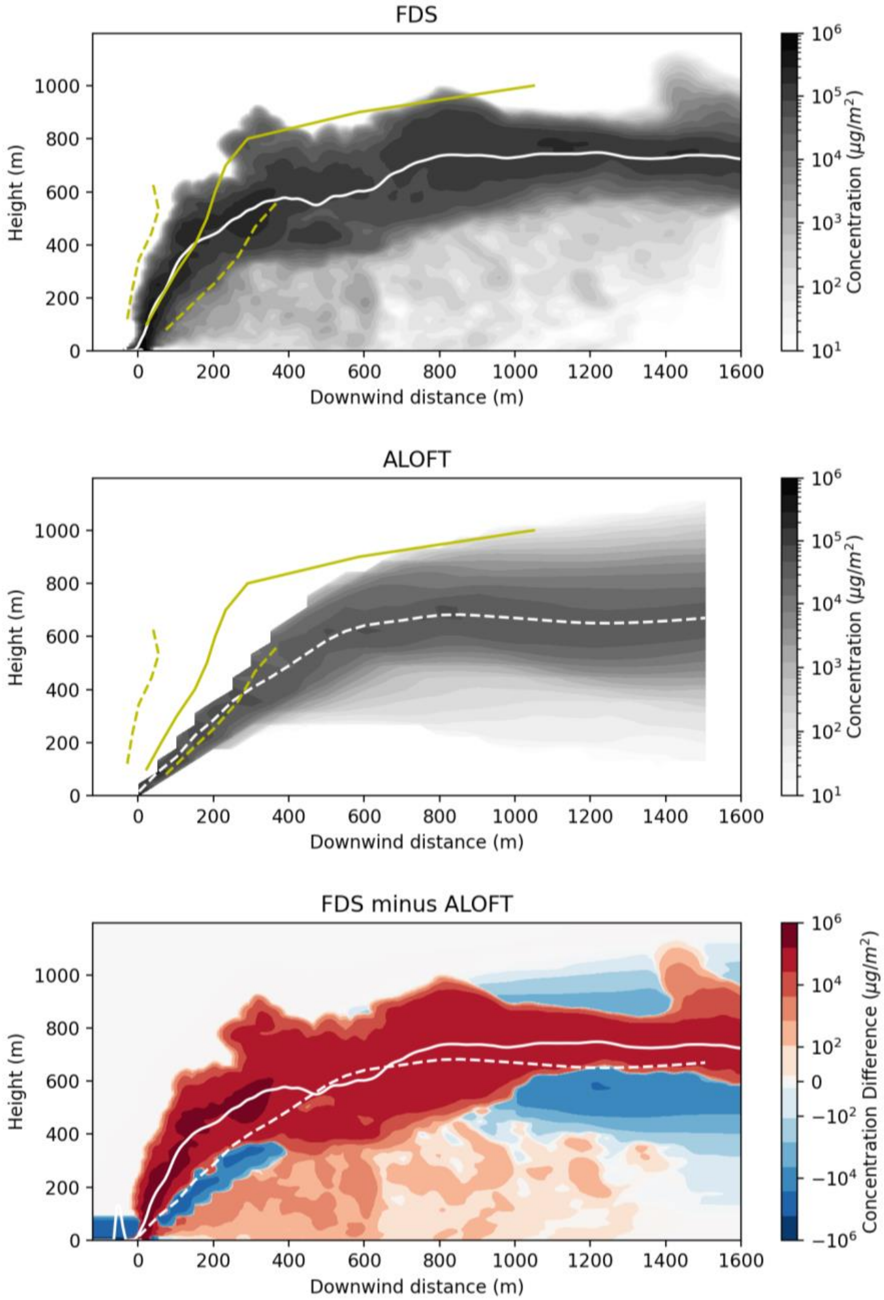

Figure 47. Crosswind-integrated concentration contours from FDS (top) and ALOFT-FT (bottom) simulations of the ***October 1973*** *Meteotron experiment. The extent of the plume as estimated from photogrammetry is shown in yellow. Bottom: difference in CWIC between the FDS and ALOFT-FT simulated plumes.*

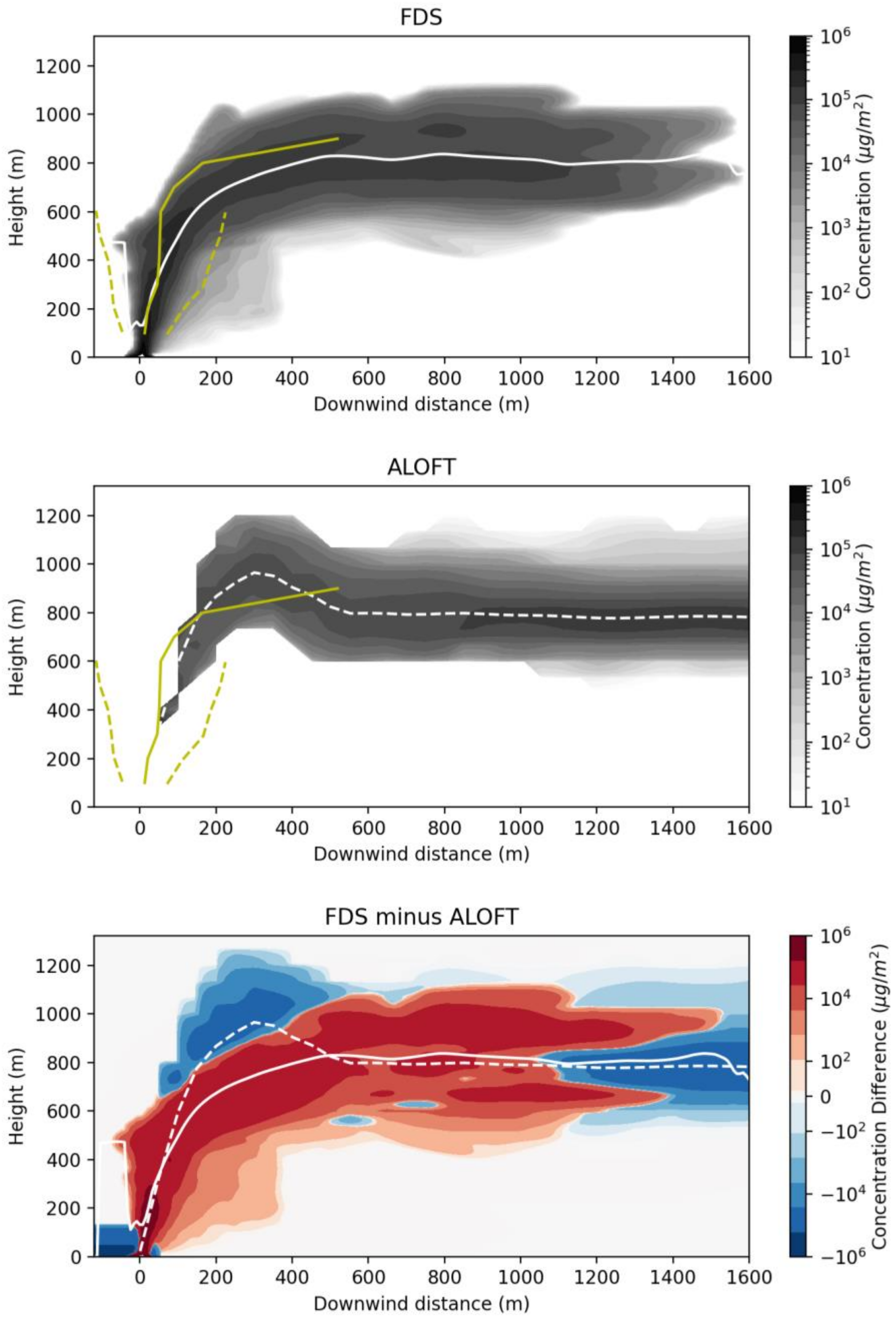

*Figure 48. Crosswind-integrated concentration contours from FDS (top) and ALOFT-FT (bottom) simulations of the **April 1973** Meteotron experiment (compare with Figure 31) simulated at a lower wind speed **(1 m/s)** than was recorded in the mixed layer (~2 m/s). The extent of the plume as estimated from photogrammetry is shown in yellow. Bottom: difference in CWIC between the FDS and ALOFT-FT simulated plumes.*

Appendix 8: Comparison of Wind Generation Methods in FDS

Wind in atmospheric simulations in FDS can be generated by three different methods (McGrattan et al. 2020). Two of those methods were employed in the simulations described in this report. In the first, referred to as the ‘wall of wind’ method, wind is blown into the domain from one or more external boundaries and exits through one or more external boundaries. Wind at inlets can be uniform in velocity or assigned power law profiles.

The second method makes use of a technique called ‘nudging’ that is commonly used in atmospheric simulations. This is implemented in FDS by means of a forcing term added to the momentum equations. Two relaxation time constants are prescribed in the forcing term. The first ensures that the mean overall flow field is similar to the prescribed field. The second constant is generally much larger than the first and drives local velocity components towards the prescribed mean over longer periods (McGrattan et al. 2020).

An advantage of the nudging method is that prescribed wind speeds and directions can vary with height and with time while the domain boundaries remain open. However, if the time constants are too constraining, the nudging method can artificially reduce turbulence and alter flow fields in ways that are unphysical. We created two types of flow simulation sets to examine the effect of nudging on plume simulations.

In the first set of simulations, a constant wind of 5 m/s was prescribed in a domain 1000 m long in the alongwind direction and 520 m x 520 m in the crosswind and vertical directions at 10 m resolution. A 20 m x 40 m block was placed in the center of the axis of flow, 120 m from the wind inlet, to trip the downwind flow. Alongwind and crosswind velocities and standard deviations were recorded at specific locations (Figure 49).

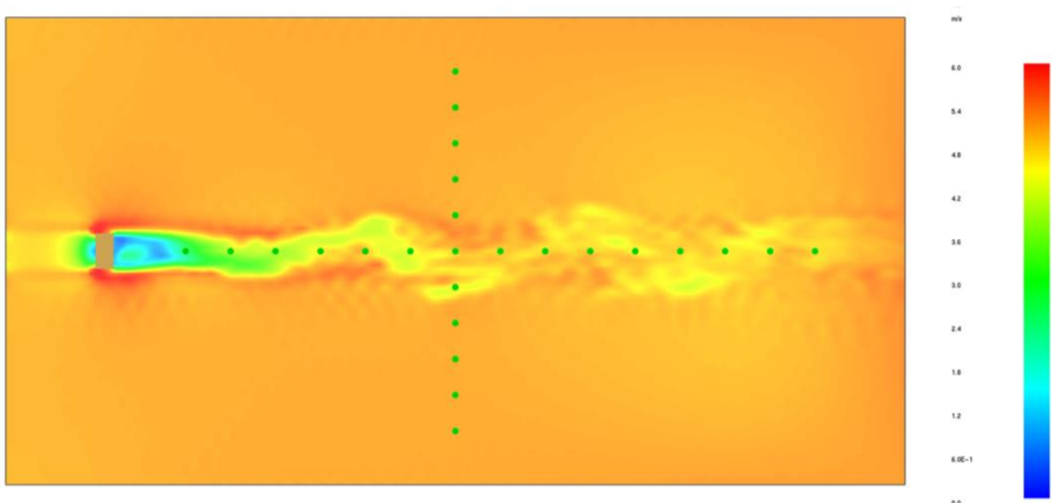

Figure 49. Cross section showing simulated wind flowing past a trip block (left side of image). Flow is from left to right. Green dots indicate locations of velocity measurements.

The initial simulation was performed using the wall-of-wind method. The simulation domain essentially acts as a large wind tunnel. Several simulations using the nudging method to drive flow were then performed and compared to the wall-of-wind simulation. The first relaxation time constant (t_1) was held at 1s in the simulations. This is the default value and should, regardless, be kept at a relatively low value to avoid numerical instabilities and unphysical flow. The second relaxation time constant (t_2) was varied from 30s to 600 s in separate simulations.

Plots comparing the alongwind and crosswind mean wind speeds and standard deviations are shown in Figure 50. Although lower values of t_2 keep the mean wind speeds nearest to the corresponding values of the wall-of-wind simulations (Figure 50, top left), they greatly dampen the *variations* in windspeed (Figure 50, top right). Values of t_2 below 100 s almost completely remove the turbulence generated by the trip (Figure 50, top & bottom right). Root mean squared errors (RMSE) with respect to the wall-of-wind case are shown for the tested values of t_2 in the bottom panels of Figure 50. The figure suggests that, at this simulated physical scale and wind speed, a t_2 value of 400 s results in the lowest RMSE values of the mean wind speeds and standard deviations together, and so provides the best balance between minimal dampening of turbulence and maintaining the prescribed wind speed.

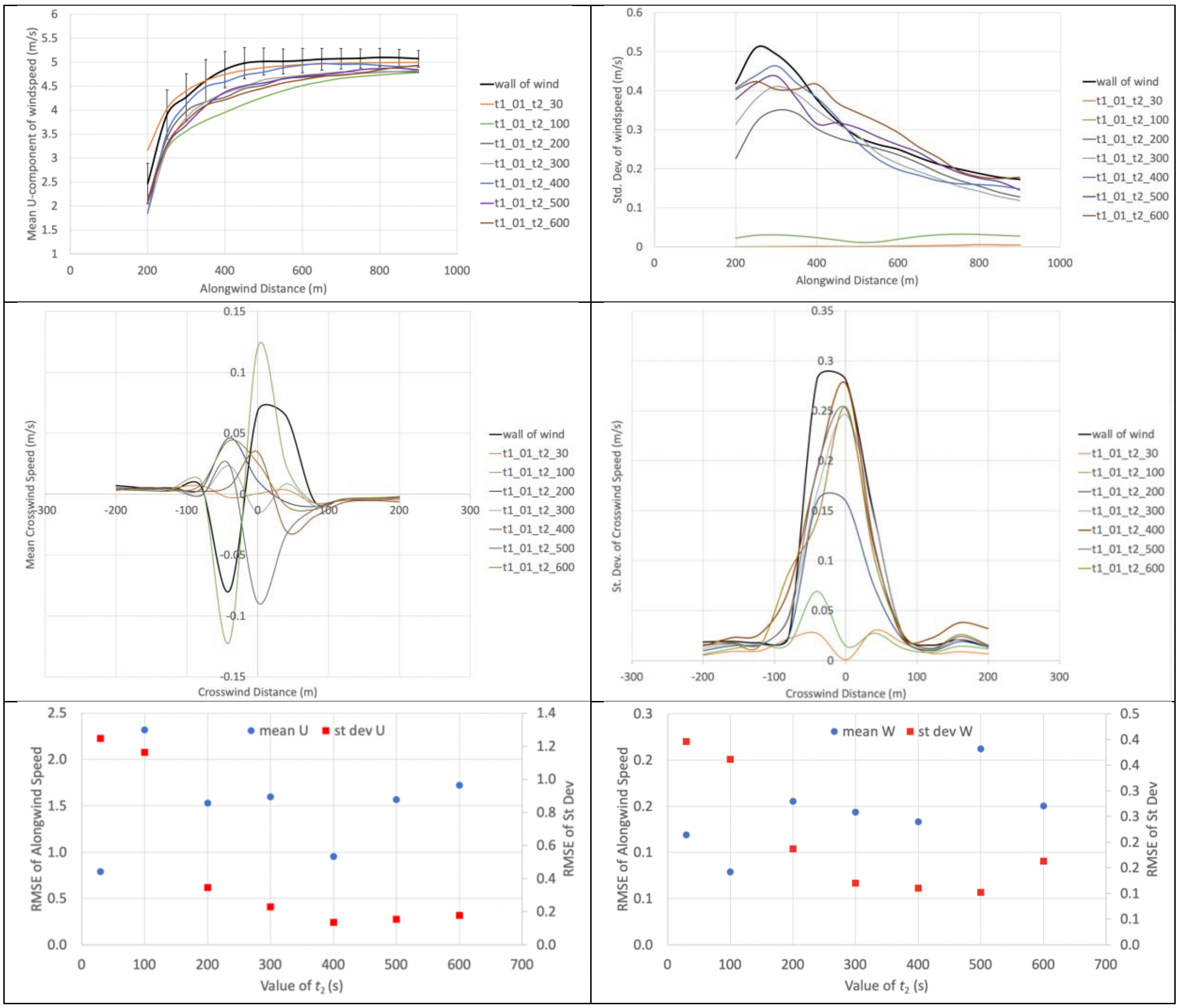

Figure 50. Effect of relaxation time on wind speeds and turbulence. Top left: mean wind speed in the alongwind direction downwind of the trip. Error bars show standard deviation of wind speed in the wall of wind simulation. Top right: Standard deviation of wind speed. Middle left: mean wind speed in crosswind direction. Middle right: standard deviation of crosswind speed. Bottom left: root mean squared errors of mean alongwind speed and standard deviation (note secondary scales). Bottom right: root mean squared errors of crosswind speed and standard deviation.

In the second simulation set, several FDS nudging simulations of plumes from a 40 m x 40 m burner with a HRR of 2 MW were conducted in a domain of the same size and resolution as the first set and compared to an equivalent wall of wind case. As before, wind speed was prescribed as 5 m/s throughout the domain in all cases.

Results are shown in Figure 51and Figure 52. Plumes from the nudging simulations have slightly lower centerline heights, and crosswind integrated concentrations tend to remain slightly greater near the plume centerlines, than in the wall of wind simulation. This suggests that plumes in the nudging simulations tend to be slightly more bent and less mixed than in the wall of wind simulations. Changing the relaxation times seems to have relatively small effects on the plume profiles.

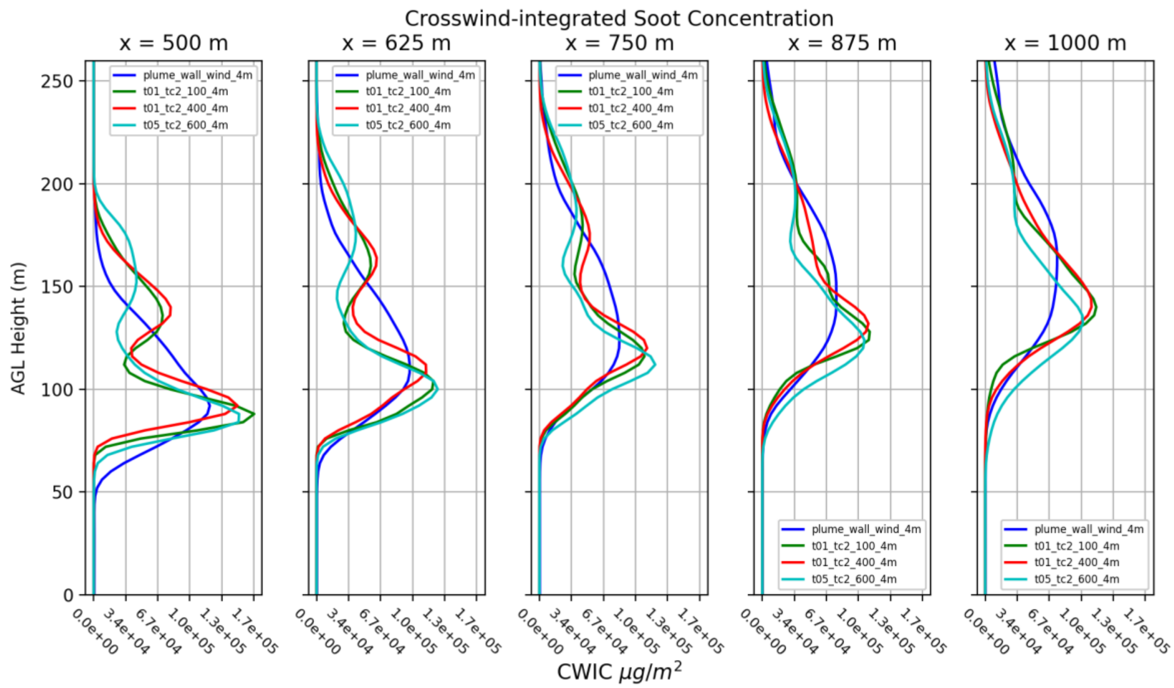

Figure 51. Vertical profiles of crosswind-integrated concentrations at specific downwind locations.

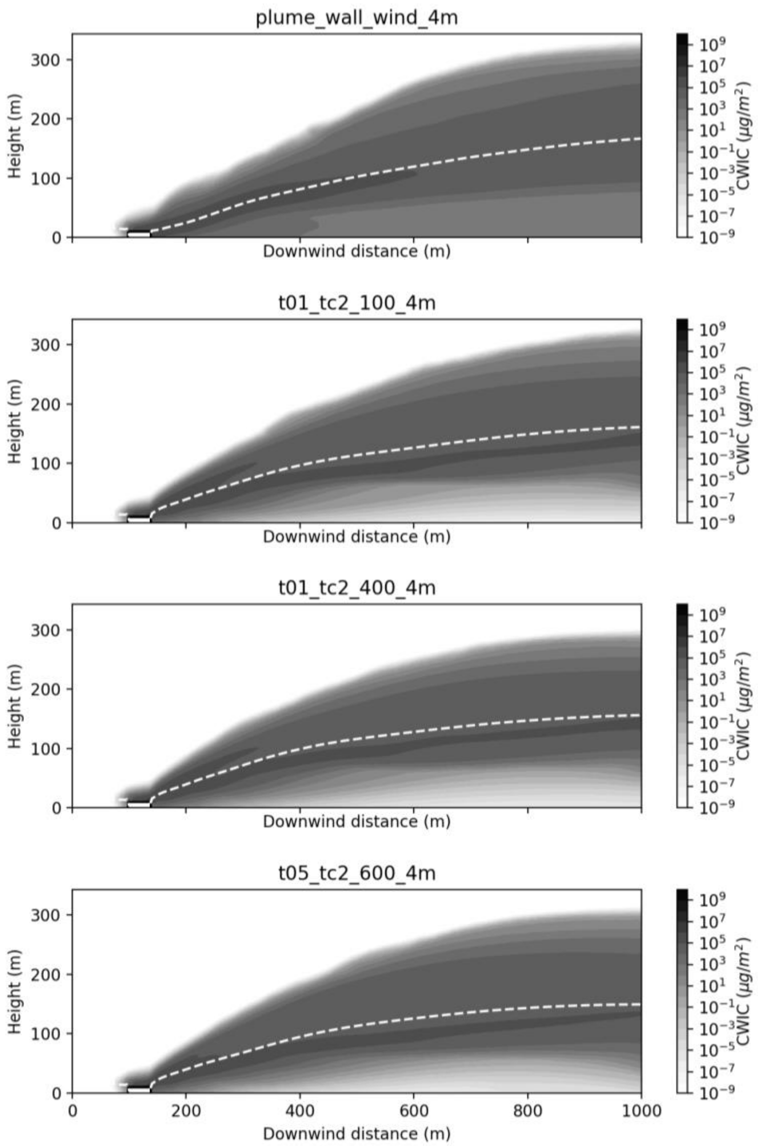

Figure 52. Contours from crosswind-integrated concentrations of plumes. From top down: wall-of-wind simulation; nudging with t_2=100 s, t_2=400 s, and t_2=600 s (t_1=5 s in the bottom panel).